This is to certify that the

thesis entitled

EFFECT OF TEMPERATURE AND LOADING TIME ON THE STIFFNESS PROPERTIES OF HMAC IN FLEXIBLE PAVEMENTS

presented by

Dong-Yeob Park

has been accepted towards fulfillment
of the requirements for

Ph.D. degree in Civil Engineering

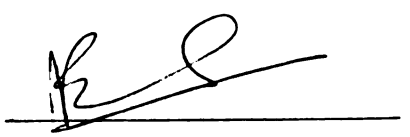

Major professor

Date 12/04/00

# EFFECT OF TEMPERATURE AND LOADING TIME ON THE STIFFNESS PROPERTIES OF HMAC IN FLEXIBLE PAVEMENTS

By

Dong-Yeob Park

A DISSERTATION

Submitted to
Michigan State University
in partial fulfillment of the requirements
for the degree of

DOCTOR OF PHILOSOPHY

Department of Civil and Environmental Engineering

2000

ABSTRACT

EFFECT OF TEMPERATURE AND LOADING TIME ON THE STIFFNESS PROPERTIES OF HMAC IN FLEXIBLE PAVEMENTS

By

Dong-Yeob Park

Surface deflections and backcalculated layer moduli of flexible pavements are significantly affected by the temperature of the asphalt concrete (AC) layer. The correction of these deflections and moduli to a reference temperature requires the determination of an effective temperature of the AC layer. In light of this, a new temperature prediction model for determining the AC temperature on the basis of a database approach is presented, and temperature correction factors for AC modulus are developed. Temperature data points (317) and deflection profiles (656) were collected from six in-service test sites in Michigan. Temperature data points (197) from three of the test sites were used to develop the temperature prediction model, and data from the remaining sites were used for validation. The developed temperature prediction model has a $R^2$ greater than 90% and an F-statistic significantly greater than 1.0. For further validation of the temperature prediction model, temperature data points (18444) from seven Seasonal Monitoring Program (SMP) sites (Colorado, Connecticut, Georgia, Nebraska, Minnesota, South Dakota, Texas) were obtained from the LTPP Database (DATAPAVE 2.0). The validation results suggest that the model could be adopted to all seasons and other climatic and geographic regions. The major improvements over existing models are: (a) the model does not require temperatures for the previous 5 days,

(b) it takes into account temperature gradients due to diurnal heating and cooling cycles, and (c) it needs fewer parameters than other published models. The effect of temperature prediction error on the performance prediction was also investigated. Temperature profiles obtained from the temperature prediction and correction study were used in the following structural analysis.

The temperature-dependent behavior of flexible pavement is due to viscoelastic properties of the AC layer. Hence, in the second part of this study, 2-D and 3-D finite element analyses (FEA) of flexible pavements were performed to investigate the influence of realistic temperature distributions and dynamic loads on pavement responses (mainly, stress, strain, and dissipated energy). Parametric studies (AC thickness, base stiffness, loading condition, and temperature distribution across the AC layer) were first conducted with a 2-D axisymmetric finite element (FE) model. Effects of three temperature distributions (night, morning, and day) and three loading types (load case I - uniform vertical load over the entire load area, load case II - uniform vertical load only under tire treads, and load case III - measured vertical and lateral stresses under tire treads) on the structural response were further investigated with a 3-D FE model. The evaluations from 2-D and 3-D analyses were consistent. These results could explain the occurrence of top-down cracking in AC pavements under certain conditions, and contribute to the development of an improved performance model and/or asphalt pavement design program based on advanced material characterization and dynamic loads.

To my family, for their support and love

ACKNOWLEDGMENTS

The author would like to express his deepest gratitude to his major advisor Dr. Neeraj Buch for his patience, guidance, and encouragement throughout this research. Gratitude is also expressed to the doctoral committee members Dr. Karim Chatti, Dr. Ronald Harichandran, and Dr. Connie Page for their valuable advice. The author expresses special thanks to Tom Hynes, Kurt Bancroft, Frederick Carian, and the traffic control crew of the Michigan Department of Transportation (MDOT) for their assistance during field data collection. The authors are grateful to Dr. Dar-Hao Chen and Dr. Mike Murphy of Texas DOT and Mr. John Rush of LTPP Customer Support Service Center for providing temperature data.

Finally, the author gratefully acknowledges the financial support provided by the MDOT, Pavement Research Center of Excellence (PRCE) and Composite Materials and Structures Center (CMSC) at Michigan State University.

## TABLE OF CONTENTS

APPENDIX

## LIST OF TABLES

## LIST OF FIGURES

# CHAPTER 1

# INTRODUCTION

## 1.1 BACKGROUND

### 1.1.1 Temperature Prediction Model and Correction Factor for AC Modulus

The use of falling weight deflectometer (FWD) data has become one of the primary means of characterizing *in situ* structural properties of flexible pavements. Structural capacity (deflection and modulus) of the asphalt concrete (AC) layer is strongly influenced by ambient and pavement temperatures. In order to accurately determine or backcalculate the AC modulus, a two-step correction procedure needs to be applied. Typically the first step consists of predicting the effective temperature of the AC layer, and the second step consists of adjusting the FWD deflection or the computed modulus to a reference temperature using a correction factor.

The 1986 AASHTO Guide for Design of Pavement Structures (AASHTO Guide, 1986) presents a temperature correction protocol for FWD deflections. This procedure requires the use of average air temperature for the previous 5-days to predict pavement temperature at selected depths. However, pavement engineers have challenged its accuracy and practicality; this procedure does not account for the temperature gradient effects due to diurnal heating and cooling cycles, which have a significant effect on the effective pavement temperature and its relationship with the AC modulus and the surface deflection (Inge and Kim, 1994; Stubstad et al., 1994).

Recognizing the urgent need to develop a more accurate and practical temperature-modulus correction procedure for pavement rehabilitation designs in the

state of Michigan, the Michigan Department of Transportation (MDOT) funded a study in 1996 to develop a new temperature prediction model. The resulting model has proven to be both robust and widely applicable. The temperature and deflection data used in this study were obtained from field measurements.

### 1.1.2 Theoretical Analysis of Flexible Pavements

Recently mechanistic analysis has become more and more essential to the design and performance evaluation of flexible pavements. With the emergence of inexpensive microcomputers and the finite element analysis (FEA), many issues associated with analyzing pavements have been overcome with numerical modeling. This capability has facilitated the transition from empirical methods to mechanistic methods in pavement design.

Flexible pavements are classified into those pavements that have an asphalt concrete (AC) surface. Flexible pavements consist of a surface course built over a base/subbase course, and compacted roadbed soil. Although one of the important characteristics of asphalt concrete (AC) is the time and temperature dependent behavior due to its viscoelastic properties, many finite element programs and methods of pavement analysis relied on elastic analysis due to their relative simplicity.

Surface deflection data collected from the FWD, which is a dynamic load, have mostly been used and analyzed to evaluate an existing pavement. Therefore, simulation of asphalt concrete pavement subjected to FWD load is the first step to understand the deflection and stress-strain behavior of flexible pavements. In the FEA, the structural and other auxiliary conditions such as material models, load model, boundary conditions,

element type, and geometry have to be correctly modeled to obtain reasonable response results.

Nonetheless, many realistic problems such as temperature variation across the AC layer and dynamic loading were simplified or not included in many viscoelastic analyses even though complex interactions can affect structural analysis and pavement performance. For instance, pavement temperature varies across the depth of AC layer with time. During heating, the lower part of the AC layer is still cool, whereas, when the surface of the asphalt is cooling, the heat transmission still causes an increase in temperature at the lower part of the asphalt layer several hours after the top layer has started to cool down. Although these temperature variations can significantly affect the analysis, it has not been carefully studied together with the FWD load pulse.

In this part of the study, structural analyses were performed based on viscoelasticity of the AC layer subjected to an FWD pulse and various temperature distributions across the AC layer. The inclusion of dynamic load effect for routine pavement design involving viscoelastic materials is yet to be realized in the future. Hence, this study can contribute to the development of an improved asphalt pavement design program based on advanced material characterization and the FWD pulse.

## 1.2 OBJECTIVE

The objectives of this research are to:

1. Develop a practical and sound model to predict the effective temperature in the AC layer and temperature correction factor for backcalculated AC moduli.
2. Investigate temperature effects on structural analysis and performance evaluation.
3. Simulate selected AC pavements using viscoelastic/elastic composite layer theories.

4. Better understand stress-strain behaviors of flexible pavements subjected to FWD load pulse and various temperature distributions across the AC layer.

## 1.3 SCOPE

The temperature prediction and correction factor part of this study addresses the development of a practical yet robust temperature prediction model and correction factor for AC modulus, which can be adopted in the field. For this reason, the developed model was validated with various methods and field data. Characterization of the base and subgrade were not within the scope of the research.

The theoretical analysis part addresses only structural analysis of flexible pavements to understand the effect of pavement temperature and FWD pulse on structural responses. Additionally, the influence of nonuniform load pressures, including the truck tire tread effect, is investigated in association with surface-initiated longitudinal wheel path cracks, in an effort to relate analysis results to field observations/applications. Development of pavement design algorithm/program, performance model, and specific mixture characteristics (mixture composition, gradation, etc.) that may affect the analysis/problem are beyond the scope of this study.

## 1.4 ORGANIZATION OF THESIS

This thesis is divided into eight chapters, including the introduction.

CHAPTER 2: Comprehensive literature review on temperature prediction models and temperature correction factors for AC modulus.

CHAPTER 3: Comprehensive literature review on structural analysis of flexible pavements, and overview of axisymmetric finite element model, the

viscoelastic characterization of the AC layer, the subgrade characterization, and applications of structural analysis to the field.

CHAPTER 4: Field data collection procedure for the development of temperature prediction model and correction factor and preliminary analysis of data.

CHAPTER 5: Introduction of boundary conditions, material properties and FEA of two- and three-dimensional models, and parametric study approach.

CHAPTER 6: Development and validation of temperature prediction model and correction factor and investigation of influence of effective temperature prediction errors on structural analysis and performance model.

CHAPTER 7: Structural analysis results of 2-D and 3-D models and discussion.

CHAPTER 8: Summary of conclusions on the research results, comments on applications to the field, and recommendations for future research.

# CHAPTER 2

# LITERATURE REVIEW I – TEMPERATURE PREDICTION MODEL AND CORRECTION FACTOR FOR AC MODULUS

## 2.1 GENERAL

Falling Weight Deflectometer (FWD) data is widely used to evaluate in-situ material properties of pavement layers. Backcalculated AC moduli are influenced by pavement temperature because asphalt concrete is viscoelastic. Therefore, an effort is usually made to obtain representative AC layer moduli of flexible pavements, in which backcalculated AC moduli are adjusted to a reference temperature. This temperature correction can be achieved in two steps: (1) determination of the temperature, the so called effective temperature, which represents the temperature of the AC layer at the time of FWD testing and (2) adjustment of the backcalculated AC moduli to a reference temperature using correction factors.

Determination of the effective temperature is currently accomplished in many ways. Southgate (1968) suggested that the surface temperature plus the 5-day mean air temperature should be used as partial inputs to determine the temperature at various depths within the AC layer. Other methods include the use of a single measured temperature either at the top or at a certain depth within the AC layer. For routine deflection testing and analysis for state highway agencies (SHA's), it is desirable, from a practical view point, to devise a nondestructive prediction method for determining the

effective AC layer temperature. Hence, numerous temperature prediction models and correction procedures have been developed.

## 2.2 REVIEW OF TEMPERATURE PREDICTION AND CORRECTION PROCEDURE FOR AC MODULI

### 2.2.1 AASHTO Guide Temperature Prediction and Correction Procedure

The 1993 AASHTO Guide does not include any specific temperature prediction procedure for the effective AC layer temperature. The 1986 AASHTO Guide presents a temperature prediction procedure that allows for the estimation of the average pavement temperature during a deflection test.

This procedure requires as input (1) the pavement surface temperature during the deflection test, and (2) the mean air temperature for the previous five days to predict pavement temperatures with depth. Using this information, the pavement temperature at various depths within the total asphalt layer thickness is obtained from Figure 2-1. The average of these values is taken as the pavement temperature during the deflection test. The AC modulus adjustment factor ($F_e$) is a function of this average pavement temperature, as illustrated in Figure 2-2. The corrected asphalt modulus value, at 70 °F (21 °C), is then determined by:

$$E_{70°F} = F_e \times E_{tp} \qquad (2\text{-}1)$$

where:

$E_{70°F}$ = corrected asphalt layer modulus used to determine the effective structural layer coefficient for the existing in situ asphalt material
$F_e$ = asphalt modulus adjustment factor
$E_{tp}$ = Uncorrected asphalt layer modulus determined from the interpretation of deflection basin measurements. (This predicted modulus corresponds to a pavement temperature condition, $t_p$, occurring during the deflection test.)

### 2.2.2 BELLS Temperature Prediction Model

Stubstad et al. (1994) and Balzer and Jansen (1994) developed a temperature prediction equation to predict temperature at one-third depth of the AC layer as an effective temperature and a temperature correction, respectively.

The BELLS temperature prediction equation is as follows (Stubstad et al., 1994):

$$T_{1/3}=8.77+0.649*IR+\{\log(d)-1.5\}\{-0.503*IR+0.786*(5\text{-day})+4.79*\sin(hr-18)\}+\{\sin(hr-14)\}\{2.20+0.044*IR\} \quad (2\text{-}2)$$

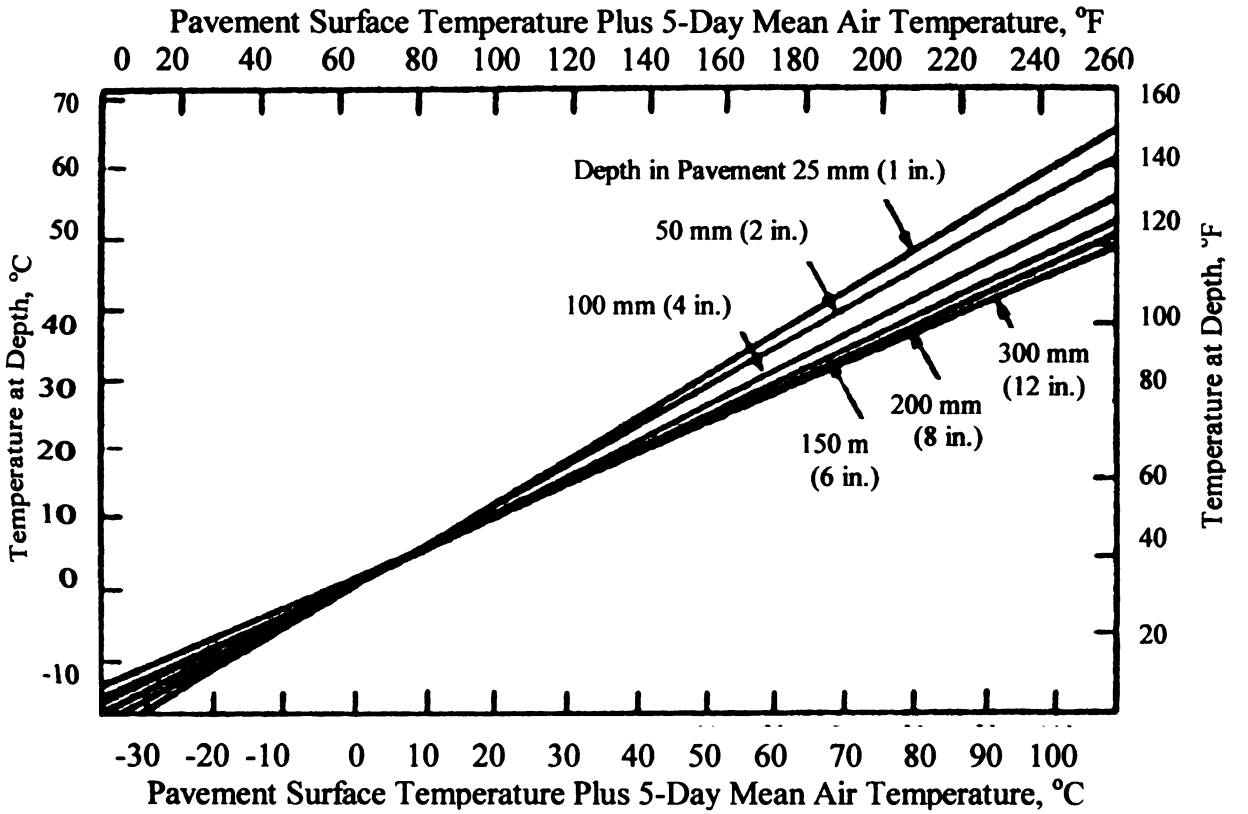


Figure 2-1. Predicted pavement temperature (AASHTO Guide, 1986)

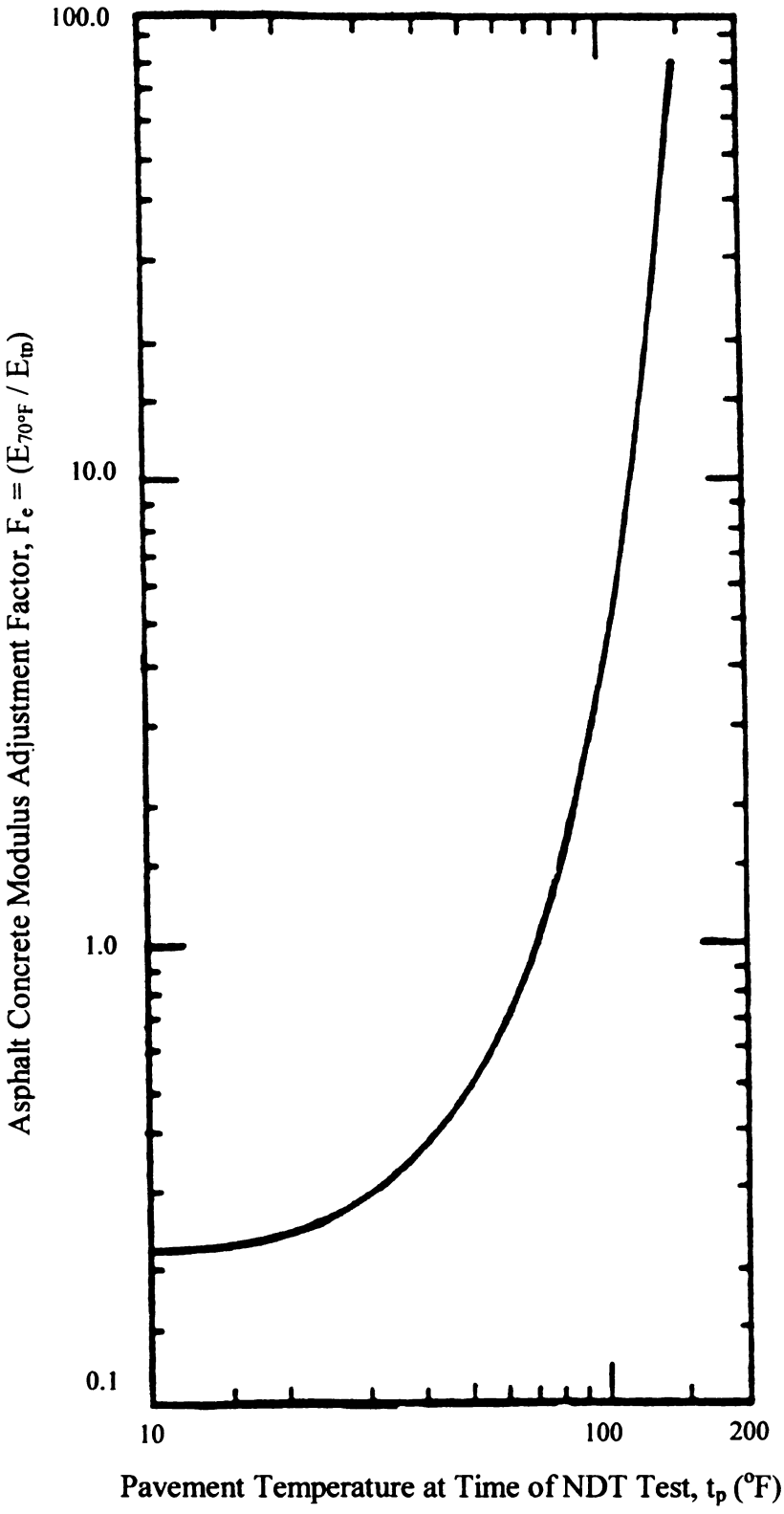


Figure 2-2. Asphalt modulus temperature adjustment factor (AASHTO Guide, 1986)

where:

| | | |
|---|---|---|
| $T_{1/3}$ | = | pavement temperature at third-point in AC mat, °C, |
| IR | = | infrared temperature reading at time of FWD test, °C, |
| log | = | base 10 logarithm, |
| d | = | depth at which mat temperature is to be determined, i.e. total AC mat thickness divided by 3, mm, |
| 5-day | = | previous mean 5-day air temperature, sum of 5 highs and 5 lows divided by 10, °C, |
| sin | = | sin function in 24 hour system. To use the time-hr function correctly, divide the number of hours in cycle by 24, multiply by $2\pi$, and apply the sin function in radians. |

Due to the heating and cooling cycles of pavement, surface temperature is higher than subsurface temperature during the daytime. On the other hand, surface temperature becomes lower than subsurface temperature during the nighttime (Figure 2-3). The BELLS model adequately takes into account the different temperature-depth gradients due to this diurnal and nocturnal cycles, which have significant effect on effective pavement temperature. However, the BELLS temperature prediction equation predicted temperature only at one-third of the AC layer.

Based on the temperature at the one-third depth of the AC layer, two correction models were presented; one is a modified correction model and the other is the new temperature correction model (Balzer and Jansen, 1994). The schematic relationship between backcalculated AC modulus and temperature at three different depths is shown in Figure 2-4. It can be seen that the AC modulus follows a different curve depending on whether the asphalt is heating or cooling. During heating, the lower part of the AC layer is still relatively stiff and has significant influence on the composite stiffness of the AC layer. Whereas, when the surface of the asphalt is cooling, the heat transmission still

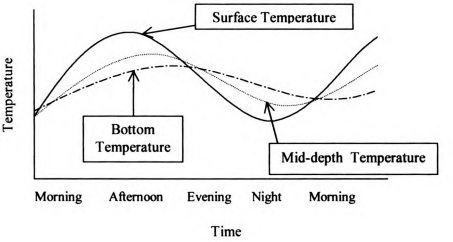


Figure 2-3. Temperature variations for a day at three different depths of an AC layer.

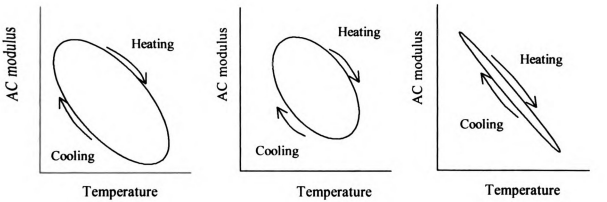


(a) Top of AC layer (b) Bottom of AC layer (c) Appr. one third of AC layer

Figure 2-4. Relationship between the AC modulus and temperature at three different depths (Modified from Balzer and Jansen (1994)).

causes an increase in temperature and softness of the lower part of the asphalt layer several hours after the top part has started to cool. This results in stagnation of the AC moduli before it starts to increase due to the lower temperature. Judging from Figure 2-4, (a) and (b), it would be very difficult to establish a temperature correction model based on the temperature at either the top or the bottom of a thick asphalt layer, as there is no definite AC modulus at any temperature chosen as standard temperature. Figure 2-4 (c) shows that temperatures at the depth of one third of the AC layer thickness exhibits a definite correlation between the temperature and the AC modulus. According to Kim et al. (1996), the middepth temperature also provides a reasonable relationship between temperature and AC modulus. At this depth (one third depth or middepth), it would be possible to calculate a definite reference AC modulus at a standard temperature.

The adjusted model is

$$E_{ref} = \frac{E_{AC}}{1 - 2.2\log(T_{AC} / T_{ref})} \tag{2-3}$$

where:

$T_{ref}$ = reference temperature, °C,
$E_{ref}$ = reference AC modulus, MPa,
$T_{AC}$ = AC temperature measured during the FWD test, at one third of the total AC thickness, °C,
$E_{AC}$ = AC modulus found from FWD testing and backcalculation, MPa

The new temperature correction model is

$$E_{ref} = 10^{-0.018\,(T_{ref} - T_{AC})}\, E_{AC} \tag{2-4}$$

where:

$E_{ref}$, $T_{ref}$, $T_{AC}$, $E_{AC}$ = same as above.

Similarly, a plot of backcalculated asphalt modulus vs. temperature was also developed by Briggs and Lukanen (2000), along with a regression equation which can be

used to determine the asphalt modulus at any temperature. The form of the regression equation is:

$$E_t = E_{ref} e^{\alpha(t-t_{ref})} \quad (2\text{-}5)$$

where:

| | | |
|---|---|---|
| $E_t$ | = | predicted asphalt modulus at temperature, t |
| $E_{ref}$ | = | asphalt modulus at reference temperature, $t_{ref}$ |
| $e$ | = | exponetial function |
| $\alpha$ | = | regression coefficient |
| t | = | temperature of asphalt, degrees C |
| $t_{ref}$ | = | reference temperature of asphalt (25 degree C) |

### 2.2.3 BELLS2 Temperature Prediction Model

Lukanen et al. (2000) developed new coefficients for BELLS temperature prediction model using temperature data from 40 sites monitored in the Seasonal Monitoring Program for the Long Term Pavement Performance (LTPP) program. In the BELLS2 model, the previous 5-day average air temperature, which was difficult to obtain, was replace by the previous day's air temperature, and the sine functions of the BELLS model were replace by two sine functions based on an18-hr cycle. The form of the resulting equation is:

$$T_d=2.78+0.912*IR+\{\log(d)-1.25\}\{-0.428*IR+0.553*(1\text{-day})+2.63*\sin(hr_{18}-15.5)\}+0.027*IR*\sin(hr_{18}-13.5) \quad (2\text{-}6)$$

where:

| | | |
|---|---|---|
| $T_d$ | = | pavement temperature at depth d, °C |
| IR | = | infrared surface temperature, °C |
| log | = | base 10 logarithm |
| d | = | depth at which mat temperature is to be predicted, mm |
| 1-day | = | average air temperature the day before testing |
| sin | = | sine function on an 18-hr clock system, with $2\pi$ radians equal to one 18-hr cycle |

$hr_{18}$ = time of day on a 24-hr clock system, but calculated using an 18-hr asphalt concrete (AC)

This new BELLS temperature prediction model became more practical by employing more easily obtainable variables such as the previous 1-day average air temperature instead of 5-day average air temperature. The model covered a wide geographical area since it used the largest and most diverse set of data from the FHWA LTPP program's SMP

The BELLS2 model was also used for temperature adjustment of backcalculated asphalt moduli. The semi-logarithmic format of the equation relating the asphalt modulus to the mid-depth asphalt temperature allows for a simple means of adjusting the backcalculated asphalt modulus for the effects of temperature. The approach is to calculate a modulus temperature adjustment factor using the following equation:

$$ATAF = 10^{slope*(T_r - T_m)} \quad (2\text{-}7)$$

Where:

$ATAF$ = asphalt temperature adjustment factor
$Slope$ = slope of the log modulus versus temperature equation (-0.0195 for the wheelpath and –0.021 for mid-lane are recommended)
$T_r$ = reference mid-depth hot-mix asphalt (HMA) temperature
$T_m$ = mid-depth HMA temperature at time of measurement

### 2.2.4 LTPP AC Pavement Temperature Models

Mohseni and Symons (1998; 1998a) presented improved LTPP low and high temperature models using the LTPP seasonal data.

The improved LTPP low temperature model is

$$T_{pav} = -1.56+0.72\,T_{air} - 0.004\,Lat^2 + 6.26\log_{10}(H+25) - z(4.4+0.52\,\sigma^2_{air})^{1/2} \quad (2\text{-}8)$$

where:

$T_{pav}$ = low AC pavement temperature below surface, °C,
$T_{air}$ = mean low air temperature, °C,
Lat = latitude of the section, degrees,
H = depth to surface, mm
$\sigma_{air}$ = standard deviation of the mean low air temperature, °C,
z = from the standard normal distribution table, z=2.055 for 98% reliability

The improved LTPP high temperature model is

$$T_{pav} = 54.32+0.78\ T_{air} - 0.0025\ Lat^2 - 15.14\ \log_{10}(H+25) - z(9+0.61\ \sigma^2_{air})^{1/2} \qquad (2\text{-}9)$$

where:

$T_{pav}$ = high AC pavement temperature below surface, °C,
$T_{air}$ = high 7-day mean air temperature, °C,
Lat = latitude of the section, degrees,
H = depth to surface, mm
$\sigma_{air}$ = standard deviation of the high 7-day mean air temperature, °C,
z = from the standard normal distribution table, z=2.055 for 98% reliability

### 2.2.5 Asphalt Institute (AI) Model

In order to account for the effect of temperature on moduli of asphalt mixtures, the relationship between mean pavement temperature, $M_p$, and mean monthly air temperature, $M_a$, based on the depth below the pavement surface was developed and implemented in the DAMA computer program (Hwang and Witczak, 1979).

$$M_p = M_a(1+\frac{1}{z+4}) - \frac{34}{z+4} + 6 \qquad (2\text{-}10)$$

where:

z = depth below surface, inches.

The temperature at the upper third point of each layer is used as the weighted average pavement temperature.

### 2.2.6 Temperature Prediction Model Based on Heat Transfer Theories and Correction Procedure

Shao et al. (1997) developed an asphalt pavement subsurface temperature prediction procedure which was based on heat transfer theories and used the surface temperature history from the previous morning. It consisted of three major steps:

1. Predicting yesterday's maximum and today's early morning minimum pavement surface temperatures on the basis of the maximum and minimum air temperature and weather conditions.
2. Generating the surface temperature history from yesterday morning to today's first temperature measurement.
3. Estimating AC layer mid-depth temperature as a function of the surface temperature history using heat conduction theory; the solution to a one-dimensional heat conduction problem is as follows:

$$T(x,t) = T_o erf(\frac{x}{2\sqrt{\alpha t}}) + \sum_{i=1}^{n} \left\{ \left[ \begin{array}{l} (A_i + B_i t) erfc(X_i) \\ + 2B_i (t - t_i)(X_i^2 erfc(X_i) - \frac{X_i}{\sqrt{\pi}} e^{-X_i^2}) \end{array} \right] - \left[ \begin{array}{l} (A_i + B_i t) erfc(X_{i+1}) \\ + 2B_i (t - t_{i+1})(X_{i+1}^2 erfc(X_{i+1}) - \frac{X_{i+1}}{\sqrt{\pi}} e^{-X_{i+1}^2}) \end{array} \right] \right\} \quad (2\text{-}11)$$

where

| | | |
|---|---|---|
| $T(x, t)$ | = | predicted temperature at a certain depth of AC, $x$, and a current time, $t$, |
| $T_o$ | = | constant (the initial temperature distribution) |
| $t$ | = | current time |
| $x$ | = | the mid-depth length of AC |
| $\alpha$ | = | the thermal diffusivity ($m^2$/sec or $m^2$/hr) |
| $T_i$ | = | measured surface temperature at the corresponding time $t_i$ |

$$B_i = \frac{T_{i+1} - T_i}{t_{i+1} - t_i} \quad \text{(no sum on i; i = 1,2,...,n)}$$

$$A_i = T_i - B_i(t_i - t_1) \quad \text{(no sum on i; i = 1,2,...,n)}$$

$$X_i = \frac{x}{2\sqrt{\alpha(t - t_i)}}$$

$$X_{i+1} = \frac{x}{2\sqrt{\alpha(t - t_{i+1})}}$$

$$erf(X) = \frac{2}{\sqrt{\pi}} \int_0^X e^{-\xi^2} d\xi \quad \text{error function, and}$$

$$erfc(X) = \frac{2}{\sqrt{\pi}} \int_X^\infty e^{-\xi^2} d\xi \quad \text{complementary error function.}$$

Based on mid-depth temperatures, correction factors were obtained as follows (Kim et al., 1996):

$$\lambda_E = 10^{m(T-To)} \tag{2-12}$$

where:

$\lambda_E$ = correction factor
m = regression constant; statewide m-value is 0.0262.
T = effective temperature at the time of the FWD testing
To = reference temperature such as 25 °C

### 2.2.7 Temperature Correction Procedure Based on the Theory of Linear Viscoelasticity

Park and Kim (1997) analytically developed a correction model based on the theory of linear viscoelasticity and the time-temperature superposition principle. The model is based on a simple temperature -modulus correction factor:

$$\lambda_E = E_{T0} / E_T \tag{2-13}$$

where:

$\lambda_\varepsilon$ = temperature-modulus correction factor,

$E_{T_0}$ = corrected modulus at temperature $T_0$,
$E_T$ = backcalculated modulus of the AC from deflections at temperature T

The theoretical correction factor is defined in Equation (2-13), and the relaxation modulus $E(\xi)$ and the time-temperature shift factor $a_T(T)$ for the asphalt mixture are defined follows:

$$\lambda_E = E(\xi_0) / E(\xi) \tag{2-14}$$

where the reduced times $\xi_0$ and $\xi$ are defined, respectively, by

$$\xi_0 = t_1 / a_T(T_0) \quad \text{and} \quad \xi = t_1 / a_T(T) \tag{2-15}$$

in which $t_1$ is the loading duration. In this correction procedure, viscoelastic properties of the AC layer were applied to the correction factor model. However, it is questionable whether it works at low temperatures because AC behaves elastically at low temperatures rather than viscoelastically.

### 2.2.8 Other Temperature Correction Methods for AC Moduli

Johnson and Baus (1992) suggested that the following formula which is based on the work done by Lytton et al. (1990) who took an approximation from the Asphalt Institute (1982):

$$\lambda_E = 10^{-0.0002175(70^{1.886} - T^{1.886})} \tag{2-16}$$

where:

$\lambda_E$ = correction factor
T = temperature at the time of the FWD testing, °F

Ullidtz (1987) developed a model based on backcalculated moduli from AASHO Road Test deflection data. The correction model is as follows:

$$\lambda_E = \frac{1}{3.177 - 1.673 \log T} \tag{2-17}$$

for T>1 °C.

### 2.2.9 Climatic Model

The climatic-material-structures model (CMS model) was developed by Dempsey et al., 1985. In the case of flexible pavements, it is generally assumed that the stiffness of the AC layer depends on pavement temperature, while unbound materials such as granular bases and subgrades depend on moisture content. This climatic model which was used to analyze flexible pavements simulates climatic conditions that control temperature and moisture conditions in the pavement layers and in the subgrade. It used sunshine percentage, windspeed, air temperature and solar radiation to compute the heat flux boundary condition on the roadway surface and the resulting temperature profile throughout the asphalt pavement. A subroutine computes accompanying changes in asphalt stiffness, resilient modulus and Poisson's ratio of the base, subbase and subgrade with time. Input of material properties, pavement geometry, pavement infiltration parameters, and many other data are required.

### 2.2.10 Summary of the Existing Temperature Prediction Models

All the models summarized in this chapter have advantages and disadvantages. Predictions of some models such as the BELLS model and the heat transfer theory based model are accurate. However, they require various input variables, or the prediction procedures are rather complex, which make them impractical in the field. For example, heat transfer theory based prediction is very reliable; prediction deviations are within ±2

°C. On the other hand, it needs many input variables and a computer program due to the iterative procedure. To obtain a previous mean 5-day air temperature in every routine test is not practical. Relatively simple (statistical) models reduce the accuracy or do not account for temperature gradient effects due to diurnal heating and cooling cycles (e.g., AI model) although the AI model is capable of accounting for monthly temperature variations.

## 2.3 APPLICATIONS TO THE FIELD/PAVEMENT DESIGN

In a mechanistic-empirical (M-E) flexible pavement design procedure, the two most critical components are structural models and transfer functions (Thompson, 1995). Development of structural models and/or a mechanistic analysis procedure is a major task in M-E pavement design. The measured deflections from a FWD are commonly used along with loading and pavement layer thickness information as input to backcalculation programs to compute a modulus for each layer of the pavement structure. The pavement layer moduli are then used in a forward calculation routine to estimate the stress/strain distributions in each of the pavement layers under expected traffic volumes and loadings. Transfer functions (distress models) relate these pavement responses to pavement performance as measured by the type and severity of distress (rutting, fatigue cracking, and so on). For flexible pavements, it is common practice to relate the horizontal strain at the bottom of the AC layer to the number of applications of that strain level to cause failure in cracking (Bonnaure et al., 1980; Buch et al., 1999; Thompson, 1987). Similarly, the vertical strain at the top of the subgrade is related to permanent deformation (rutting) (Buch et al., 1999; Kenis, 1977; Owusu-Antwi, 1998). These transfer functions are quite

sensitive to small changes in strain levels (Briggs and Lukanen, 2000). Therefore, it is crucial to accurately determine the effective (pavement) temperature and adjust the moduli to the reference/standard temperature because the stress/strain distribution in the pavement structure is dependent on the stiffness or moduli of each of the pavement layers, and the stiffness of the AC layer varies with pavement temperature.

# CHAPTER 3

# LITERATURE REVIEW II – OVERVIEW OF THEORETICAL ANALYSIS OF FLEXIBLE PAVEMENTS

## 3.1 INTRODUCTION OF VISCOELASTICITY TO THE FLEXIBLE PAVEMENT ANALYSIS

The structural analysis of layered systems such as layered soil deposits and pavements have long been pursued by many geotechnical and pavement engineers. Based on Love's stress function (Love, 1927) and a Bessel function expansion of the load applied on a finite boundary surface, Burmister (1943, 1945) developed solutions for a two-and three-layer systems. Using Burmister's analytical solutions, afterwards, tabular and graphical summaries of stresses and displacements in two- and three-layer systems for various combinations of geometrical and material parameters were presented (Acum and Fox, 1951; Jones, 1962; Peattie, 1962; Huang, 1969).

Due to their relatively simple analysis, many finite element programs and methods of pavement analysis for mechanistic pavement design rely on elastic analysis, for example, of layered systems in the *Shell Pavement Design Manual*. Design to limit permanent deformation is often related to vertical elastic strain on the top of the AC/subgrade layer(s). Similarly, fatigue cracking for design criterion is related to tensile strain at the bottom of the AC layer. The use of elastic analysis methods alone has limitations and can result in incorrect characterization of pavement performance unless material temperatures as well as loading time are specified (Lu and Wright, 2000).

Huhtala et al. (1990) reported strains measured under moving wheel loads in a test track. Yun and Chatti (1996) compared viscoelastic and dynamic responses obtained by a moving load solution very well with field data. It was observed that, in the longitudinal direction, compressive strains occur which are followed by a tensile peak and then compressive strains again, whereas, in the transverse direction, the strain is all tensile. Viscoelastic responses led to asymmetric strain pulses, but elastic analysis predicted symmetric strain pulses (Huhtala et al., 1992; Nilsson et al., 1996). Good agreement was found between the measured deflections and computed deflections by using viscoelastic analysis (Uddin, 1998). It has been reported that the resilient modulus of asphalt mixtures is very sensitive to pavement temperature. It was also estimated that the difference in asphalt mixture stiffness on the top and bottom of the AC layer can be as high as a factor of 4 if temperatures at the top and bottom are 44 and 30 °C, respectively (Van de Loo, 1978). Brown and Snaith (1978) found that strain of asphalt mixture is much more sensitive to the variation of experiment temperature than to the change of loading magnitude.

Hence, many researchers have considered the viscoelastic analysis in flexible pavements. Perloff and Moavenzadeh, (1967) studied the surface deflection of homogeneous viscoelastic halfspace under moving loads. Stresses and displacements in viscoelastic multi-layer systems were also investigated (Chou and Larew, 1969; Elliot and Moavenzadeh, 1971; Huang, 1973). In order to predict the structural responses of layered viscoelastic systems and the integrity of flexible pavement, a computer program named VESYS (Kenis, 1977 and 1978), was developed by the Federal Highway Administration. Huang (1993) also presented a computerized procedure for the analysis

of linear elastic, nonlinear elastic, and/or viscoelastic layer systems. Kim et al. (1996) developed a procedure for the analysis of stresses and displacements in a viscoelastic layered system subjected to transient loading and transient and spatially homogeneous temperature conditions. They used the viscoelastic solutions through a linear convolution integral of the unit response functions and the time rate of loading and the existing elastic solutions to determine the unit response functions for the corresponding viscoelastic problem.

Subsequent sections of this chapter briefly review the viscoelastic characterization of the AC layer and the axisymmetric finite element model and the subgrade characterization typically used for the analysis of flexible pavement. The final section addresses how this analytical evaluation can be used in the field.

## 3.2 VISCOELASTICITY

The mechanical behavior of elastic materials is independent of loading time and temperature and obeys *Hooke's law*: the stress is proportional to the strain. On the other hand the behavior of viscoelastic materials is that the response to an applied stress or strain depends upon the rate or time period of loading. For linear viscoelastic materials, the uniaxial stress-strain relationship can be expressed by

$$\sigma(t) = \int_0^t E(t-\tau)\frac{d\varepsilon(\tau)}{d\tau}d\tau \qquad (3\text{-}1)$$

where $\sigma(t)$ is the stress at time t, E(t) is the uniaxial relaxation modulus, and $\varepsilon(t)$ is the strain at time t.

The relaxation modulus can be obtained from a one-step strain test.

If $\varepsilon(t)$ is a step function:

$$\varepsilon(t) = 0 \quad \text{if } t \leq 0, \tag{3-2}$$

$$\varepsilon(t) = \varepsilon_0 \quad \text{if } t > 0, \tag{3-3}$$

where $\varepsilon(t)$ is strain at time t, and $\varepsilon_0$ is constant.

Then, the relaxation modulus is obtained as follows:

$$E(t) = \frac{\sigma(t)}{\varepsilon_0} \tag{3-4}$$

Similarly, under a constant stress $\sigma_0$, the creep compliance, D(t), is defined as

$$D(t) = \frac{\varepsilon(t)}{\sigma_0} \tag{3-5}$$

In general, the mechanical property of viscoelastic materials depends not only on loading time but also on temperature. Especially some of the mechanical properties of amorphous polymers have a strong dependence upon temperature. There exists a special class of viscoelastic materials whose temperature dependence of mechanical properties is amenable to analytical description. This class is referred to as being thermorheologically simple materials. The simplifying feature of the thermorheologically simple materials is that, when the unit response function (e.g., creep compliance or relaxation modulus) curve measured at different constant temperatures are all plotted against time on a logarithmic scale, the curves can be superposed so as to form a single curve, defined as a master curve, corresponding to an arbitrary fixed temperature (i.e. reference temperature) by means of horizontal translation only. This makes it possible to cover times outside the range that is not easily accessible by practical experiments. The horizontal distance (representing the shift factor, $a_T$) between the master curve and any one of the isothermal curves is independent of time.

This feature has a very significant consequence in that the dependence of the material property upon both time and temperature can be represented by dependence upon a single variable called reduced time, and the feature is often referred to as time-temperature superposition or reduced-time methods. For example, the uniaxial relaxation modulus in mathematical notation is expressed as:

$$E(t, T) = E_M(t_r) \tag{3-6}$$

where $E_M(t_r)$ is the master relaxation modulus corresponding to a reference temperature ($T_R$), and for constant temperature,

$$t_r = \frac{t}{a_T} \tag{3-7}$$

where $t_r$ and $a_T$ are the reduced time and the time-temperature shift factor, respectively. The $a_T$ is a temperature dependent material function that reflects the influence of temperature on internal viscosity of the material. One may obtain the relaxation modulus E(t,T) if the master relaxation modulus $E_M(t_r)$ and the shift factor $a_T(T)$ are given; or, conversely, one may obtain $E_M(t_r)$ when E(t,T) and $a_T(T)$ are given.

The method of relating the horizontal shifts along log time scale to temperature changes was developed by Williams, Landel, and Ferry so called the WLF equation as shown in Equation 3-8. For temperature above the glass transition temperature of the material, the shift factor $a_T$ for thermorheologically simple materials is usually expressed in the following form:

$$\log a_T = -\frac{c_1(T - T_r)}{c_2 + (T - T_r)} \tag{3-8}$$

where $a_T$ is the shift factor, $c_1$ and $c_2$ are constants, and $T_r$ is the reference temperature.

The constants, $c_1$ and $c_2$, can be obtained by plotting $(T-T_r)$ against $(T-T_r)/\log a_T$. The slope and the intercept of the plotted line are $-c_1$ and $-c_2$, respectively.

By Equations 3-6 and 3-7, the uniaxial stress-strain relationship of Equation 3-1 at a given time, t, and a given temperature T can be rewritten as

$$\sigma(t) = \int_0^t E(\frac{t-\tau}{a_T})\frac{d\varepsilon(\tau)}{d\tau}d\tau \tag{3-9}$$

where $\sigma(t)$ is the stress at time t and temperature T, $E(t_r)$ is the uniaxial relaxation modulus which becomes a temperature independent relaxation modulus of a temperature dependent "reduced time", and $\varepsilon(t)$ is the strain at time t.

(Young et al., 1991; Sperling, 1993; Kim et al., 1996)

## 3.3 AXISYMMETRIC FINITE ELEMENT ANALYSIS

Solids and shells whose geometry is axisymmetric (bodies of revolution), which have material properties and loads that also are axially symmetric, can be modeled using cylindrical coordinates r, $\theta$, and z. With these assumptions, a three dimensional problem can be reduced to a two dimensional one. However, flexible pavements must be assumed to be continuous (no cracks) and infinitely wide. Therefore the edge (shoulder) effect cannot be considered.

In an axisymmetric state of stress, only four stress components, $\sigma_r$, $\sigma_\theta$, $\sigma_z$, and $\tau_{zr}$, are non-zero (Figure 3-1). The major and minor principal stresses along the axis of symmetry (r=0) coincide with either $\sigma_r$ ($=\sigma_\theta$) or $\sigma_z$ depending on the vertical position z. Cook (1989) formulates the plane linear isoparametric element which can be revised to obtain the axisymmetric element. The global coordinates (radial and vertical), and the

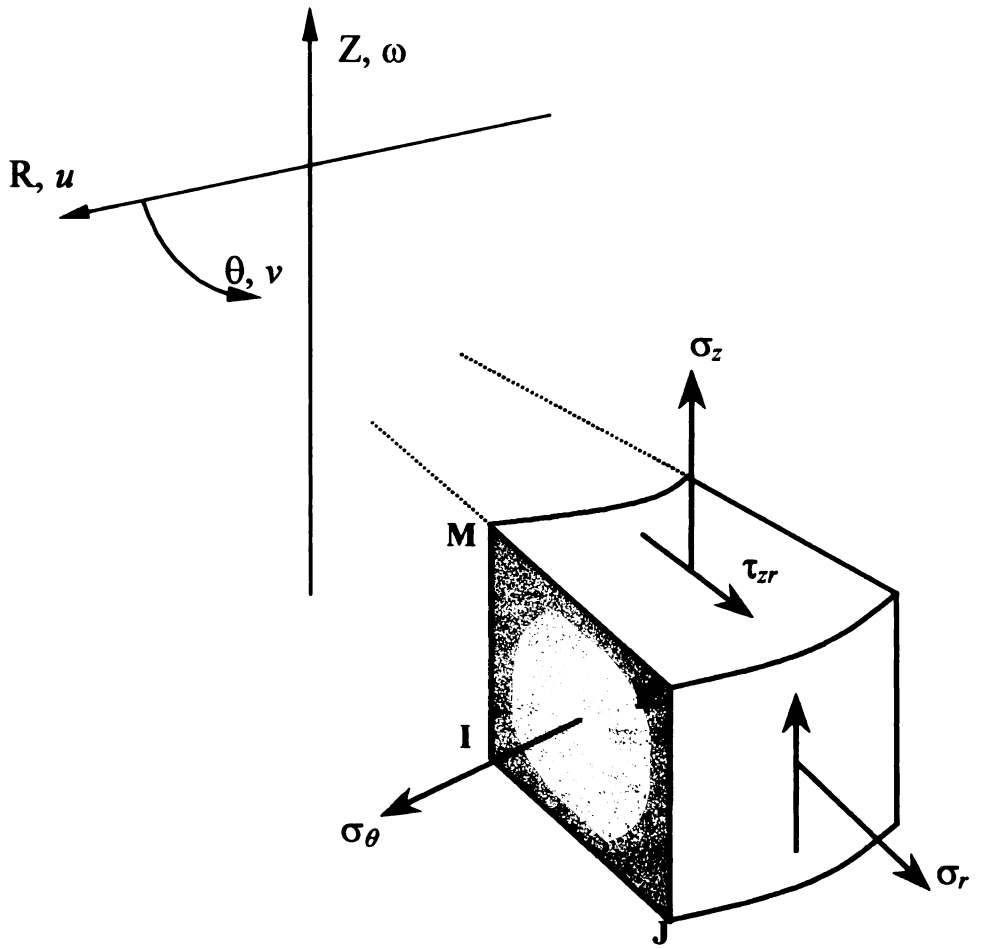


(a) isometric view

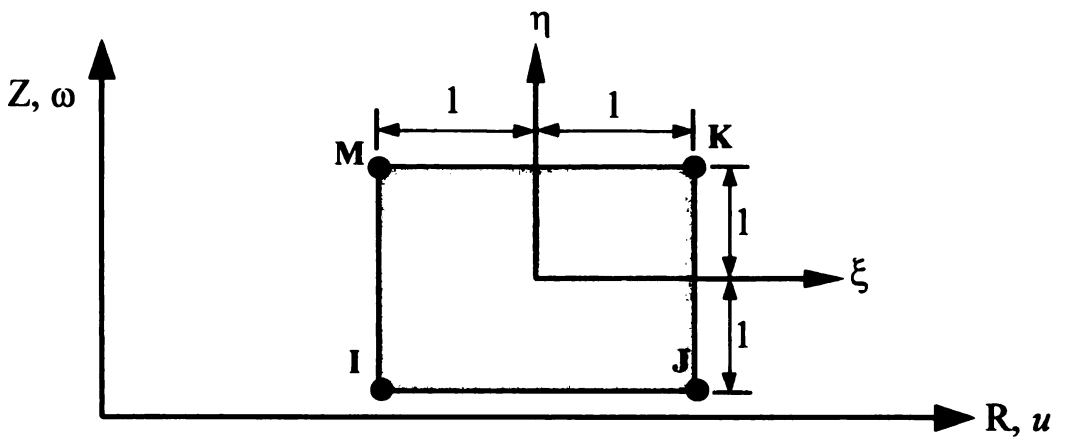


(b) the four-node isoparametric element

Figure 3-1. A typical axisymmetric finite element

corresponding displacements at an internal point can be related to the corresponding nodal quantities through shape functions:

$$\begin{Bmatrix} u \\ w \end{Bmatrix} = \begin{bmatrix} N_i & 0 & N_j & 0 & N_k & 0 & N_m & 0 \\ 0 & N_i & 0 & N_j & 0 & N_k & 0 & N_m \end{bmatrix} \begin{Bmatrix} u_i \\ w_i \\ u_j \\ \vdots \\ w_m \end{Bmatrix} \tag{3-10}$$

where the individual shape functions are

$$N_I = \frac{(1 \pm \xi)(1 \pm \eta)}{4}, \qquad \text{where I = i, j, k, m}$$

(Cook et al., 1989)

## 3.4 3-D HEXAHEDERAL AND TRIANGULAR ISOPARAMETRIC ELEMENTS

3-D hexahederal (brick) and triangular elements are rarely used in pavement analysis because 2-D axisymmetric elements usually produce satisfactorily accurate results with greater economy. However, 3-D elements may still be appropriate to investigate the complicated interactions among environmental factors, nonuniform loads and pavement layers which are not necessarily treated appropriately by 2-D elements. As long as the mesh is properly designed, reliable and valuable results are produced from the 3-D model.

In three dimensions, the isoparametric procedure is similar to the 2-D development. For brick element geometry and the field quantity $\phi$ of a solid

isoparametric element, $x$, $y$, and $z$ are coordinates interpolated from nodal values of $x_i$, $y_i$, and $z_i$:

$$x = \Sigma N_i x_i, \quad y = \Sigma N_i y_i, \quad z = \Sigma N_i z_i, \quad \phi = \Sigma N_i \phi_i, \tag{3-11}$$

where $i$ ranges over the number of nodes in the element. Shape functions $N_i$ are functions of isoparametric coordinates $\xi$, $\eta$, and $\zeta$. Similarly, for triangular element:

$$x = \Sigma N_i x_i, \quad y = \Sigma N_i y_i, \quad \phi = \Sigma N_i \phi_i, \tag{3-12}$$

(Cook et al., 1989)

## 3.5 SUBGRADE CHARACTERIZATION

In order to mechanically or mathematically model the particular characteristics of soil behavior, the linear elastic idealization is usually adopted. The Winkler and elastic solid foundations are the most commonly used linear foundation models. In the analysis of this study, the subgrade is characterized as an elastic solid foundation.

### 3.5.1 Winkler Foundation

The Winkler foundation model represents soil as closely spaced linear elastic springs (Winkler, 1867) (Figure 3-2 (a)). The Winkler foundation was first applied in the pavement field in order to determine the critical stresses in an infinitely large concrete slab under a single load for three cases of loadings: corner, edge, and interior (Westergaard, 1926). Since the Winkler foundation models the subgrade with only one support, k, and is capable of modelling edge or corner loading more realistically than the elastic solid model, it was commonly used in concrete pavement analysis.

### 3.5.2 Elastic Solid Foundation

The elastic solid foundation is another well-known model for pavement support. This is ideal for cases where there is no joints or cracks, and for a single uniform slab thickness and subgrade support. Hence, it is widely used for flexible pavement modeling. The soil is modeled as a linear elastic, isotropic, homogeneous solid. The elastic solid model may be more realistic than the Winkler foundation in some aspects since real subgrade supports experiences shear stresses to some extent. The significant difference between an elastic solid foundation and the Winkler foundation is shown in Figure 3-2.

## 3.6 APPLICATIONS OF STRUCTURAL ANALYSIS TO THE FIELD

As pointed out in the previous chapter, the estimated stress/strain distributions for each layer of the pavement structure are related to pavement performance by transfer functions (distress model), and this is a major task in mechanistic-empirical (M-E) pavement design.

The structural analyses based on viscoelasticity can be also related to the design and/or performance evaluation. Some applications of the viscoelastic analysis to the field were reviewed in the earlier section. Besides them, recently, Rowe et al. (1995 and 1997) and Collop et al. (1995) presented viscoelastic approaches to fatigue cracking/rutting.

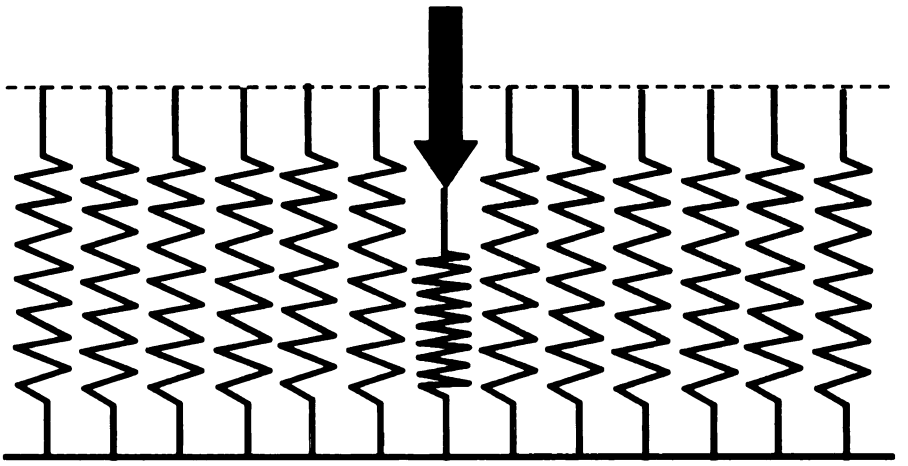

(a) Winkler Foundation

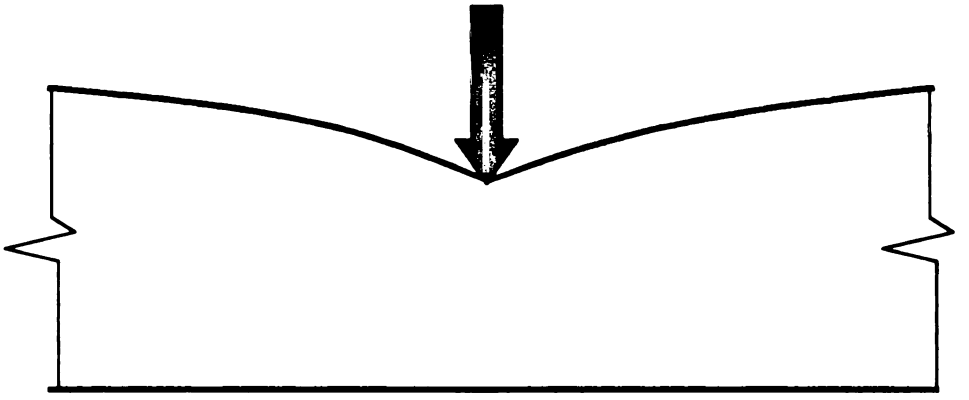

(b) Elastic Solid Foundation

Figure 3-2. Comparison of Winkler Foundation with Elastic Solid Foundation (After Tabatabaie-Raissi, 1977)

Rowe et al. predicted fatigue performance by considering the energy dissipated (work done) in asphaltic materials under loading with the damage being proportional to the cumulative dissipated energy. The calculation of the fatigue life was proposed in the previous work as follows (Rowe, 1993):

$$N1 = 205 \times Vb^{6.44} \times w_o^{-2.01} \times \Psi_{N1}^{1.64} \qquad (3\text{-}13)$$

where:

| | | |
|---|---|---|
| N1 | = | number of load cycles to "crack initiation" |
| Vb | = | volume of binder (%) |
| $w_o$ | = | dissipated energy per cycle at start of test ($J/m^2$) |
| $\Psi_{N1}$ | = | work ratio, calculated from the initial complex modulus and phase angle and input into the statistical analysis as a calculated parameter. |

This dissipated energy fatigue criterion replaced the "(tensile) strain criterion" currently used for fatigue damage.

Lee et al. (1998) investigated a mechanistic approach to uniaxial viscoelastic constitutive modeling of asphalt concrete that accounts for damage evolution under cyclic loading conditions. The constitutive equation developed from the controlled-strain fatigue tests satisfactorily predicted the stress-strain behavior of asphalt concrete all the way up to failure under the controlled-stress mode as well as under the monotonic loading with varying strain rates. Uddin (1998) also found good agreement between the measured field deflections and computed deflections by viscoelastic analysis (Figure 3-3).

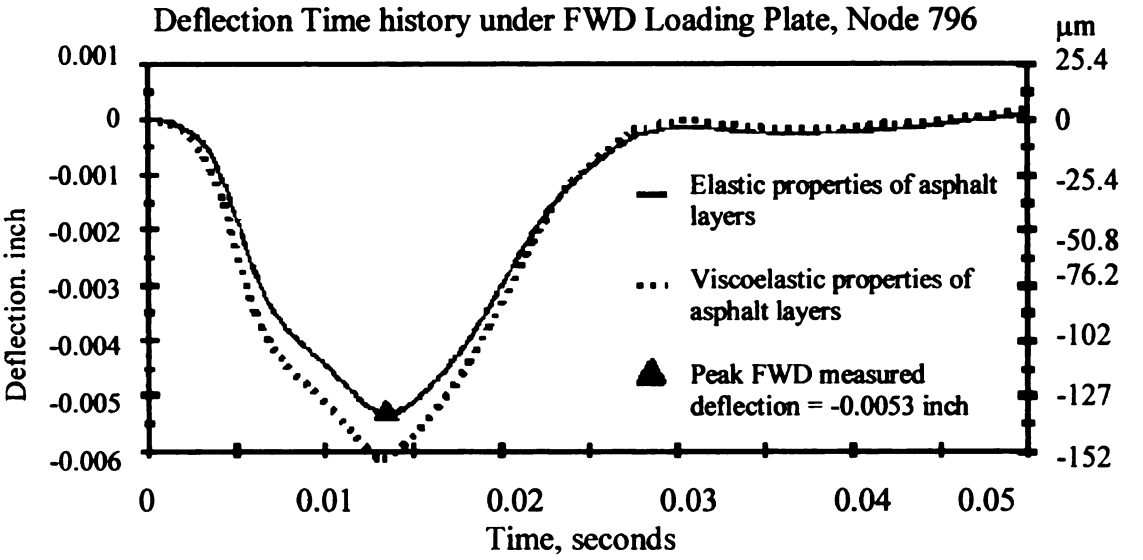


Figure 3-3. Deflection-time history plot of computed dynamic deflection bowl under the FWD loading plate using viscoelastic parameters for asphalt layers (Uddin, 1998)

## 3.7 SURFACE-INITIATED CRACKING

It has been reported that surface-initiated cracking had become more prevalent in recent years (CROW, 1990; Myers et al., 1998; Uhlmeyer et al., 2000). Figures 3-4 and 3-5 show surface-initiated longitudinal wheel path cracks and core with surface-initiated longitudinal wheel path cracks, respectively. However, the mechanism for this type of failure has not been clearly identified.

Gerritsen et al. (1987) concluded that both thermal and load related effects caused the surface initiated cracks that did not extend into the lower bituminous base layers. Dauzats et al. (1987) noted that surface cracking were initially caused by thermal stresses and then further propagated by traffic loads, and a rapid hardening of the mix binder likely contributed to this type of cracks. Nunn (1998) suggested from field observations

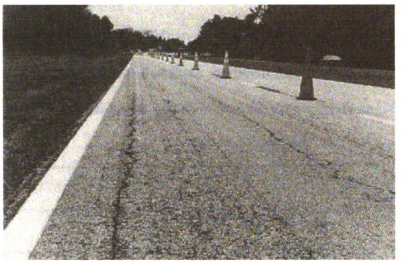

Figure 3-4. Overview of surface-initiated longitudinal wheel path cracks (Myers et al., 1998)

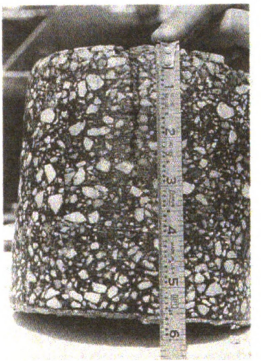

Figure 3-5. Core showing surface-initiated longitudinal wheel path cracks (Myers et al., 1998)

that a very different failure mechanism occurs at the "breakpoint" thickness, and the cracks propagated from the top of the pavement surface downward for full depth cracks in thinner pavements. Recently, Uhlmeyer et al. (2000) reported field observations in Washington State. They claimed that these top-down cracks were typically longitudinal, appeared in or near the wheelpaths, and decreased in width with depth.

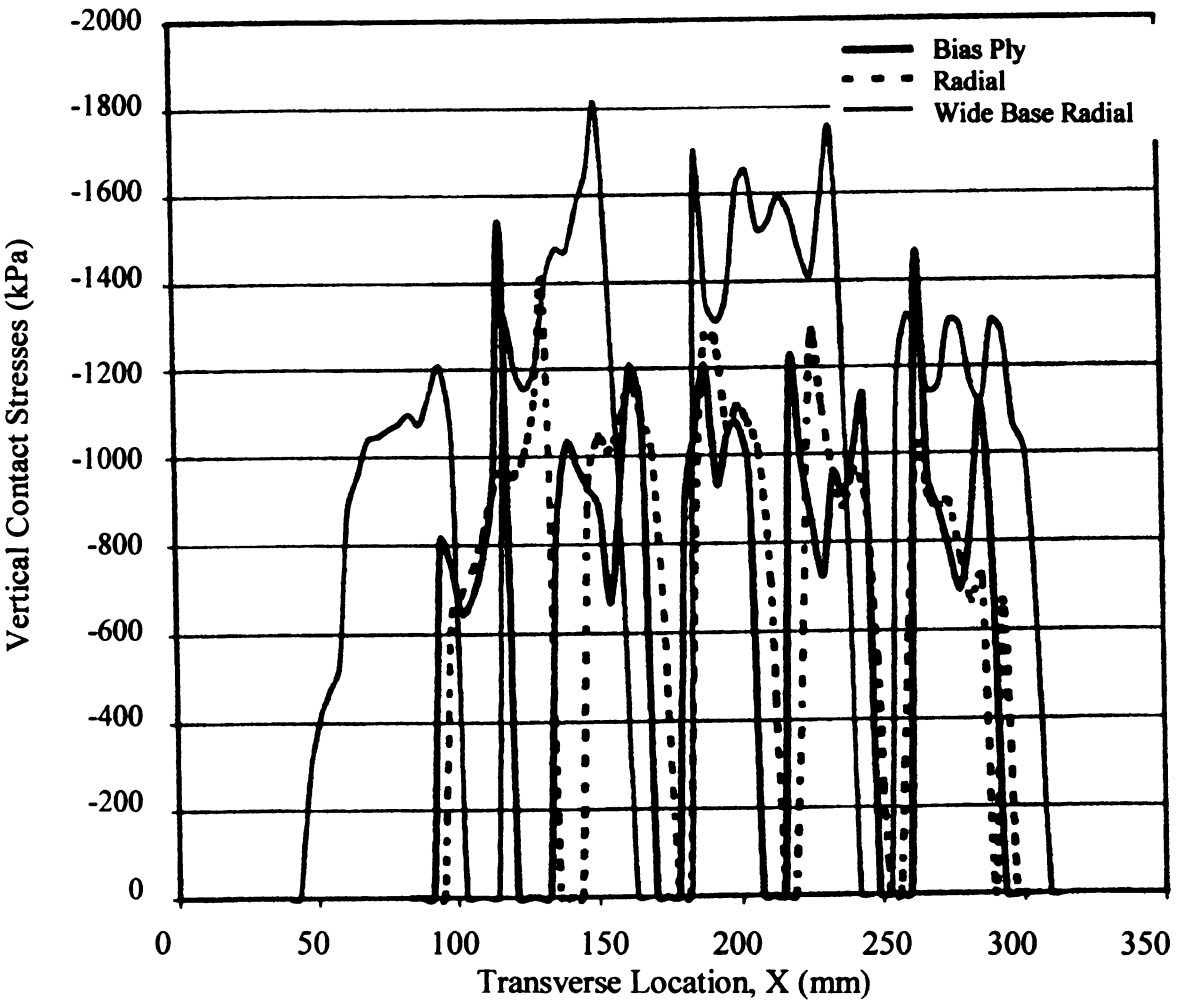


Figure 3-6. Vertical contact stresses measured for bias ply, radial, and wide-base radial tires at appropriate rated load and inflation pressure (Myers et al., 1999)

It should be noted that the predominant tire used by trucks on the roads today is the radial over the bias ply tire. This is due to their increased load carrying capacity,

better traction, handling, and fuel efficiency (Myers et al., 1998). The main structural differences between the radial and bias ply tires are that radial tires have a more flexible wall and rigid tread structure. Figure 3-6 shows the vertical stress distribution across the tire for three tire treads: bias ply, radial, and wide base radial (Myers et al., 1999). Himeno et al. (1997) and de Beer et al (1997) presented measurements of tire forces that were non-uniform contact pressures. Numerous researchers investigated the effects of nonuniform vertical stress distributions on pavement performance (Marshek et at., 1986; Marshek et at., 1986a; Chen et al.,1986). However, their work was limited to the effects of stresses and strains at the bottom of the AC layer. Myers et al. (1998) investigated the effects of tire treads and combination of vertical and lateral tire-pavement interface stresses and concluded that tensile stresses under the treads of tire were the primarily cause of the cracks.

# CHAPTER 4

# DATA COLLECTION – TEMPERARTURE PREDICTION MODEL AND CORRECTION FACTOR

## 4.1 TEST SITES AND DATA COLLECTION

The objective of this study was to (a) develop a model to predict effective temperature of the AC layer at any depth based on field data, and (b) adjust the backcalculated modulus to a reference temperature using the predicted effective AC layer temperature and modulus correction factors.

Six in-service Michigan flexible pavement sites were selected in 1997, 1998, and 1999. The inventory data for the Michigan sections is summarized in Table 4-1 and the data from the special pavement studies (SPS-1) is summarized in Table 4-2. All the Michigan test sites were instrumented with temperature sensors connected to a OM-220 Portable Data Logger (Omega Engineering, INC).

In order to profile the temperature gradient, test holes (approximately 2.5 cm in diameter) were drilled and partially filled with a viscous fluid (mineral oil). A digital thermometer probe was inserted, and temperature readings were recorded at 30 minute intervals. Figure 4-1 shows a schematic of the manual temperature measurement layout.

MDOT's KUAB FWD was used to determine the deflection basins. In order to investigate temperature effects on deflections and backcalculated AC moduli and develop correction factors, deflection and temperature data were collected simultaneously from the FWD and sensors/thermocouples. These tests were conducted throughout the day.

Table 4-1. Test Site Location and Inventory Data

| Site No. | Location | Cross-Section | | | Sensor for Air Temperature | Sensor for Surface Temperature | Depth of Mid-range Sensor (cm) | Depth of Bottom Sensor (cm) | Manually Measured Depth (Hole Depth) (cm) |
|---|---|---|---|---|---|---|---|---|---|
| | | AC (cm) | Base (cm) | Sub-base (cm) | | | | | |
| 25 | Route: I-94 WB; New Buffalo, MI | 25.9 | 15.2 | | Available | Available | 17.8 | 25.4 | 7.6, 13.0 |
| 45 | Route: M-37 NB; Traverse City, MI | 14.0 | 25.4 | 40.6 | Available | Available | 14.0 | 25.4 | 5.7, 12.7 |
| 69* | Route: US-2 EB; Brevort, MI | 14.0 | 20.3 | | Available | Available | 12.7 | 25.4 | |
| 88 | Route: M-28 WB; Deerton, MI | 17.8 | 50.8 | | Available | Not Available | 16.5 | 36.8 | 6.4, 8.9, 16.5 |

*Data from this site used for validation.



Table 4-2. Location of SPS1 and SMP Sections, Sensor Location, and Pavement Cross-Section Data

| | Section ID | Location | Sensor Location (cm) | Cross-Section | | |
|---|---|---|---|---|---|---|
| | | | | AC (cm) | Base (cm) | Subbase (cm) |
| SPS 1 Site | K24 | St. Johns, MI | 5.1, 8.9, 13.3* | 17.8 | 30.5 | 10.2 |
| | K59 | St. Johns, MI | 4.4, 8.3, 12.7* | 16.5 | 20.3 | 61.0 |
| SMP Site | 8-1053-1 | County: Delta, CO | 1.3, 6.1, 10.9 | 11.7 | 11.4 | 59.7 |
| | 9-1803-1 | County: New London, CT | 2.5, 8.9, 15.3 | 18.3 | 30.5 | |
| | 13-1005-1 | County: Houston, GA | 2.5, 8.4, 14.3 | 19.6 | 23.1 | |
| | 31-0114-1 | County: Thayer, NE | 2.5, 9.9 | 17.0 | 30.5 | 61.0 |
| | 27-6251-1 | County: Beltrami, MN | 2.5, 8.3, 14.0 | 18.8 | 25.9 | |
| | 46-9187-2 | County: Meade, SD | 2.3, 6.5, 10.6 | 15 | 15.2 | 7.6 |
| | 48-1068-1 | County: Lamar, TX | 2.5, 12.8, 23.2 | 27.7 | 15.2 | 20.3 |
| | US281S1 | TX | 1.3, 8.9, 16.5** | 18.42 | 38.1 | |

*Manual operation

**Temperature Data provided by Texas DOT (Chen et al., 2000)

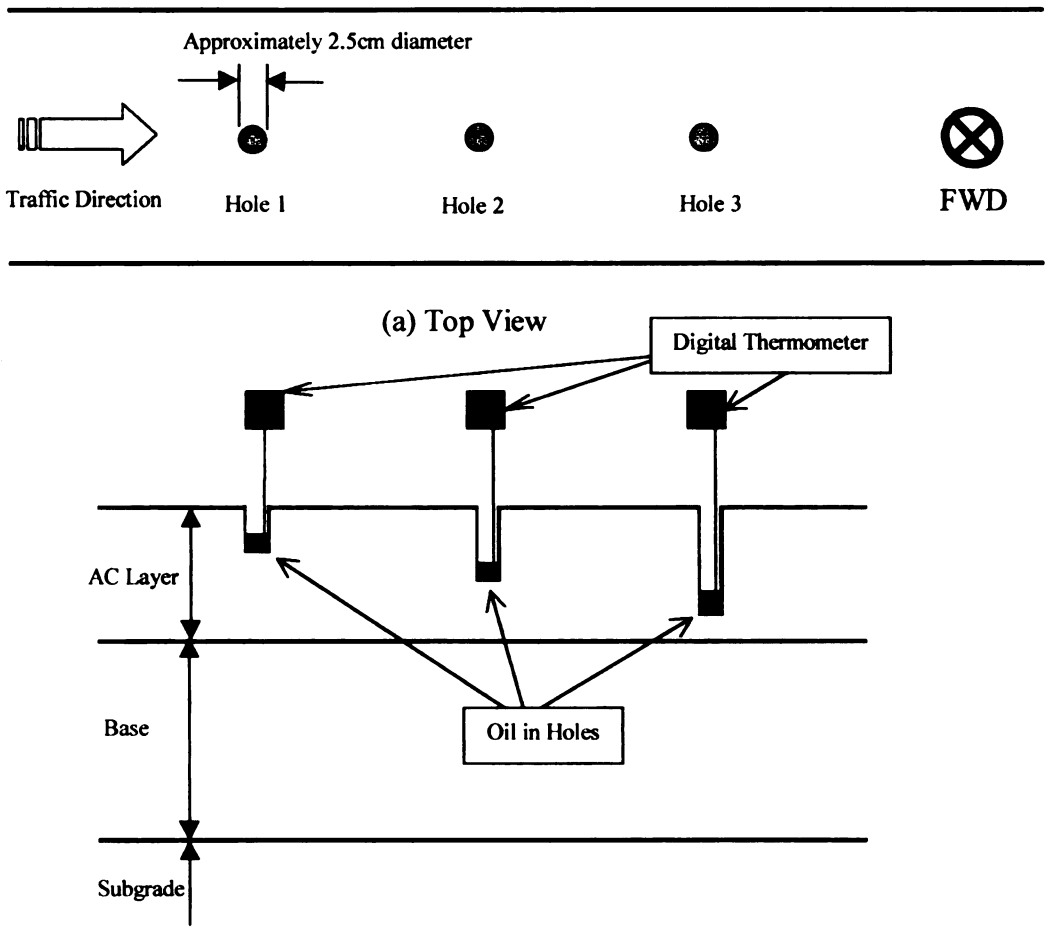


Figure 4-1. Schematic of manual temperature measurements.

## 4.2 TEMPERATURE PREDICTION MODEL AND CORRECTION FACTOR DEVELOPMENT

Data from three of the six test sites (sites 25, 45, 88) were used to develop the temperature prediction model. The model was validated and calibrated using data from site 69 in Brevort, MI, two Special Pavement Studies (SPS1) sites near St. Johns, MI, and eight Seasonal Monitoring Program (SMP) sites in Colorado, Connecticut, Georgia, Nebraska, Minnesota, South Dakota, and Texas. The SMP data was obtained from DATAPAVE 2.0 (1997). Inventory and temperature sensor location information for these sites is summarized in Table 4-2. Data presented by Stubstad et al. (1994) was also used for comparing the newly developed model with other popular models.

Temperature correction factors for backcalculated AC layer moduli of all four test sites (sites 25, 45, 88, 69) and two SPS1 sites were computed based on measured and predicted middepth temperature of the AC layer, using 317 temperature data points and 656 deflection basins (Table 4-3). Table 4-4 summarizes the data from Stubstad et al. (1994), which was used for the validation.

## 4.3 INFLUENCE OF TEMPERATURE PREDICTION ERROR ON PERFORMANCE PREDICTION

For structural (performance prediction) models and/or mechanistic analysis procedure in M-E pavement design, the measured deflections from a FWD are commonly used along with loading and pavement layer thickness information as input to

Table 4-3. (a) Measured Temperature at Site 25 (New Buffalo, MI)

| Time | Measured Temperature | | | | | | | |
|---|---|---|---|---|---|---|---|---|
| | Air | | Surface | | 3" (7.62 cm) | | 5.1" (12.95 cm) | |
| | °C | °F | °C | °F | °C | °F | °C | °F |
| 8:30 AM | 18.0 | 63.9 | 22.0 | 71.1 | 24.5 | 75.6 | 26.0 | 78.2 |
| 9:00 AM | 20.0 | 67.5 | 23.0 | 72.9 | 24.1 | 74.8 | 25.0 | 76.5 |
| 9:30 AM | 21.0 | 69.3 | 23.0 | 72.9 | 24.0 | 74.7 | 24.8 | 76.1 |
| 10:00 AM | 21.0 | 69.3 | 24.0 | 74.7 | 24.3 | 75.2 | 24.8 | 76.0 |
| 10:30 AM | 21.0 | 69.3 | 24.0 | 74.7 | 24.5 | 75.6 | 24.8 | 76.1 |
| 11:00 AM | 22.0 | 71.1 | 24.0 | 74.7 | 24.7 | 75.9 | 24.9 | 76.3 |
| 11:30 AM | 23.0 | 72.9 | 24.0 | 74.7 | 25.0 | 76.5 | 25.1 | 76.6 |
| 1:00 PM | 26.0 | 78.3 | 29.0 | 83.7 | 27.0 | 80.1 | 26.3 | 78.8 |
| 1:30 PM | 25.0 | 76.5 | 29.0 | 83.7 | 27.5 | 81.0 | 26.9 | 79.8 |
| 2:00 PM | 25.0 | 76.5 | 29.0 | 83.7 | 27.9 | 81.7 | 27.2 | 80.3 |
| 2:30 PM | 25.0 | 76.5 | 30.0 | 85.5 | 28.6 | 82.9 | 27.7 | 81.3 |
| 3:00 PM | 27.0 | 80.1 | 34.0 | 92.7 | 30.3 | 86.0 | 28.2 | 82.2 |
| 3:30 PM | 28.0 | 81.9 | 38.0 | 99.9 | 32.0 | 89.1 | 29.5 | 84.5 |
| 4:00 PM | 27.0 | 80.1 | 36.0 | 96.3 | 33.3 | 91.4 | 30.1 | 85.6 |
| 4:30 PM | 27.0 | 80.1 | 38.0 | 99.9 | 34.0 | 92.7 | 31.1 | 87.4 |
| 5:00 PM | 26.0 | 78.3 | 36.0 | 96.3 | 34.8 | 94.1 | 31.7 | 88.5 |
| 5:30 PM | 26.0 | 78.3 | 35.0 | 94.5 | 34.7 | 93.9 | 32.1 | 89.2 |
| 6:00 PM | 25.0 | 76.5 | 35.0 | 94.5 | 35.2 | 94.8 | 32.5 | 90.0 |
| 6:30 PM | 25.0 | 76.5 | 34.0 | 92.7 | 35.2 | 94.8 | 33.0 | 90.8 |
| 7:00 PM | 24.0 | 74.7 | 33.0 | 90.9 | 34.9 | 94.3 | 32.9 | 90.6 |
| 7:30 PM | 24.0 | 74.7 | 32.0 | 89.1 | 34.1 | 92.8 | 32.6 | 90.1 |
| 8:00 PM | 23.0 | 72.9 | 30.0 | 85.5 | 33.3 | 91.4 | 32.2 | 89.4 |
| 8:30 PM | 23.0 | 72.9 | 27.0 | 80.1 | 31.9 | 88.9 | 31.7 | 88.4 |
| 9:00 PM | 22.0 | 71.1 | 27.0 | 80.1 | 31.1 | 87.4 | 31.0 | 87.3 |

Table 4-3. (b) Measured Temperature at Site 45 (Traverse City, MI)

| Time | Measured Temperature | | | | | | | |
|---|---|---|---|---|---|---|---|---|
| | Air | | Surface | | 2.25" (5.72 cm) | | 5.0" (12.7 cm) | |
| | °C | °F | °C | °F | °C | °F | °C | °F |
| 10:00 AM | 22.0 | 71.1 | 29.0 | 83.7 | 25.6 | 77.5 | | |
| 10:30 AM | 23.0 | 72.9 | 31.0 | 87.3 | 27.9 | 81.7 | | |
| 11:00 AM | 24.0 | 74.7 | 32.0 | 89.1 | 29.4 | 84.4 | 26.0 | 78.3 |
| 11:30 AM | 26.0 | 78.3 | 35.0 | 94.5 | 30.8 | 86.8 | 26.9 | 79.9 |
| 12:30 PM | 27.0 | 80.1 | 37.0 | 98.1 | 33.6 | 91.9 | 28.5 | 82.8 |
| 1:00 PM | 28.0 | 81.9 | 39.0 | 101.7 | 35.4 | 95.2 | 29.4 | 84.4 |
| 1:30 PM | 27.0 | 80.1 | 40.0 | 103.5 | 36.6 | 97.3 | 30.7 | 86.7 |
| 2:00 PM | 28.0 | 81.9 | 41.0 | 105.3 | 37.7 | 99.2 | 31.1 | 87.4 |
| 2:30 PM | 29.0 | 83.7 | 41.0 | 105.3 | 38.9 | 101.4 | 32.0 | 89.1 |
| 3:00 PM | 29.0 | 83.7 | 42.0 | 107.1 | 39.4 | 102.4 | 32.9 | 90.7 |
| 3:30 PM | 28.0 | 81.9 | 43.0 | 108.9 | 39.8 | 103.0 | 33.5 | 91.8 |
| 4:00 PM | 29.0 | 83.7 | 42.0 | 107.1 | 39.8 | 103.0 | 34.0 | 92.7 |
| 4:30 PM | 28.0 | 81.9 | 42.0 | 107.1 | 39.4 | 102.3 | 34.0 | 92.7 |
| 5:00 PM | 30.0 | 85.5 | 40.0 | 103.5 | 40.1 | 103.6 | 34.6 | 93.7 |

Table 4-3. (c) Measured Temperature at Site 69 (Brevort, MI)

| Time | Measured Temperature | | | | | |
|---|---|---|---|---|---|---|
| | Air | | Surface | | 5.0" (12.7 cm) | |
| | °C | °F | °C | °F | °C | °F |
| 5:57 AM | 7.2 | 44.4 | 14.1 | 56.8 | 17.8 | 63.5 |
| 6:27 AM | 8.1 | 46.0 | 14.4 | 57.4 | 17.5 | 63.0 |
| 6:57 AM | 9.2 | 48.0 | 14.4 | 57.4 | 17.3 | 62.6 |
| 7:57 AM | 17.9 | 63.7 | 15.8 | 59.9 | 17.1 | 62.2 |
| 8:27 AM | 18.7 | 65.1 | 18.8 | 65.3 | 17.4 | 62.8 |
| 8:57 AM | 21.4 | 70.0 | 21.8 | 70.7 | 18.2 | 64.2 |
| 9:27 AM | 23.3 | 73.4 | 24.3 | 75.2 | 19.1 | 65.8 |
| 9:57 AM | 22.9 | 72.7 | 26.5 | 79.2 | 20.2 | 67.8 |
| 10:27 AM | 19.6 | 66.7 | 28.6 | 82.9 | 21.2 | 69.6 |
| 10:57 AM | 22.5 | 72.0 | 30.8 | 86.9 | 22.6 | 72.1 |
| 11:27 AM | 22.3 | 71.6 | 31.5 | 88.2 | 23.7 | 74.1 |
| 12:27 PM | 21.6 | 70.3 | 35.4 | 95.2 | 25.8 | 77.9 |
| 12:57 PM | 26.2 | 78.6 | 36.3 | 96.8 | 27.1 | 80.2 |
| 1:27 PM | 27.9 | 81.7 | 37.4 | 98.8 | 27.9 | 81.7 |
| 1:57 PM | 25.2 | 76.8 | 38.2 | 100.2 | 28.9 | 83.5 |
| 2:27 PM | 30.1 | 85.6 | 38.8 | 101.3 | 29.8 | 85.1 |
| 2:57 PM | 27.8 | 81.5 | 38.3 | 100.4 | 30.3 | 86.0 |
| 3:27 PM | 33.4 | 91.6 | 37.3 | 98.6 | 30.8 | 86.9 |
| 3:57 PM | 29.6 | 84.7 | 37.6 | 99.1 | 31.2 | 87.6 |
| 4:27 PM | 25.0 | 76.5 | 36.8 | 97.7 | 31.4 | 88.0 |
| 4:57 PM | 29.8 | 85.1 | 35.2 | 94.8 | 31.6 | 88.3 |

Table 4-3. (d) Measured Temperature at Site 88 (Deerton, MI)

| Time | Measured Temperature | | | | | | | | | |
|---|---|---|---|---|---|---|---|---|---|---|
| | Air | | Surface | | 2.5" (6.35 cm) | | 3.5" (8.89 cm) | | 6.5" (16.5 cm) | |
| | °C | °F | °C | °F | °C | °F | °C | °F | °C | °F |
| 7:58 AM | 15.0 | 58.5 | 19.0 | 65.7 | | | | | | |
| 8:30 AM | 20.0 | 67.5 | 22.0 | 71.1 | | | | | | |
| 9:01 AM | 26.0 | 78.3 | 22.0 | 71.1 | | | | | | |
| 9:30 AM | 25.0 | 76.5 | 26.0 | 78.3 | | | | | | |
| 10:00 AM | 25.0 | 76.5 | 29.0 | 83.7 | 25.3 | 77.0 | 24.9 | 76.2 | 24.9 | 76.3 |
| 10:30 AM | 24.0 | 74.7 | 31.0 | 87.3 | 26.4 | 79.0 | 26.2 | 78.6 | 24.8 | 76.1 |
| 11:01 AM | 24.0 | 74.7 | 32.0 | 89.1 | 28.6 | 82.9 | 27.2 | 80.4 | 25.2 | 76.8 |
| 11:30 AM | 26.0 | 78.3 | 35.0 | 94.5 | 29.9 | 85.3 | 28.6 | 82.9 | 26.0 | 78.3 |
| 12:59 PM | 26.0 | 78.3 | 40.0 | 103.5 | 35.0 | 94.5 | 32.7 | 90.2 | 28.5 | 82.8 |
| 1:34 PM | 26.0 | 78.3 | 41.0 | 105.3 | 36.6 | 97.3 | 34.3 | 93.2 | 29.2 | 84.0 |
| 2:00 PM | 27.0 | 80.1 | 43.0 | 108.9 | 38.3 | 100.4 | 35.3 | 95.0 | 30.2 | 85.8 |
| 2:30 PM | 26.0 | 78.3 | 43.0 | 108.9 | 38.5 | 100.8 | 36.2 | 96.6 | 30.8 | 86.9 |
| 3:01 PM | 27.0 | 80.1 | 44.0 | 110.7 | 40.4 | 104.2 | 37.7 | 99.2 | 32.1 | 89.2 |
| 3:33 PM | 25.0 | 76.5 | 43.0 | 108.9 | 42.4 | 107.8 | 38.4 | 100.6 | 32.4 | 89.8 |
| 4:00 PM | 27.0 | 80.1 | 43.0 | 108.9 | 41.4 | 106.0 | 39.1 | 101.8 | 33.1 | 91.0 |
| 4:30 PM | 26.0 | 78.3 | 43.0 | 108.9 | 41.5 | 106.2 | 39.4 | 102.3 | 33.6 | 91.9 |
| 5:00 PM | 25.0 | 76.5 | 43.0 | 108.9 | 41.8 | 106.7 | 39.5 | 102.5 | 34.2 | 93.0 |
| 5:31 PM | 25.0 | 76.5 | 42.0 | 107.1 | 41.5 | 106.2 | 39.9 | 103.2 | 35.1 | 94.6 |
| 5:59 PM | 24.0 | 74.7 | 41.0 | 105.3 | 41.6 | 106.3 | 39.8 | 103.1 | 35.1 | 94.6 |

Table 4-3. (e) Measured Temperature at SPS Site K24

| Time | Measured Temperature | | | | | | | | | |
|---|---|---|---|---|---|---|---|---|---|---|
| | Air | | Surface | | 2.0" (5.1 cm) | | 3.5" (8.89 cm) | | 5.25" (13.4 cm) | |
| | °C | °F | °C | °F | °C | °F | °C | °F | °C | °F |
| 7:30 AM | 21.0 | 69.3 | 23.0 | 72.9 | 22.8 | 72.5 | 24.0 | 74.6 | 24.5 | 75.6 |
| 8:00 AM | 22.0 | 71.1 | 24.0 | 74.7 | 23.6 | 73.9 | 23.6 | 73.9 | 23.7 | 74.1 |
| 8:30 AM | 24.0 | 74.7 | 27.0 | 80.1 | 24.8 | 76.1 | 24.4 | 75.4 | 24.0 | 74.7 |
| 9:00 AM | 26.0 | 78.3 | 29.0 | 83.7 | 26.8 | 79.7 | 25.6 | 77.5 | 24.8 | 76.1 |
| 9:30 AM | 27.0 | 80.1 | 32.0 | 89.1 | 28.5 | 82.8 | 27.1 | 80.2 | 25.5 | 77.4 |
| 10:00 AM | 28.0 | 81.9 | 34.0 | 92.7 | 30.6 | 86.5 | 28.4 | 82.5 | 26.5 | 79.2 |
| 10:30 AM | 28.0 | 81.9 | 35.0 | 94.5 | 32.4 | 89.8 | 30.0 | 85.4 | 27.7 | 81.3 |
| 11:40 AM | 27.0 | 80.1 | 38.0 | 99.9 | 36.7 | 97.5 | 33.6 | 91.9 | 30.4 | 86.2 |
| 12:00 PM | 28.0 | 81.9 | 40.0 | 103.5 | 37.8 | 99.5 | 34.4 | 93.4 | 31.2 | 87.6 |
| 12:30 PM | 28.0 | 81.9 | 42.0 | 107.1 | 39.3 | 102.2 | 35.3 | 95.0 | 31.7 | 88.5 |
| 1:00 PM | 29.0 | 83.7 | 42.0 | 107.1 | 40.5 | 104.4 | 36.8 | 97.6 | 33.4 | 91.6 |
| 1:30 PM | 29.0 | 83.7 | 43.0 | 108.9 | 41.3 | 105.8 | 38.0 | 99.8 | 34.3 | 93.2 |
| 2:00 PM | 30.0 | 85.5 | 44.0 | 110.7 | 42.5 | 108.0 | 39.2 | 102.0 | 35.3 | 95.0 |
| 2:30 PM | 31.0 | 87.3 | 46.0 | 114.3 | 43.1 | 109.0 | 39.9 | 103.2 | 35.9 | 96.1 |
| 3:00 PM | 30.0 | 85.5 | 45.0 | 112.5 | 43.4 | 109.6 | 40.3 | 103.9 | 36.5 | 97.2 |
| 3:30 PM | 29.0 | 83.7 | 44.0 | 110.7 | 44.6 | 111.7 | 41.5 | 106.1 | 37.6 | 99.1 |
| 4:00 PM | 29.0 | 83.7 | 44.0 | 110.7 | 44.4 | 111.4 | 41.6 | 106.3 | 38.0 | 99.9 |

Table 4-3. (f) Measured Temperature at SPS Site K59

| Time | Measured Temperature | | | | | | | | | |
|---|---|---|---|---|---|---|---|---|---|---|
| | Air | | Surface | | 1.75" (4.4 cm) | | 3.25" (8.3 cm) | | 5.0" (12.7 cm) | |
| | °C | °F | °C | °F | °C | °F | °C | °F | °C | °F |
| 7:30 AM | 24.0 | 74.7 | 26.0 | 78.3 | 24.6 | 75.7 | 24.5 | 75.5 | 25.0 | 76.5 |
| 8:00 AM | 26.0 | 78.3 | 27.0 | 80.1 | 25.8 | 77.9 | 25.2 | 76.8 | 25.1 | 76.6 |
| 8:30 AM | 28.0 | 81.9 | 29.0 | 83.7 | 27.6 | 81.1 | 26.0 | 78.2 | 25.3 | 77.0 |
| 9:00 AM | 30.0 | 85.5 | 33.0 | 90.9 | 30.0 | 85.5 | 27.6 | 81.1 | 26.3 | 78.8 |
| 9:30 AM | 30.0 | 85.5 | 32.0 | 89.1 | 30.5 | 86.4 | 28.5 | 82.8 | 26.8 | 79.7 |
| 10:00 AM | 32.0 | 89.1 | 35.0 | 94.5 | 32.4 | 89.8 | 29.4 | 84.4 | 27.5 | 81.0 |
| 10:30 AM | 31.0 | 87.3 | 38.0 | 99.9 | 34.3 | 93.2 | 31.3 | 87.7 | 28.8 | 83.3 |
| 12:00 PM | 33.0 | 90.9 | 43.0 | 108.9 | 39.8 | 103.1 | 35.6 | 95.5 | 32.2 | 89.4 |
| 12:30 PM | 34.0 | 92.7 | 44.0 | 110.7 | 41.5 | 106.2 | 36.9 | 97.8 | 33.3 | 91.4 |
| 1:00 PM | 33.0 | 90.9 | 46.0 | 114.3 | 41.7 | 106.5 | 38.0 | 99.9 | 34.2 | 93.0 |
| 1:30 PM | 34.0 | 92.7 | 45.0 | 112.5 | 41.6 | 106.3 | 38.7 | 101.1 | 35.1 | 94.6 |
| 2:00 PM | 34.0 | 92.7 | 45.0 | 112.5 | 41.8 | 106.7 | 39.4 | 102.4 | 35.7 | 95.7 |
| 2:30 PM | 34.0 | 92.7 | 45.0 | 112.5 | 42.0 | 107.1 | 39.8 | 103.0 | 36.4 | 97.0 |
| 3:00 PM | 33.0 | 90.9 | 43.0 | 108.9 | 41.6 | 106.3 | 39.6 | 102.7 | 36.8 | 97.7 |
| 3:30 PM | 34.0 | 92.7 | 43.0 | 108.9 | 41.2 | 105.6 | 39.9 | 103.3 | 37.3 | 98.6 |
| 4:00 PM | 32.0 | 89.1 | 41.0 | 105.3 | 40.7 | 104.7 | 40.1 | 103.6 | 37.5 | 99.0 |

Table 4-4. Database from Stubstad et al. (1994)

| Location | Time | AC Thickness (inches/cm) | Measured Temeprature | | | |
|---|---|---|---|---|---|---|
| | | | Surface | | One-Third Depth | |
| | | | °C | °F | °C | °F |
| Nebraska | 10:00 AM | | 6.7 | 43.5 | 8.6 | 46.9 |
| Arapaho | 11:34 AM | | 18.1 | 64.0 | 13.9 | 56.5 |
| | 12:52 PM | | 21.9 | 70.9 | 18.5 | 64.8 |
| | 2:34 PM | | 26.1 | 78.4 | 22.6 | 72.1 |
| | 9:37 AM | | 8.9 | 47.5 | 13.4 | 55.6 |
| | 11:00 AM | 7.2/18.3 | 11.2 | 51.6 | 14.4 | 57.4 |
| | 12:54 PM | | 18.6 | 64.9 | 18.0 | 63.9 |
| | 3:07 PM | | 23.1 | 73.0 | 21.4 | 70.0 |
| | 9:10 AM | | 33.1 | 91.0 | 29.8 | 85.1 |
| | 10:20 AM | | 37.8 | 99.5 | 33.0 | 90.9 |
| | 12:10 PM | | 45.0 | 112.5 | 38.0 | 99.9 |

backcalculation programs to compute the modulus for each layer of the pavement structure. The backcalculated modulus of the AC layer is then adjusted to a reference or standard temperature. The adjusted backcalculated layer moduli are then used in a forward calculation routine to estimate the stress/strain distributions in each of the pavement layers and structural performance under expected traffic volumes and loadings. Hence, the sensitivity of temperature prediction on performance prediction was also investigated because the temperature prediction is eventually used for temperature correction and structural performance prediction. Cross-section and deflection data collected from sites 25, 45, 88, 69 and two SPS1 sites were used as input to the MICHBACK program (Harichandran et al., 1994) to compute layer moduli. The computed AC layer modulus at each site was temperature-corrected based on both measured and predicted layer middepth temperatures. This layer modulus information along with pavement cross-section information was then used to compute layer responses such as, surface deflection, horizontal strain at the bottom of the AC layer, vertical strain at the base, and vertical strain at the subgrade. The CHEVRONX program (Warren et al., 1963) was used for determining the structural responses. The layer moduli, pavement responses, and mixture properties were incorporated into a rut prediction model (Kim et al., 2000) to compute predicted rut depth.

The results from the data analysis will be presented and discussed in Chapter 6.

# CHAPTER 5

# FINITE ELEMENT MODEL

## 5.1 GENERAL

Due to the relatively simple geometry, flexible pavement analyses are usually approached by two-dimensional (2-D) axisymmetric models. Many finite element programs based on 2-D models have been satisfactorily used in analyzing flexible pavement problems. However, many realistic problems are beyond the capability of 2-D models. A three-dimensional model is needed to solve these problems.

The 2-D finite element analysis/program for flexible pavements has the following advantages:

- The model is efficient and relatively simple.
- Such models/programs are widely used and available.
- Most 2-D pavement programs have been satisfactorily validated with theoretical solutions and field data.

However, realistic pavement behavior can be far more complex than the 2-D model idealization. Among the problems that 2-D models/programs cannot accurately and conveniently model are the following:

- Nonuniform contact pressure distribution under the load (Figure 5-1)
- Realistic lateral forces pressure (e.g., lateral stresses in various directions) between tire and pavement surface.

These limitations can be solved by multiple 2-D analyses and superposition; however this usually leads to complicated and time-consuming procedures.

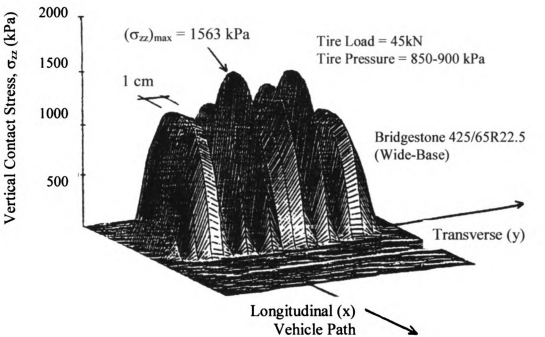


Figure 5-1. Nonuniform vertical stress distribution under a wide-base tire (De Beer et al., 1996)

In this study, 2-D analysis was performed to carry out parametric studies in which temperature distribution across the asphalt concrete (AC) layer, AC thickness, base stiffness, and load pressure distribution were varied. The 3-D analyses were used to investigate the effect of temperature distribution and nonuniform load pressure such as tire tread effects as shown in Figure 5-1.

The following sections describe the viscoelastic model for the AC layer, boundary conditions and inputs, application of the load pulse, and two-dimensional and three-dimensional models used in this study.

## 5.2 MODELING

It is assumed that only the mechanistic properties of the viscoelastic (AC) layer depend on temperature and those of the elastic (base and subgrade) layers are not affected by temperature. Base/subbase and subgrade were modeled as a linearly elastic, isotropic, and homogeneous solid. Because of the relatively small effect of Poisson ratio $\upsilon$ on pavement behavior, constant Poisson's ratios were used in the analysis. The 2-D and 3-D finite element models (FEM) were developed using the I-DEAS graphical software (I-DEAS *Master Series*, 1997) and the analysis was performed using the ABAQUS FEM software package (ABAQUS *User Manual*, 1993).

### 5.2.1 Viscoelastic Material Model for the AC Layer

In this model, the relaxation at a given temperature, T, is described by a temperature-independent relaxation function in terms of a temperature dependent "reduced time ($t_r$)" which is defined as $t_r = t/a_T$, as follows:

$$\sigma(t) = \int_0^t E(\frac{t-\tau}{a_T})\frac{d\varepsilon(\tau)}{d\tau}d\tau \qquad (3\text{-}9)$$

where $\sigma(t)$ is the stress at time t and temperature T, $E(t_r)$ is the uniaxial relaxation modulus which becomes a temperature-independent relaxation modulus by using the "reduced time", and $\varepsilon(t)$ is the strain at time t.

The shift factor $a_T$ is defined in the following form (Williams, Landel, and Ferry (WLF) equation):

$$h(T) = -\log a_T = \frac{c_1(T-T_r)}{c_2+(T-T_r)} \qquad (3\text{-}8)$$

where h(T) is a time shift function, $a_T$ is the shift factor, $c_1$ and $c_2$ are constants, and $T_r$ is a reference temperature.

The time shift function h(T) can be used to extrapolate the relaxation data to very short or long times. This study requires the relaxation data of very short times due to the relatively short duration of the FWD load (approximately 30 milliseconds). The extrapolation procedure is described below.

Relaxation experiments are carried out with the stress measured in a given time range under the applied constant strain, for example between t=1 sec and t=1000 sec, at different temperatures, e.g., at $T = T_o$ and $T = T_o \pm \Delta T$. Let $T_o$ be selected as the reference temperature: $h(T_o) = 0$ and results can be plotted on a logarithmic time scale as shown in Figure 5-2. The master curve is made by shifting the data along the horizontal axis.

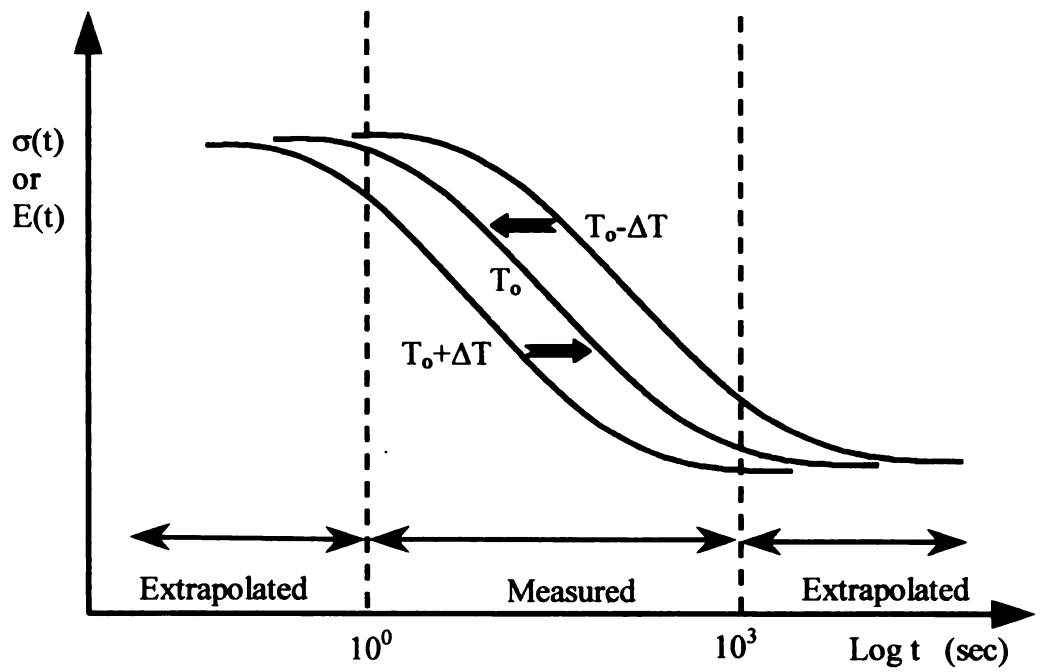


Figure 5-2. An example of stress-relaxation data obtained at different temperature (modified from ABAQUS *User Manual*, 1993)

The measured curves make it possible to determine the shift functions $h(T_o-\Delta T)$ and $h(T_o+\Delta T)$. The shift functions can in turn be used to extrapolate the relaxation curves beyond the measured domain as shown in Figure 5-2. By carrying out stress relaxation tests over a wide enough range of temperatures, a complete relaxation curve spanning many decades in time can be obtained. Figure 5-3 shows master relaxation modulus and shift factor of the asphalt mixtures used in the analysis.

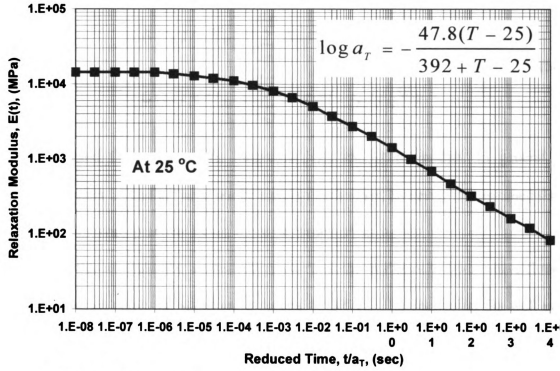


*Note*: 1 MPa = 145 psi

Figure 5-3. Master relaxation modulus and shift factor of the asphalt mixtures used in the analysis (Kim et al., 1996)

### *5.2.1.1 Time Integration Procedure*

The basic hereditary integral formulation for linear isotropic viscoelasticity is:

$$\sigma(t) = \int_0^t 2G(t_r - t_r')\dot{e}dt' + I\int_0^t K(t_r - t_r')\dot{\phi}dt' \qquad (5\text{-}1)$$

where $e$ and $\phi$ are the mechanical deviatoric and volumetric strains; I is a unit matrix, K is the bulk modulus and G is the shear modulus, which are functions of the reduced time $t_r$; and $\dot{}$ denotes differentiation with respect to t'.

With a series of exponentials known as the Prony series, the relaxation functions K(t) and G(t) can be defined individually:

$$\begin{aligned} K(t_r) &= K_\infty + \sum_{i=1}^{n_K} K_i \exp(-t_r / {t_{ri}}^K) \\ G(t_r) &= G_\infty + \sum_{i=1}^{n_G} G_i \exp(-t_r / {t_{ri}}^G) \end{aligned} \qquad (5\text{-}2a)$$

where $K_\infty$ and $G_\infty$ represent the long-term bulk and shear moduli. In general, the relaxation times ${t_{ri}}^K$ and ${t_{ri}}^G$ need not be equal to each other; however, it is assumed that $t_{ri} = {t_{ri}}^K = {t_{ri}}^G$. In many practical cases, it can be assumed that $n_K = 0$.

For this analysis, the master relaxation modulus in Figure 5-3 was curve fitted to the Prony series using the statistical program, SYSTAT. The regression fits well up to approximately 10 seconds, which is a period long enough to cover the analysis since the period of FWD pulse is 30 milliseconds (Figure 5-4). The regression equation for the master curve is as follows:

$$E(t) = 14285 - 2209*(1-\exp(-t_r/1.1447957)) - 4427.6*(1-\exp(-t_r/0.0006052)) - 4454.6*(1-\exp(-t_r/0.0173438)) - 2637.2*(1-\exp(-t_r/0.0000131)) \qquad (5\text{-}2b)$$

with $R^2 = 99\%$.

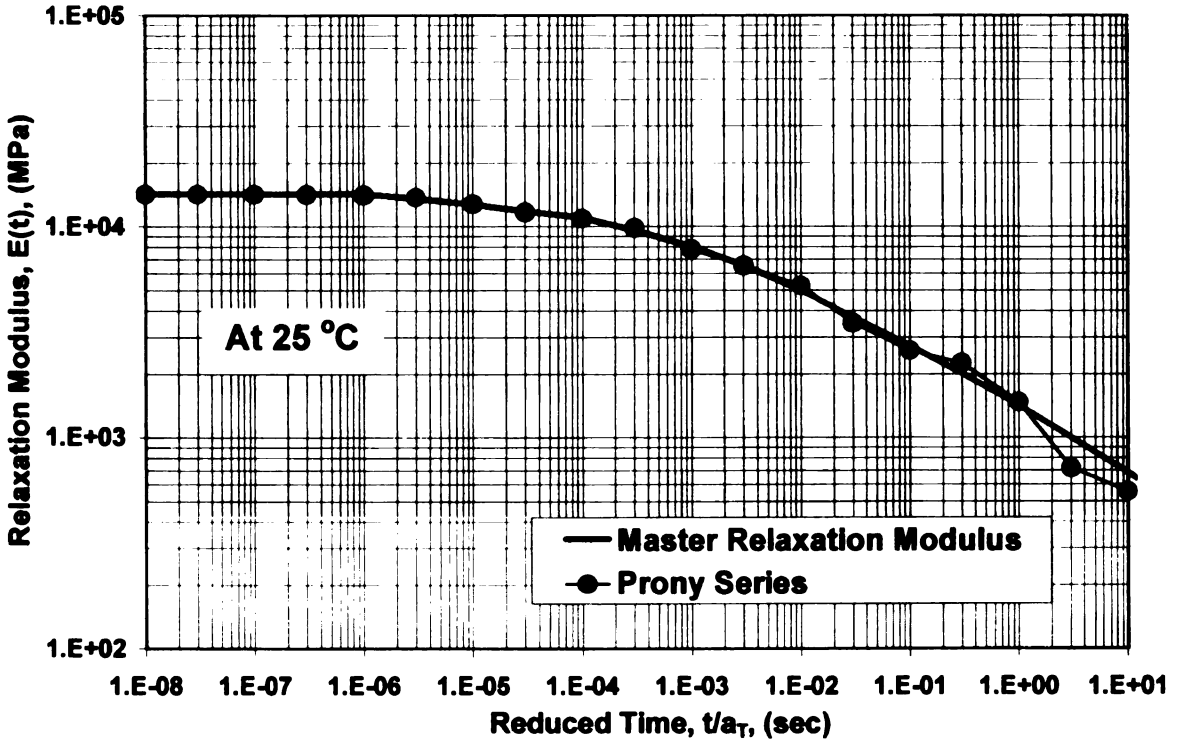


*Note*: 1 MPa = 145 psi

Figure 5-4. Curve fit of master relaxation modulus to the Prony series

The deviatoric integral equation is

$$S = \int_0^t 2(G_\infty + \sum_{i=1}^{n_G} G_i \exp((t'_r - t_r)/t_{ri})\dot{e}dt' \tag{5-3}$$

This equation can be written in the form

$$S = 2G_o\left(e - \sum_{i=1}^{n} \alpha_i e_i\right) \tag{5-4}$$

where $G_o = G_\infty + \Sigma^n_{i=1} G_i$ is the instantaneous shear modulus, $\alpha_i = G_i/G_o$ is the relative modulus for term *i* and

$$e_i = \int_0^{t_r} (1 - \exp((t'_r - t_r)/t_{ri})) \frac{de}{dt'_r} dt'_r \tag{5-5}$$

is the viscous strain in each term of the series of spring-dashpot elements (Figure 5-5).

For finite element analysis, this equation must be integrated over a finite increment of time. To carry out this integration, it is assumed that during the increment, the total strain varies linearly with time, and hence $de/dt_r' = \Delta e/\Delta t_r$. To use this relation, Equation 5-5 is broken up into two parts:

$$e_i^{n+1} = \int_0^{t_r^n} (1 - \exp((t_r' - t_r^n)/t_{ri}))\frac{de}{dt_r'}dt_r' + \int_{t_r^n}^{t_r^{n+1}} (1 - \exp((t_r' - t_r^{n+1})/t_{ri}))\frac{de}{dt_r'}dt_r' \quad (5\text{-}6)$$

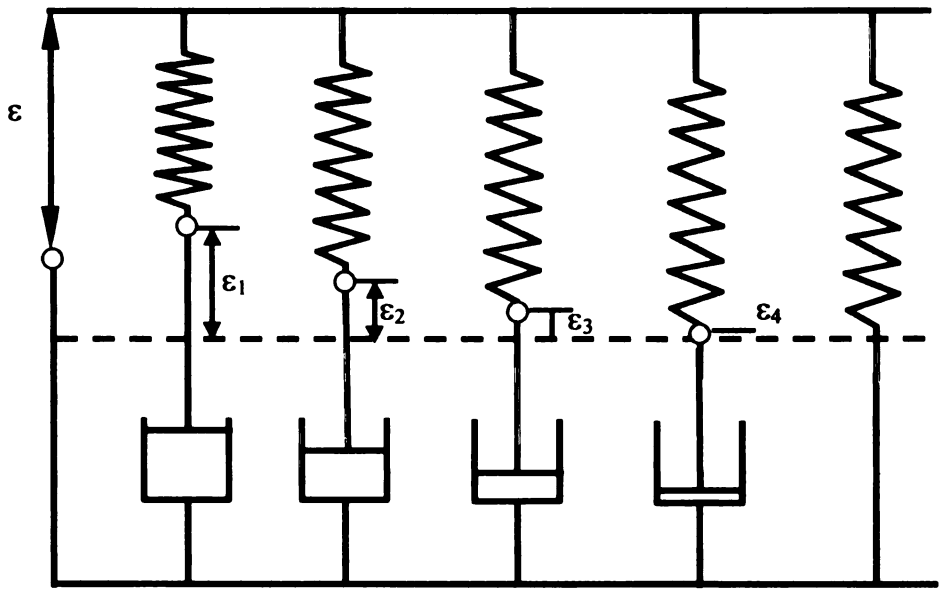


Figure 5-5. Prony series strains (ABAQUS *User Manual*, 1993)

Observing that

$$1 - e^{(t_r' - t_r^{n+1})/t_{ri}} = 1 - e^{-\Delta t_r/t_{ri}} + e^{-\Delta t_r/t_{ri}}(1 - e^{(t_r' - t_r^n)/t_{ri}}) \quad (5\text{-}7)$$

use of this expression and the approximation for $de/dt_r'$ during the increment yields

$$e_i^{n+1} = (1 - e^{-\Delta t_r / t_{ri}}) \int_0^{t_r^n} \frac{de}{dt_r'} dt_r'$$

$$+ e^{-\Delta t_r / t_{ti}} \int_0^{t_r^n} (1 - e^{(t_r' - t_r^n)/t_{ri}}) \frac{de}{dt_r'} dt_r' \qquad (5\text{-}8)$$

$$+ \frac{\Delta e}{\Delta t_r} \int_{t_r^n}^{t_r^{n+1}} (1 - e^{(t_r' - t_r^{n+1})/t_{ri}}) dt_r'$$

The first and last integrals in this equation are readily evaluated, whereas the second integral represents the viscous strain in the $i^{th}$ term at the beginning of the increment. Hence the change in the $i^{th}$ viscous strain is

$$\Delta e_i = (1 - e^{-\Delta t_r / t_{ri}}) e^n + (e^{-\Delta t_r / t_{ri}} - 1) e_i^n + (\Delta t_r - t_{ri}(1 - e^{-\Delta t_r / t_{ri}})) \frac{\Delta e}{\Delta t_r} \qquad (5\text{-}9)$$

In an increment, the above equation is used to compute the new value of the viscous strains. Equation (5-4) is then used subsequently to obtain the new value of the stresses. (ABAQUS *User Manual*, 1993)

#### *5.2.1.2 Implementation of Temperature Effects*

In order to relate the reduced time increment, $\Delta t_r$, to the actual time increment, $\Delta t$, it is assumed that the (time) shift factor ($a_T$) applies to the rate of change of reduced time when the temperature changes in the analysis:

$$dt_r = \frac{1}{a_T} dt \qquad (5\text{-}10)$$

where $t_r$ is the reduced time corresponding to the change in temperature and t is the actual time at the reference temperature.

For a finite time increment, the increment of reduced time, $\Delta t_r$, is calculated based on the assumption that the shift function, h(T), is generally a smoothly varying function of temperature which is well approximated by a linear function of temperature over an increment, and temperature T is a linear function of time t. Then, one finds the relationship to be:

$$h(T) = -\ln a_T = A + Bt \qquad \text{or} \qquad a_T^{-1} = e^{A+Bt} \tag{5-11}$$

with

$$A = \frac{1}{\Delta t}\left[t^{T+\Delta T} h(T) - t^{T} h(T+\Delta T)\right] \tag{5-12}$$

$$B = \frac{1}{\Delta t}\left[h(T+\Delta T) - h(T)\right]$$

This yields to the following relationship

$$\Delta t_r = \int_t^{T+\Delta T} e^{A+Bt}\, dt = \frac{1}{B}(e^{A+Bt^{T+\Delta T}} - e^{A+Bt^{T}}) \tag{5-13}$$

As a result, the increment of reduced time is calculated as

$$\Delta t_r = \frac{1/a_{T+\Delta T} - 1/a_T}{h(T+\Delta T) - h(T)} \Delta t \tag{5-14}$$

It is readily verified that

$$\Delta t_r \to \frac{1}{a_T} \Delta t \qquad \text{if } \Delta t \to 0 \tag{5-15}$$

(ABAQUS *User Manual*, 1993)

### 5.2.2 Boundary Conditions (Temperature)

Temperature was specified at each node or node sets. It was assumed that temperature varied only with depth and does not change with time because of the short time period. Thus, each layer of nodes across the AC layer was assigned a temperature value. The temperature distribution was obtained from field data and the developed temperature prediction model in this study (as explained in Chapters 4 and 6).

In order to investigate temperature gradient effects on the structural analysis, four typical temperature distribution cases were considered (Figure 5-6):

- morning (uniform temperature distribution),
- daytime (temperature at the surface is higher than at the bottom),
- average temperature of daytime (uniform temperature distribution of average temperature of daytime), and
- nighttime (temperature at the surface is lower than at the bottom)

Very low temperature distribution cases were not selected in this study because viscoelastic materials behave like elastic materials at very low temperatures. Figure 5-6 shows temperature distributions of three AC thickness cases: 3" (7.6 cm), 7" (17.8 cm), and 15" (38 cm) thick AC layers. These three different AC thickness cases were used in the analyses for the parametric study.

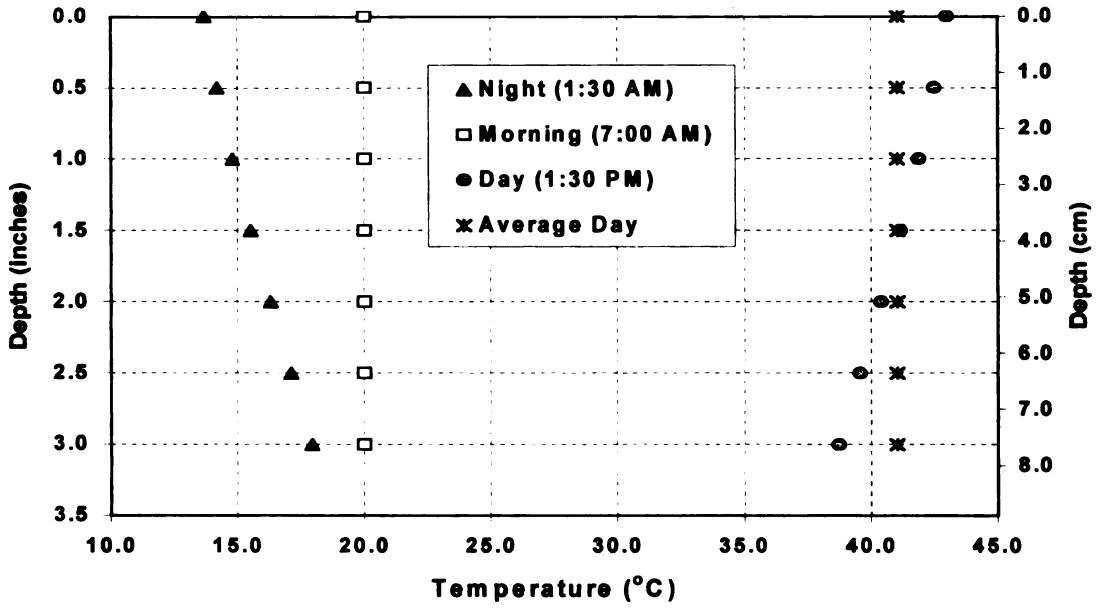


(a) 3" (7.6 cm) thick AC layer

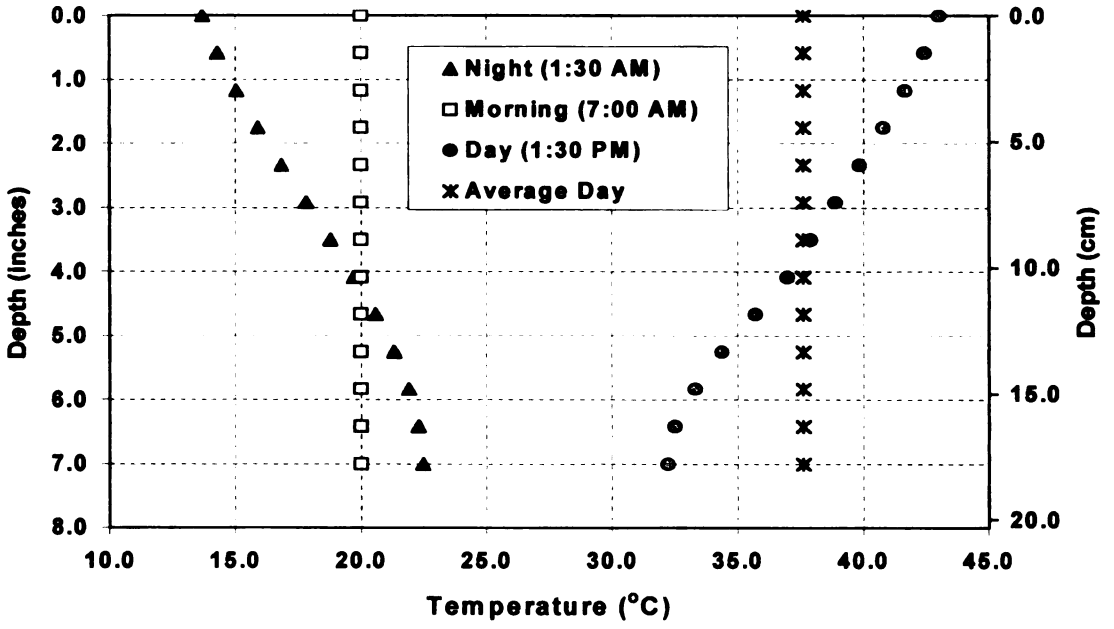


(b) 7" (17.8 cm) thick AC layer

Figure 5-6. Temperature distributions along the AC layer used in the analysis

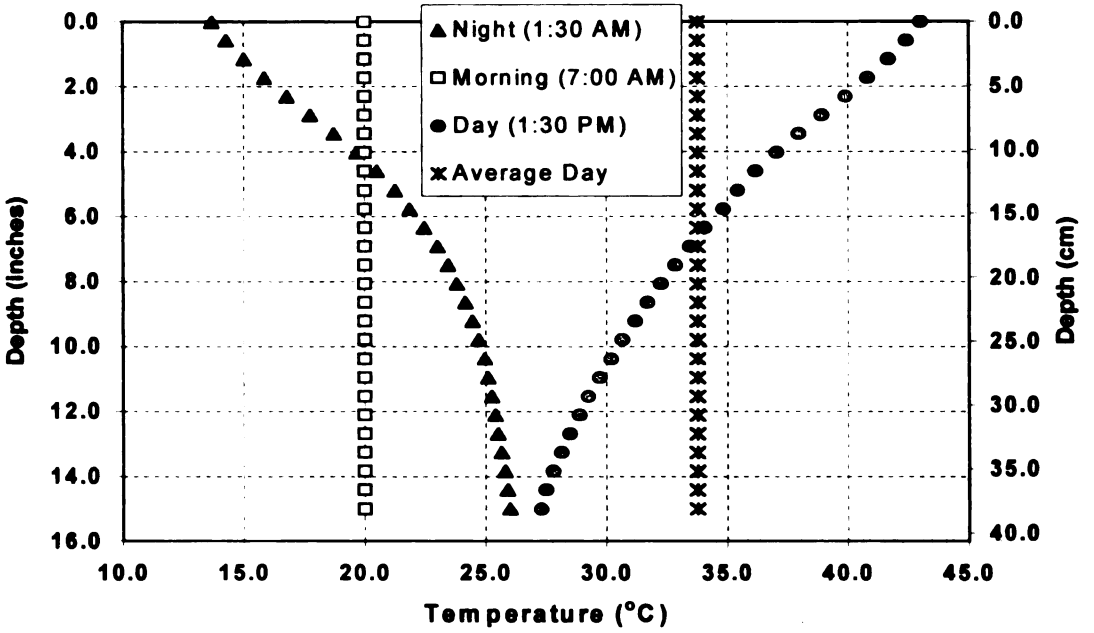


(c) 15" (38 cm) thick AC layer

Figure 5-6. Temperature distributions along the AC layer used in the analysis (continued)

### 5.2.3 Loading

When the applied excitation is time-varying, the dynamic effects (damping) need to be considered. However, the damping effects can be neglected if the time rate of input is reasonably small. In this study, the damping effects were not considered since the FWD load time history based on a typical FWD pulse of 33msec duration was used to simulate the FWD impact load. The peak FWD load was taken as 40 kN (9000 lbs) distributed over an area of 707.9 sq. cm (109.7 sq. inches). Figure 5-7 shows the FWD load pulse used in this study.

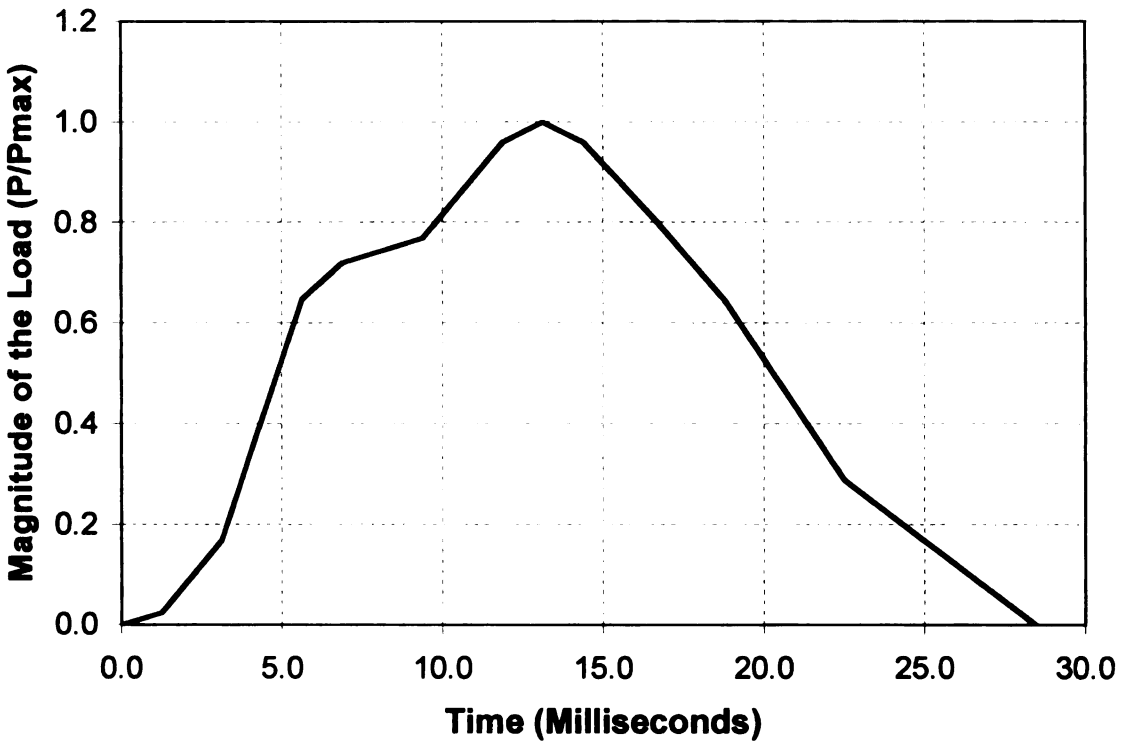


Figure 5-7. FWD load pulse used in the analysis (Uddin, 1998)

In order to implement the FWD pulse in the analysis, it was divided into many steps. The load magnitude was varied linearly over the step from the value at the end of the previous step (or zero, at the start of the analysis) to the value at the end of the current step. This pulse was also adopted for the tire pressure, and the peak load pressure was taken as 115 psi (793 kPa) for the uniform load pressure distribution. Detailed load pressure values are presented in the later sections.

### 5.2.4 Two-Dimensional Finite Element (FE) Model

In the first step of this research, 2-D models were developed and a parametric study was conducted to gain experience in correctly building a model. The following factors relative to the viscoelastic response were investigated:

(a) The effect of temperature distribution across the AC layer

(b) The effect of AC thickness

(c) The effect of rigidity of the base

(d) The effect of loading condition.

This experience facilitated the use of a more complicated 3-D model. For the 2-D model, the axisymmetric model was used, which assumes that the pavement geometry and loading are both axisymmetric. Figure 5-8 and Table 5-1 present the geometry and mesh of the 2-D model and the experimental design for the parametric study, respectively. The range and type of variation of the above four parameters were determined on a realistic assessment of practical pavement applications:

- Temperature distribution
  - Details were presented in the earlier section.
- AC layer thickness
  - Thin (7.6 cm (3")) and thick (38 cm (15")) AC layer were analyzed besides the typical 17.8 cm (7") layer.
- Rigidity of the base
  - Modulus varied between 138 MPa (20 ksi) and 6895 MPa (1000 ksi), to separate granular, asphalt and cement-stabilized bases.

Table 5-1. Experimental design matrix for the parametric study

| AC Thickness (cm) | | 7.6 | | | | 17.8 | | | | 38.1 | | |
|---|---|---|---|---|---|---|---|---|---|---|---|---|
| Base Modulus (MPa) | | 138 | 345 | 689 | 6895 | 138 | 345 | 689 | 6895 | 138 | 345 | 689 |
| Loading Condition | | | | | | | | | | | | |
| Temperature Condition | | | | | | | | | | | | |
| Day | Uniform | 1 | 2 | 3 | 4 | 5 | 6 | 7 | 8 | 9 | 10 | 11 |
| | High Center | 12 | 13 | 14 | 15 | 16 | 17 | 18 | 19 | 20 | 21 | 22 |
| | High Egde | 23 | 24 | 25 | 26 | 27 | 28 | 29 | 30 | 31 | 32 | 33 |
| Average Day uniform | Uniform | 34 | 35 | 36 | 37 | 38 | 39 | 40 | 41 | 42 | 43 | 44 |
| | High Center | 45 | 46 | 47 | 48 | 49 | 50 | 51 | 52 | 53 | 54 | 55 |
| | High Egde | 56 | 57 | 58 | 59 | 60 | 61 | 62 | 63 | 64 | 65 | 66 |
| Night | Uniform | 67 | 68 | 69 | 70 | 71 | 72 | 73 | 74 | 75 | 76 | 77 |
| | High Center | 78 | 79 | 80 | 81 | 82 | 83 | 84 | 85 | 86 | 87 | 88 |
| | High Egde | 89 | 90 | 91 | 92 | 93 | 94 | 95 | 96 | 97 | 98 | 99 |
| Morning uniform | Uniform | 100 | 101 | 102 | 103 | 104 | 105 | 106 | 107 | 108 | 109 | 110 |
| | High Center | 111 | 112 | 113 | 114 | 115 | 116 | 117 | 118 | 119 | 120 | 121 |
| | High Egde | 122 | 123 | 124 | 125 | 126 | 127 | 128 | 129 | 130 | 131 | 132 |

Note. 1 cm = 0.394 in.
1 MPa = 145 psi.

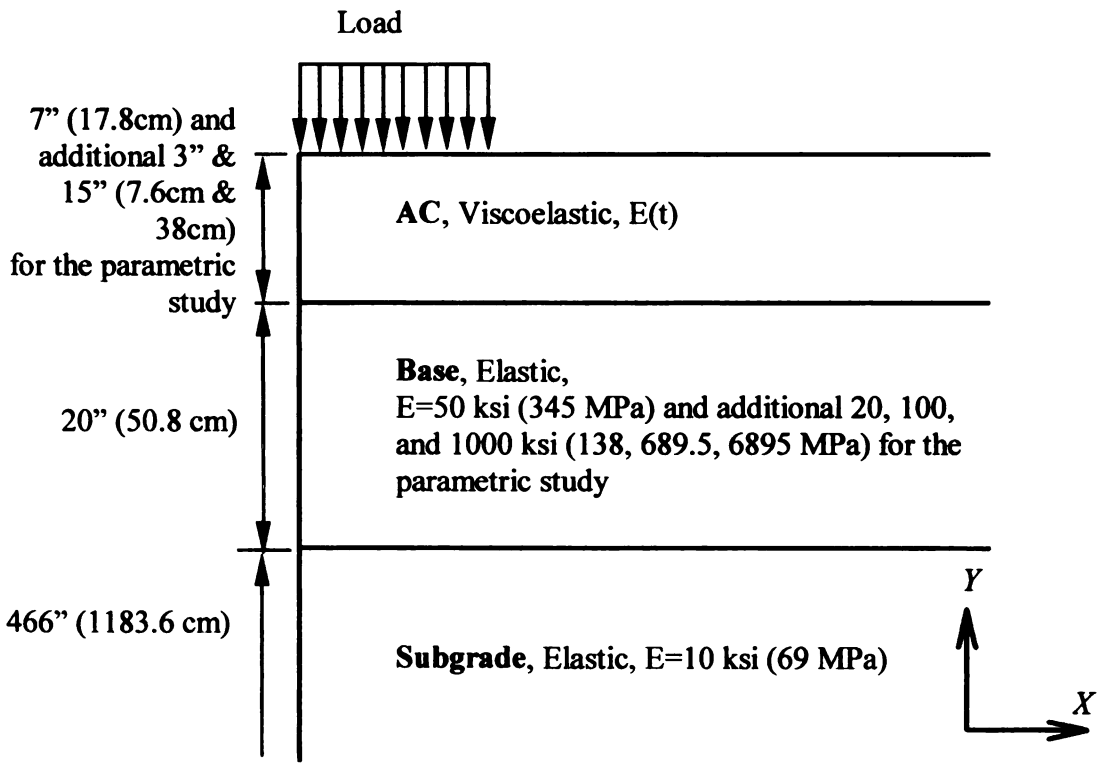


(a) Geometry

Figure 5-8. Two-dimensional model for a three-layer system

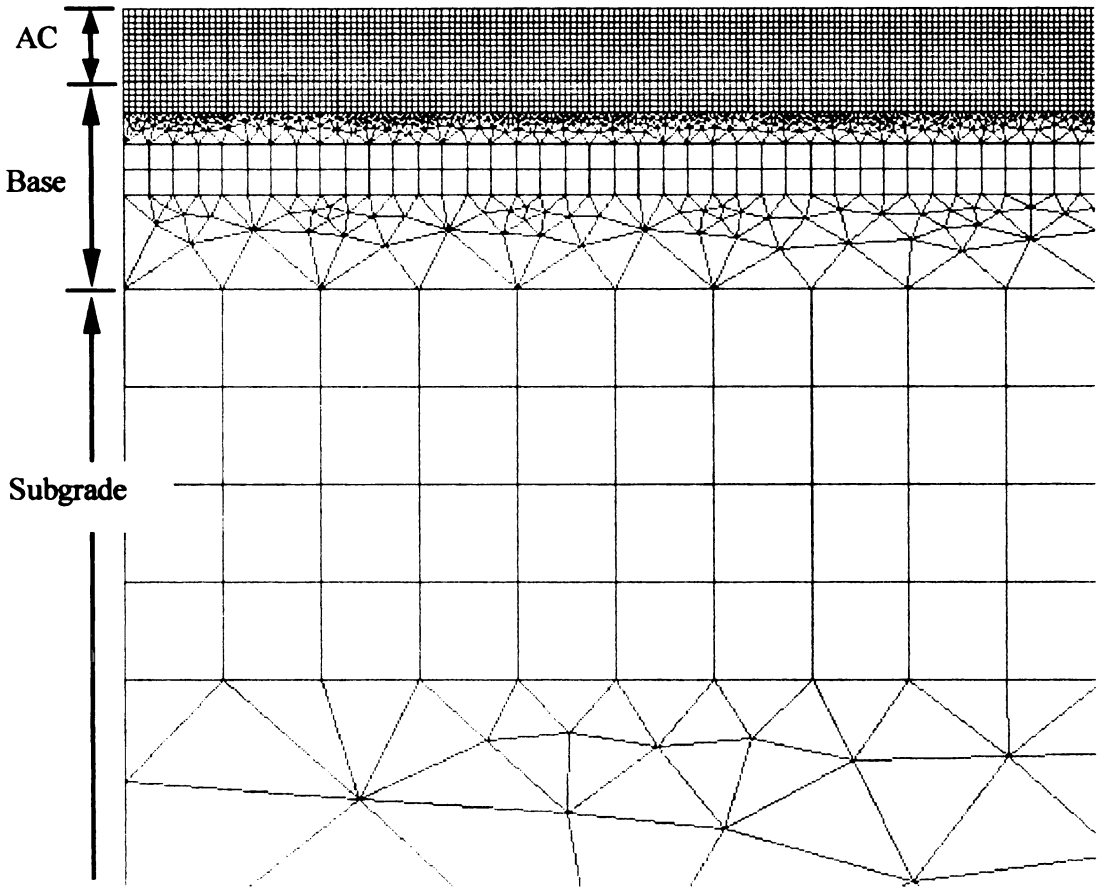


(b) Mesh

Figure 5-8. Two-dimensional model for a three-layer system (continued)

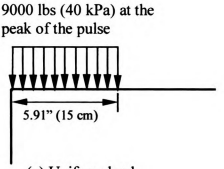


(a) Uniform load

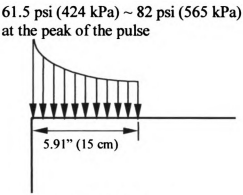


(b) Nonuniform load
(higher pressure at the load center),

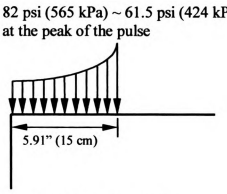


(c) Nonuniform load
(higher pressure at the load edge)

Figure 5-9. Illustration of applied loads in the 2-D axisymmetric analysis

- Loading condition
  - Nonuniform load cases (higher pressures at the load center and edge) were analyzed as well as a standard uniform FWD pressure of 565 kPa (82 psi) at the peak of the pulse (Figure 5-9). Figure 5-10 shows nonuniform pressures versus time and location. The FWD pulse was adopted for the pulse of nonuniform.

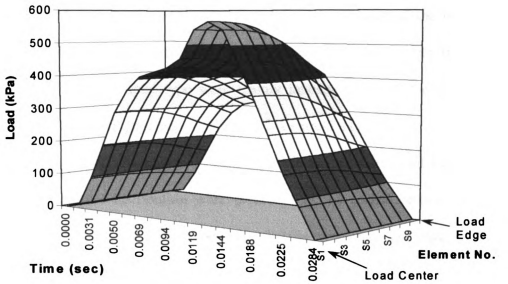


(a) Higher pressure at the load center

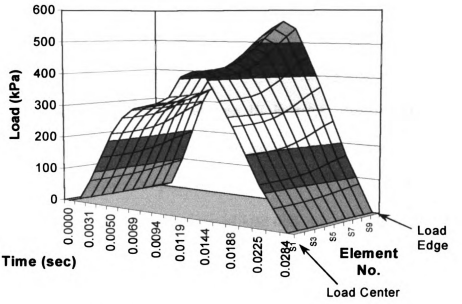


(b) Higher pressure at the load edge

Figure 5-10. Applied nonuniform pressure versus time and location

### 5.2.5 Three-Dimensional FE Model

The development of a 3-D model allows the investigation of the more realistic problem that is not easily simulated with a 2-D model. Hence, the effects of temperature distribution and different load type were mainly investigated with the 3-D model. A typical 7" (17.8 cm) thick pavement was selected (Figure 5-11).

Three temperature distribution cases (Morning, Daytime, and Nighttime) were simulated. Details of temperature distribution were presented in the earlier section. In order to investigate the effects of load, three types of load cases were applied (Figure 5-12):

(a) Load case I: uniform vertical load over the entire load area (no lateral stress),

(b) Load case II: uniform vertical load only under tire treads (no lateral stress), and

(c) Load case III: measured vertical and lateral stresses under tire treads (as measured by Myers et al., 1998).

The uniform vertical load for the load cases I and II is 793 MPa (115 psi) at the peak of the pulse. Measured tire-pavement interface stresses presented by Myers et al., 1998 were modified for the load case III. The load case III includes vertical and lateral tire-pavement interface stresses. Details of measured stresses are illustrated in Figure 5-13. The FWD pulse was adopted for the pulse of all loads applied in this analysis.

Because there is no distributed tangential load option in ABAQUS, an alternative method was used to apply lateral stresses to the model. A layer of membrane elements was first added to the loaded area. The membrane elements were parallel to the global *XZ* plane as shown in Figure 5-11. Body forces equivalent to the lateral stresses were then applied to these elements in the desired lateral direction. The membrane elements had

negligible stiffness (for instance, 6.9E-6 kPa (1.0E-6 psi)) in order to avoid restricting the responses of the pavement. However, applied loads are transmitted to the pavement since loads computed at nodes (i.e., nodal loads) are not associated with the element stiffness (Cook et al., 1989). Discussion of results will be presented in Chapter 7.

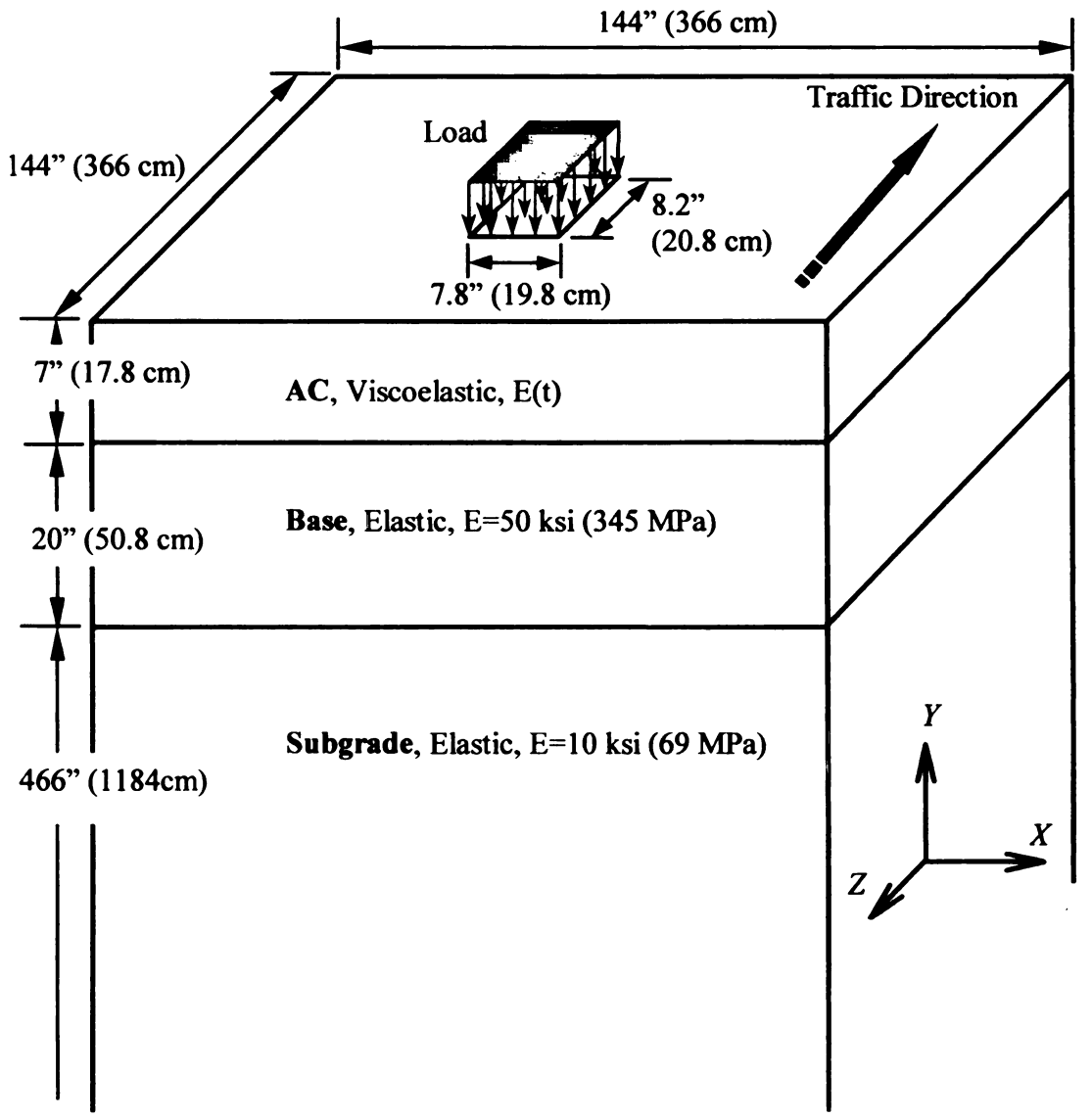


(a) Geometry

Figure 5-11. Three-dimensional model for a three-layer system

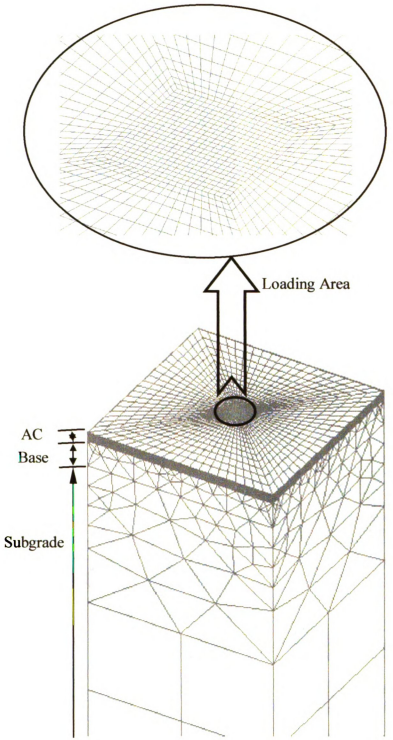


(b) Mesh

Figure 5-11. Three-dimensional model for a three-layer system (continued)

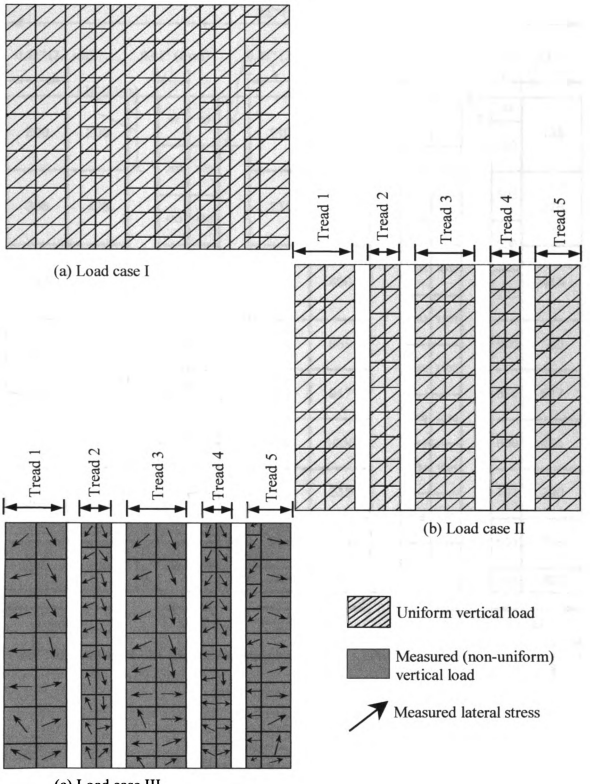


Figure 5-12. Illustration of applied loads in the 3-D analysis

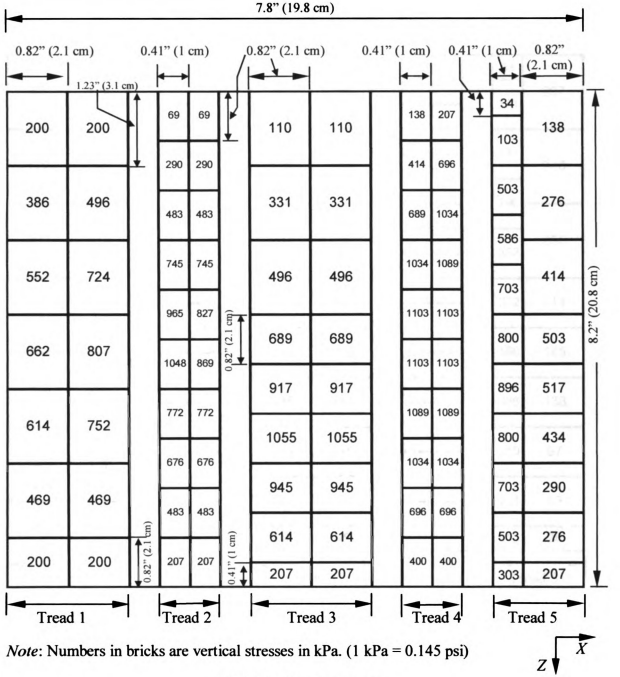


*Note*: Numbers in bricks are vertical stresses in kPa. (1 kPa = 0.145 psi)

(a) Vertical contact stress

Figure 5-13. Measured tire pressure used in the analysis
(modified from Myers et al., 1998)

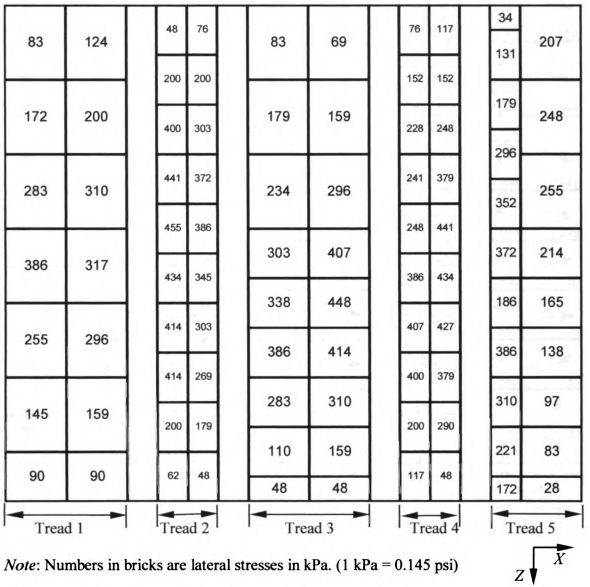


*Note*: Numbers in bricks are lateral stresses in kPa. (1 kPa = 0.145 psi)

(b) Lateral tire-pavement interface stresses

Figure 5-13. Measured tire pressure used in the analysis (modified from Myers et al., 1998) (continued)

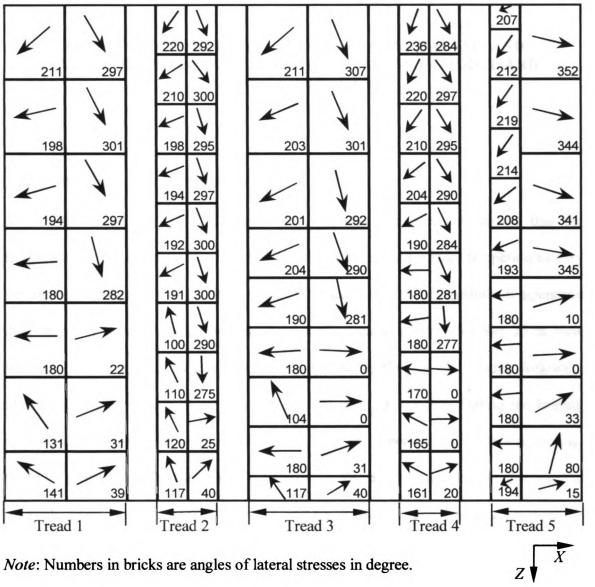


*Note*: Numbers in bricks are angles of lateral stresses in degree.

(c) Orientation of lateral tire-pavement interface stresses

Figure 5-13. Measured tire pressure used in the analysis (modified from Myers et al., 1998) (continued)

# CHAPTER 6

# RESULTS AND DISCUSSION I – FIELD DATA ANALYSIS AND DEVELOPMENT OF TEMPERATURE PREDICTION MODEL AND CORRECTION FACTOR

## 6.1 TEMPERATURE MEASUREMENTS

Data from Site 45 in Traverse City, Michigan (Figure 6-1) shows that the temperature at the bottom of the AC layer as well as the air and surface temperatures vary during the day. Figures 6-2 (a) and (b) illustrate backcalculated AC modulus-temperature data based on temperatures measured at the surface and mid-depth for Site 25 in New Buffalo. Based on these three illustrations it is evident that the AC moduli follows a different curve depending on whether the AC is heating or cooling. During the heating cycle, the AC sublayers are still relatively stiff; whereas, when the AC surface is cooling, the AC sublayers are relatively soft. These cycles have significant impact on the backcalculated modulus of the AC layer, making it difficult to establish a temperature correction model based on the temperature recorded at the top or the bottom of the AC layer.

Figure 6-3 presents a change in temperature gradients recorded in July at site 25. The air and AC surface temperatures fluctuated whereas temperatures at lower depths were relatively stable, resulting in cone-shaped temperature gradient plots. Temperature gradient slopes changed as the pavement alternated between heating and cooling cycles. For example, even though the surface temperatures measured at 3:00 PM and 7:00 PM were close, the subsurface temperatures differed by more than 5 °C (9 °F).

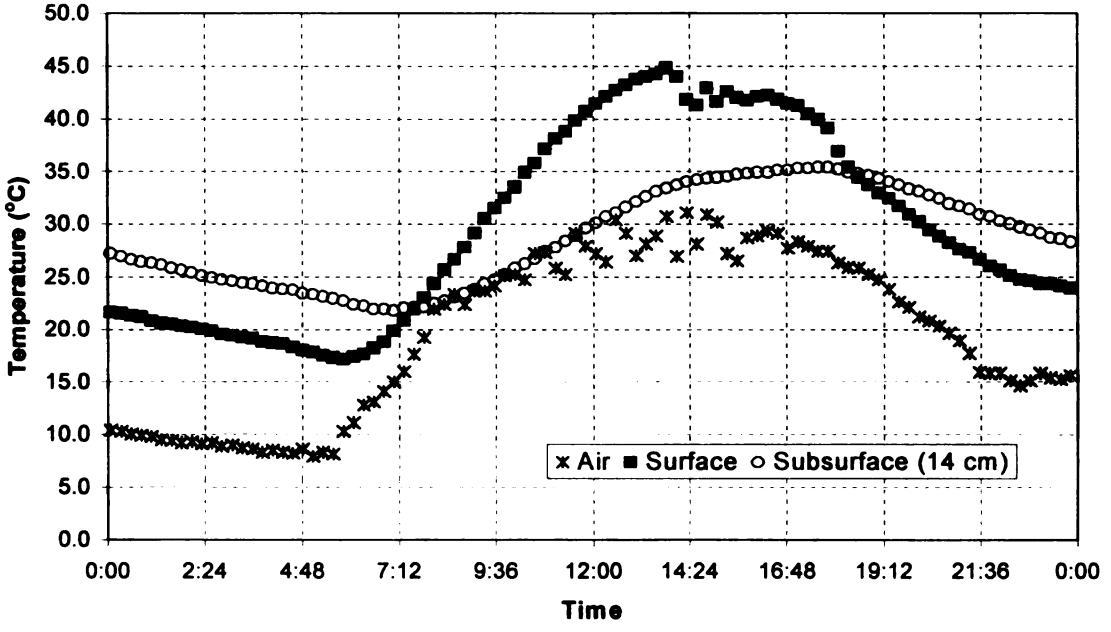


Figure 6-1. Variation of air, surface, and subsurface temperature over a 24 hour period at site 45 (Traverse City, MI)

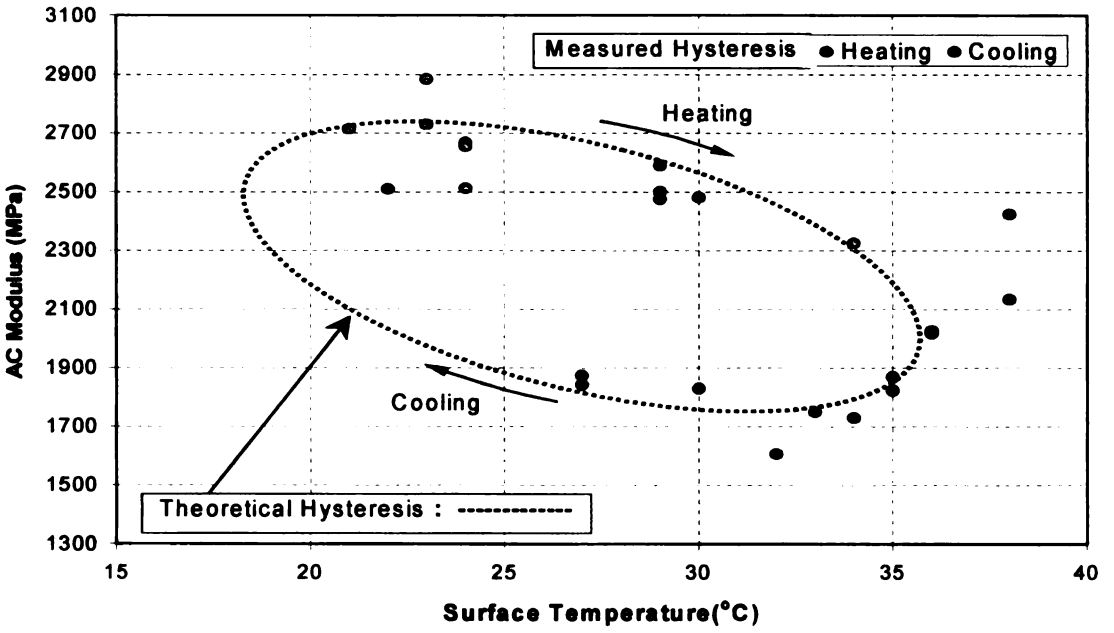


(a)

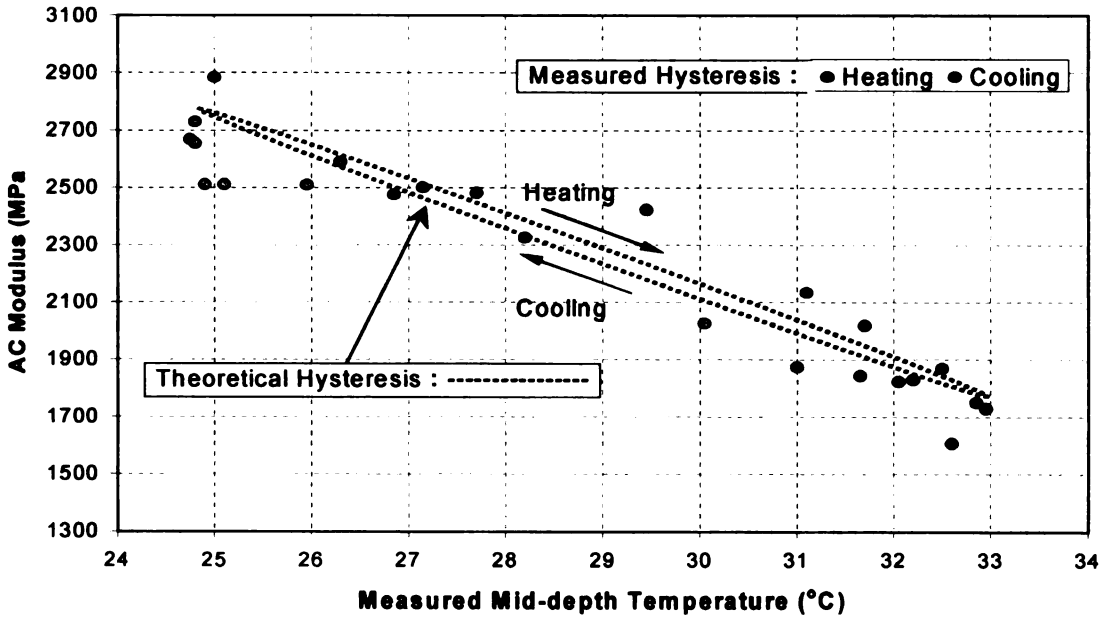


(b)

Figure 6-2. Measured temperature at the surface (a) and the mid-depth (b) vs. AC modulus at site 25 (New Buffalo, MI)

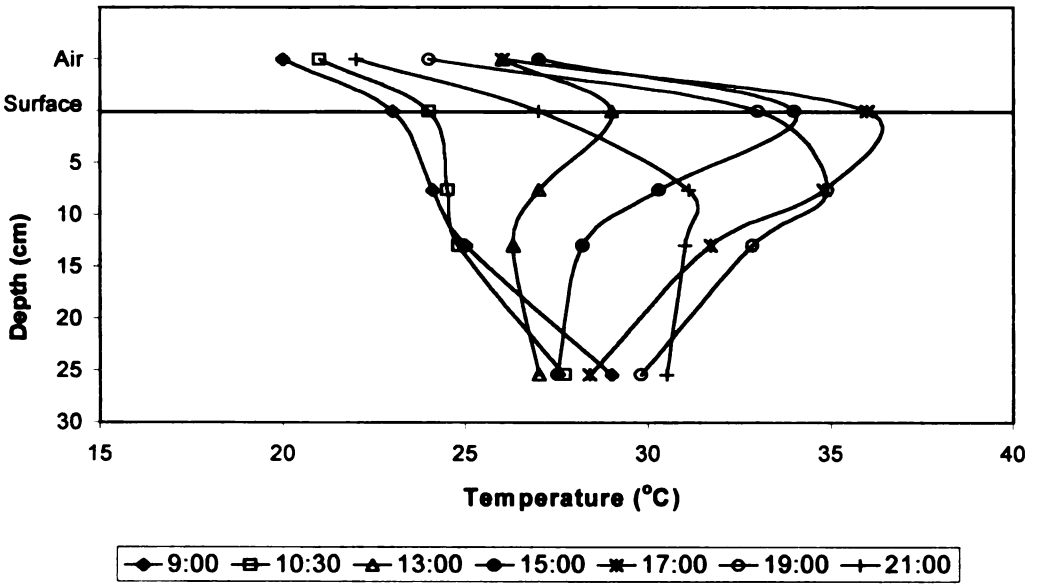


Figure 6-3. Temperature change as a function of pavement depth and time of measurement at site 25 (New Buffalo, MI)

Therefore, both pavement depth and time of FWD testing should be included as input variables in a temperature prediction model.

## 6.2 TEMPERATURE PREDICTION MODEL

In light of the above discussion, a temperature prediction model was developed using 197 data points from the three sites summarized in Tables 4-1 and 4-3. Using non-linear regression techniques and numerical optimization, pavement depth, time of FWD testing, and pavement surface temperature were selected as input variables for the model, and the following model was developed:

$$T_z = T_{surf} + (-0.3451z - 0.0432z^2 + 0.00196z^3) \times \sin(-6.3252t + 5.0967) \qquad (6\text{-}1)$$

where: $T_z$ = AC pavement temperature at depth z, °C
$T_{surf}$ = AC pavement temperature at the surface, °C
$z$ = Depth at which temperature is to be determined, cm.
sin = Sine function, radians
$t$ = Time when the AC surface temperature was measured, days
(0<t <1, e.g., 1:30 p.m. = 13.5/24 = 0.5625 days)

The developed temperature prediction model has a $R^2$ of 99.34%.. Table 6-1 summarizes the statistical parameters associated with this model. Figure 6-4 compares the measured temperature to the predicted temperature for sites 25, 45, and 88. Results from the model overlap the 1:1 or 45° line indicating a very good fit. Site 25 (New Buffalo) showed a slight noise compared to other sites. This was because of field conditions on the test day: heavy traffic and slight rain before measurements.

Table 6-1. Statistical Results of Nonlinear Regression Analysis

| SOURCE | SUM-OF-SQUARES | DEGREE OF FREEDOM | MEAN-SQUARE | F | P-value |
|---|---|---|---|---|---|
| REGRESSION | .206E+06 | 5 | .412E+05 | 5882.346 | 6.334E-208 |
| RESIDUAL | .134E+04 | 192 | 6.997 | | |
| TOTAL | .203E+06 | 197 | | | |
| CORRECTED | .412E+04 | 196 | | | |

RAW R-SQUARED (1-RESIDUAL/TOTAL) = 0.9934

| PARAMETER | ESTIMATE | A.S.E. | CONFIDENCE INTERVAL (95%) | |
|---|---|---|---|---|
| | | | LOWER BOUND | UPPER BOUND |
| a1 | -6.325 | 0.175 | -6.670 | -5.980 |
| a2 | 5.097 | 0.104 | 4.892 | 5.302 |
| a3 | -0.877* | 0.436 | -1.737 | -0.016 |
| a4 | -0.279* | 0.125 | -0.525 | -0.033 |
| a5 | 0.032* | 0.009 | 0.015 | 0.049 |

*a3, a4, and a5 are based on inches. In Equation 6-1, they were converted for centimeters (cm).

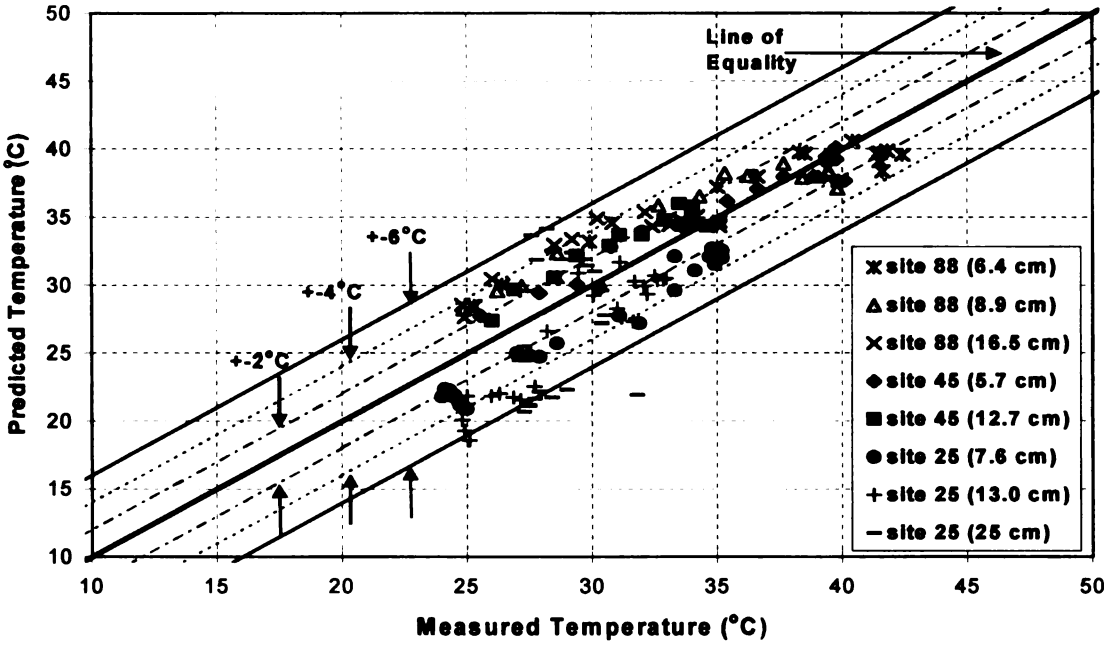


Figure 6-4. Measured temperature vs. predicted temperature at test sites (88, 45, 25)

## 6.3 VALIDATION OF THE TEMPERATURE MODEL

To test the accuracy and robustness of the model presented in Equation 6-1 independent temperature and cross-section information from site 69, two SPS1 sites, eight SMP sites, and one additional site from Arapaho, Nebraska (data obtained from Stubstad et al. (1994)) were acquired. Data from the SMP sites covers a one year period (one week of each month). The data for the site in Texas covers a period from September through January. Figure 6-5, for example, shows a comparison of measured and predicted temperature changes as a function of pavement depth and time of measurement at SPS1 site K24 (St. Johns, MI). Figures 6-6 through 6-14 illustrate the comparison between the measured and predicted at some of the above validation sites.

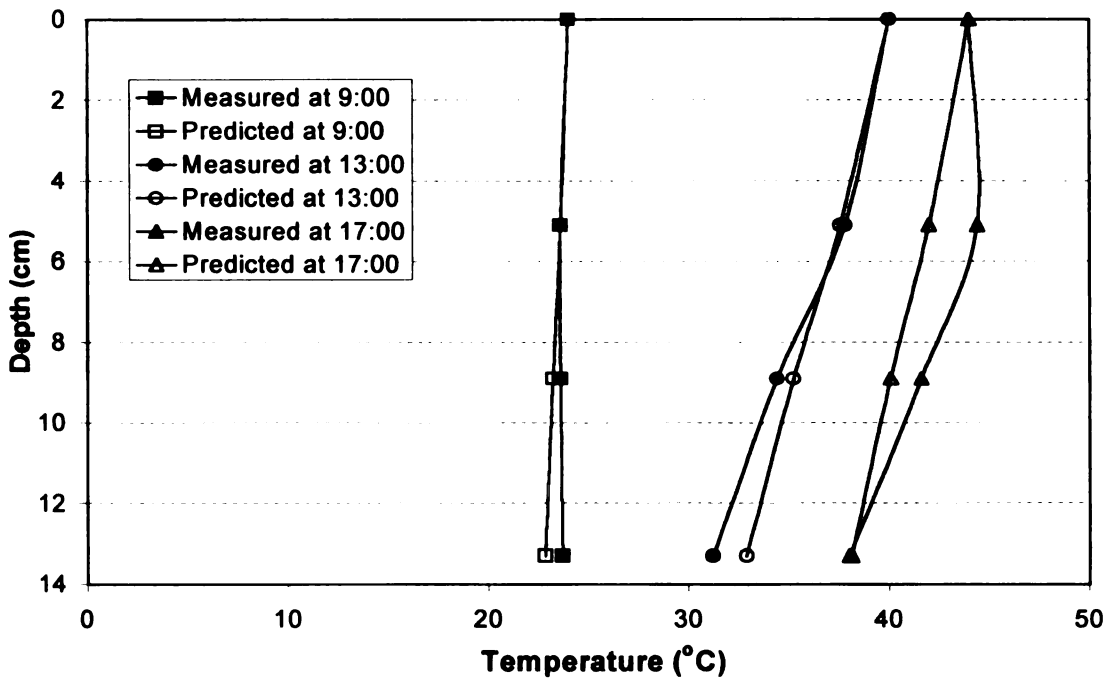


Figure 6-5. Comparison of measured and predicted temperature changes as a function of pavement depth and time of measurement at SPS1 site K24 (St. Johns, MI)

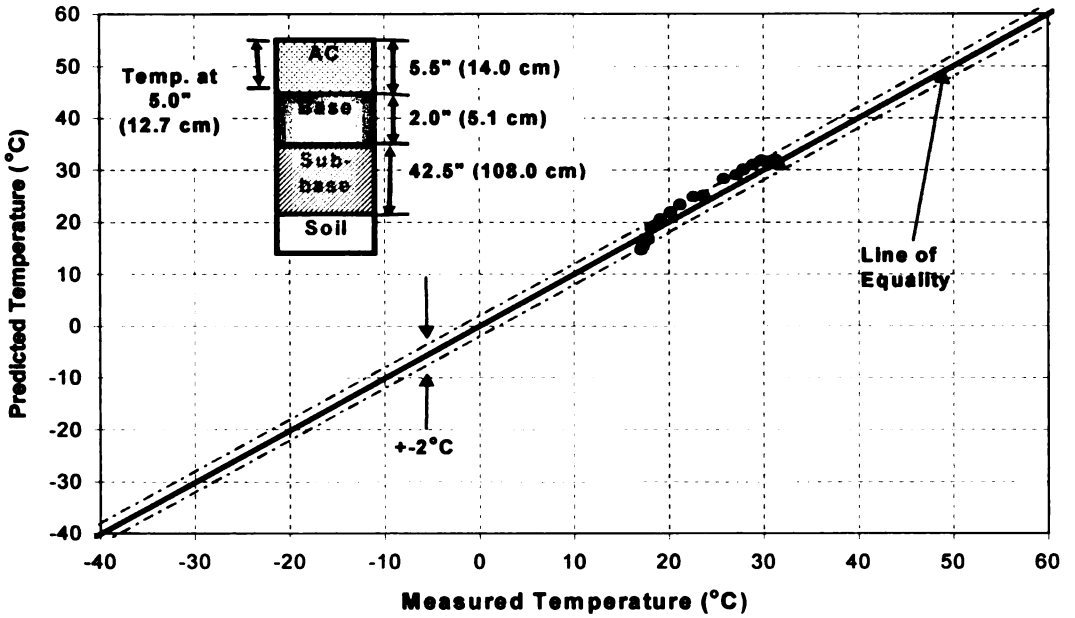


Figure 6-6 (a). Validation: measured temperature vs. predicted temperature at site 69 (Brevort, MI)

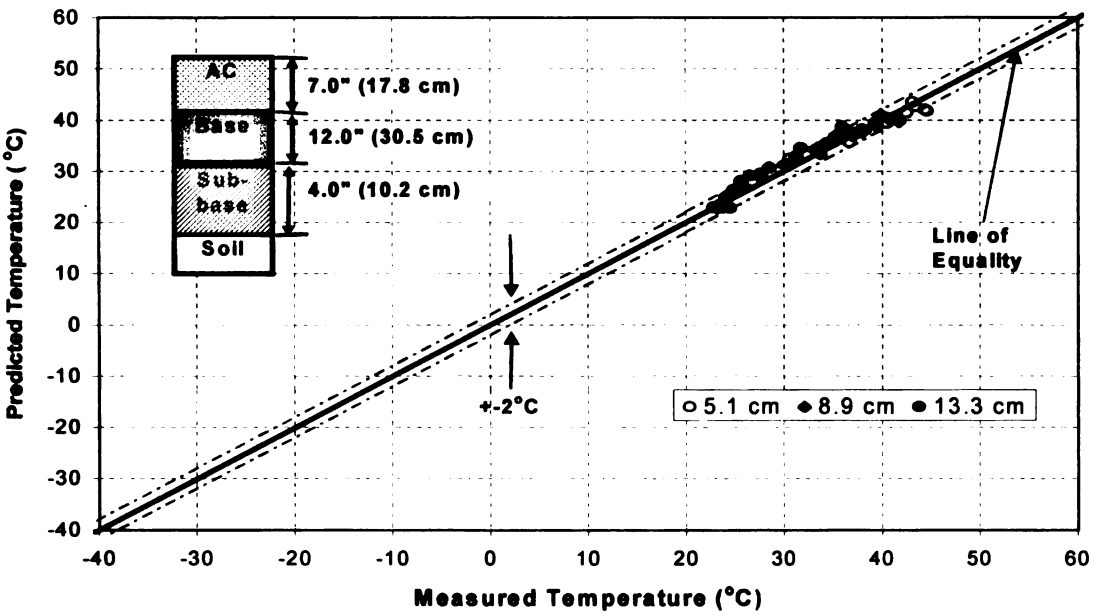


Figure 6-6 (b). Validation: measured temperature vs. predicted temperature at SPS1 site K24 (St. Johns, MI)

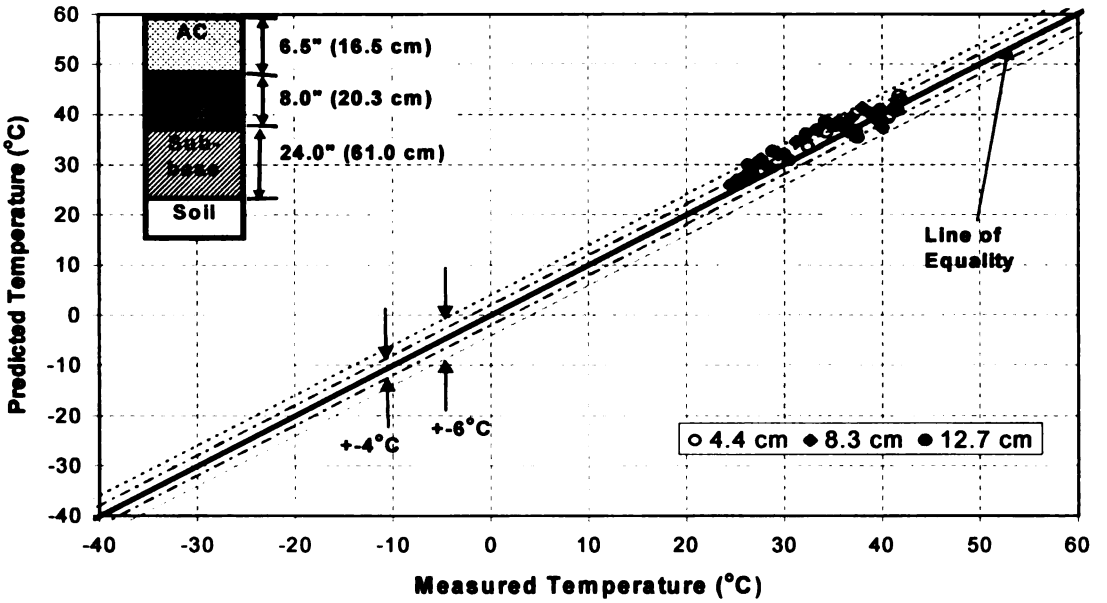


Figure 6-6 (c). Validation: measured temperature vs. predicted temperature at SPS1 site K59 (St. Johns, MI)

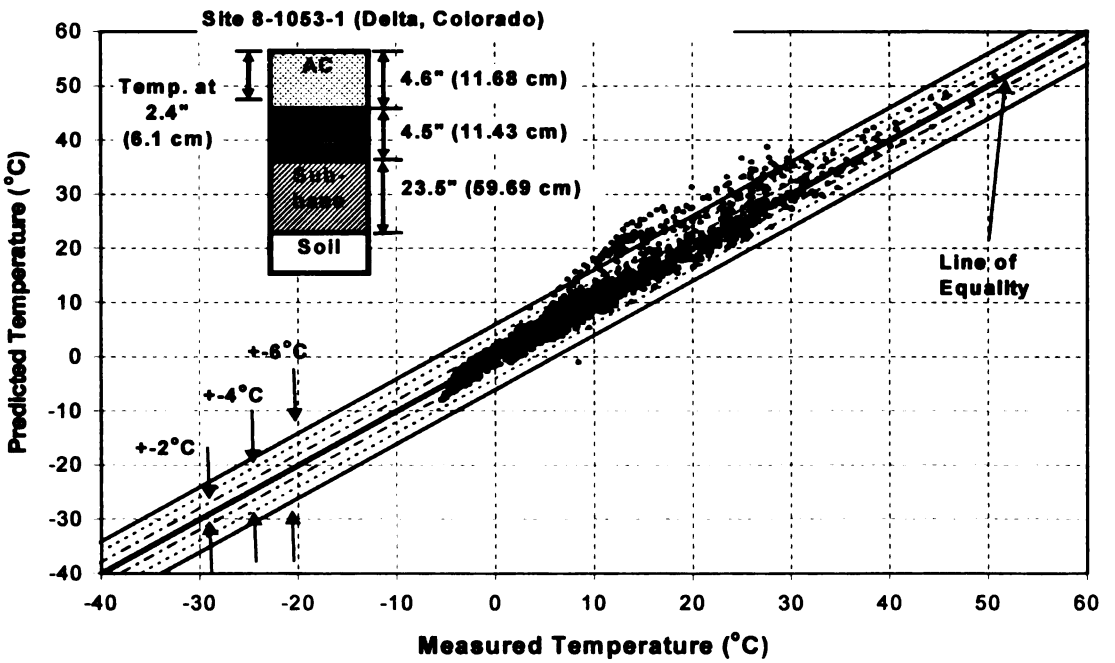


Figure 6-7 (a). Validation: measured temperature vs. predicted temperature at the middepth of 6.1 cm (site 8-1053-1, Colorado)

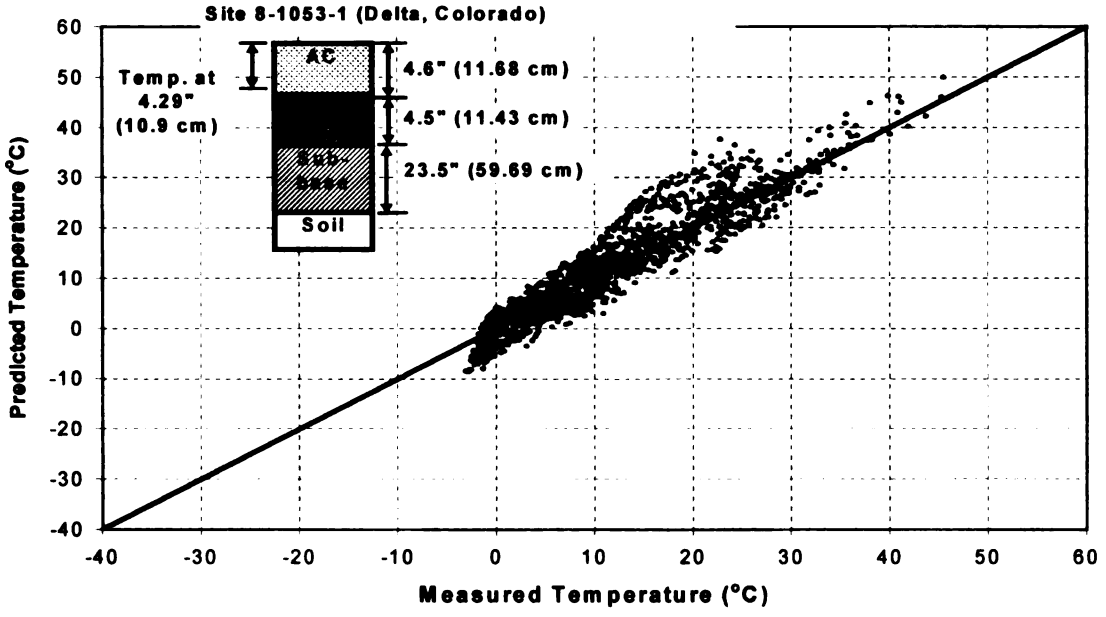


Figure 6-7 (b). Validation: measured temperature vs. predicted temperature at the bottom (site 8-1053-1, Colorado)

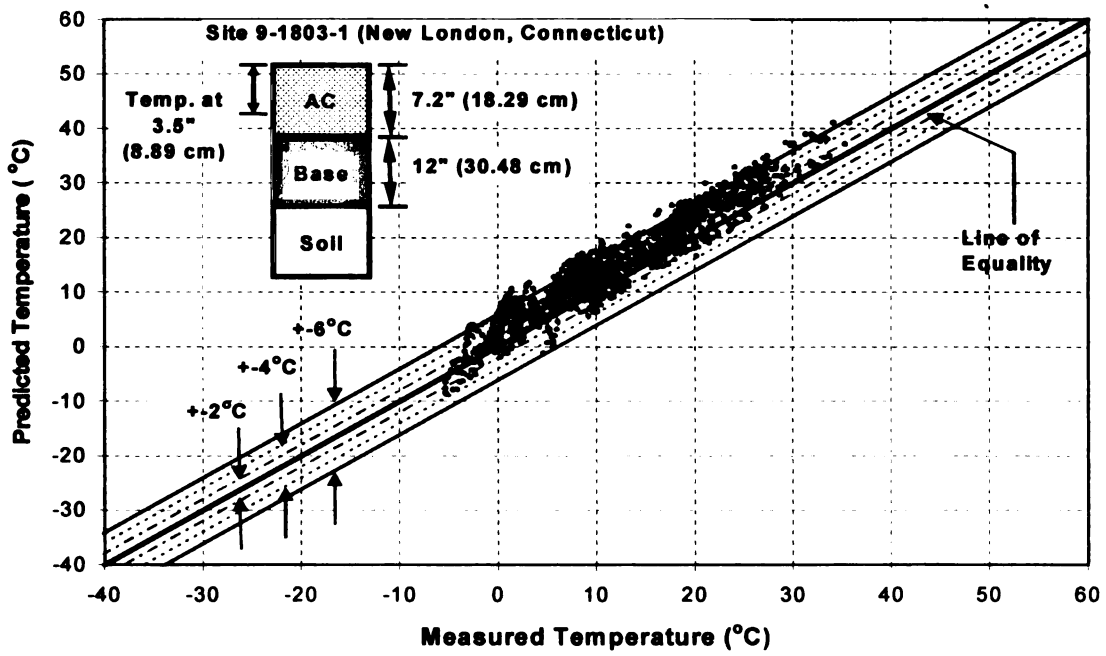


Figure 6-8 (a). Validation: measured temperature vs. predicted temperature at the middepth of 8.89 cm (site 9-1803-1, Connecticut)

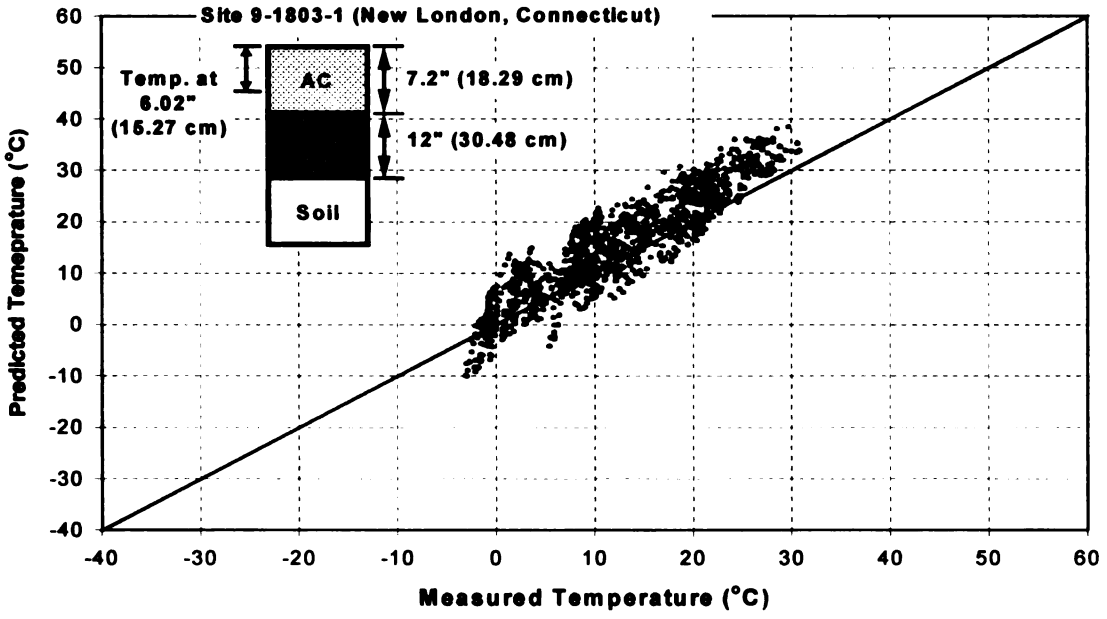


Figure 6-8 (b). Validation: measured temperature vs. predicted temperature at the bottom (site 9-1803-1, Connecticut)

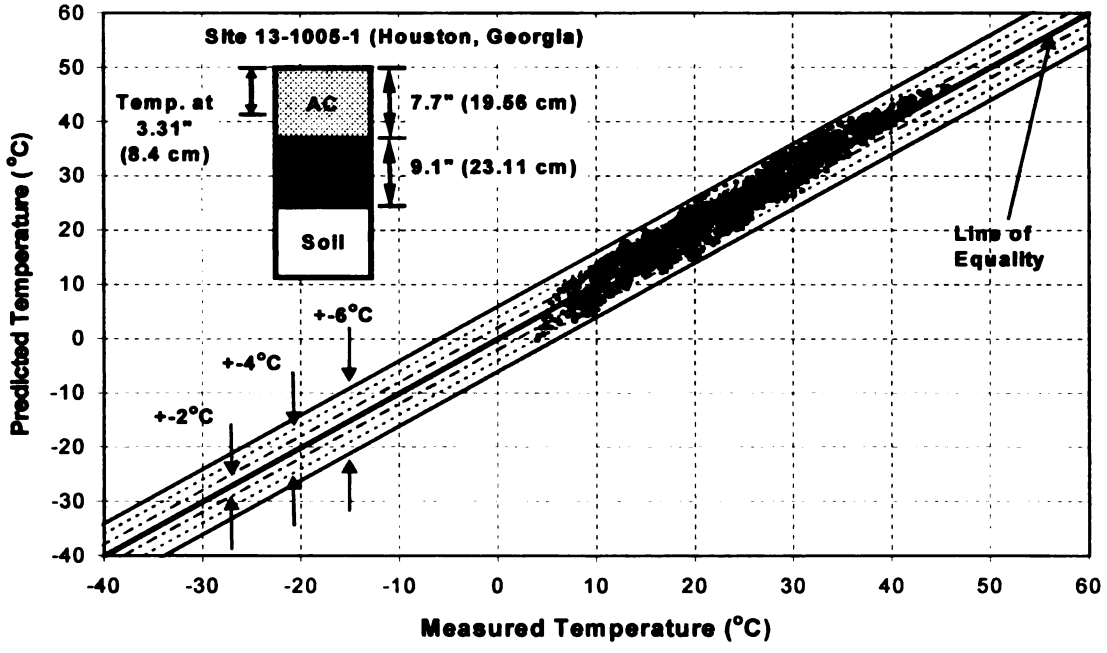


Figure 6-9 (a). Validation: measured temperature vs. predicted temperature at the middepth of 8.4 cm (site 13-1005-1, Georgia)

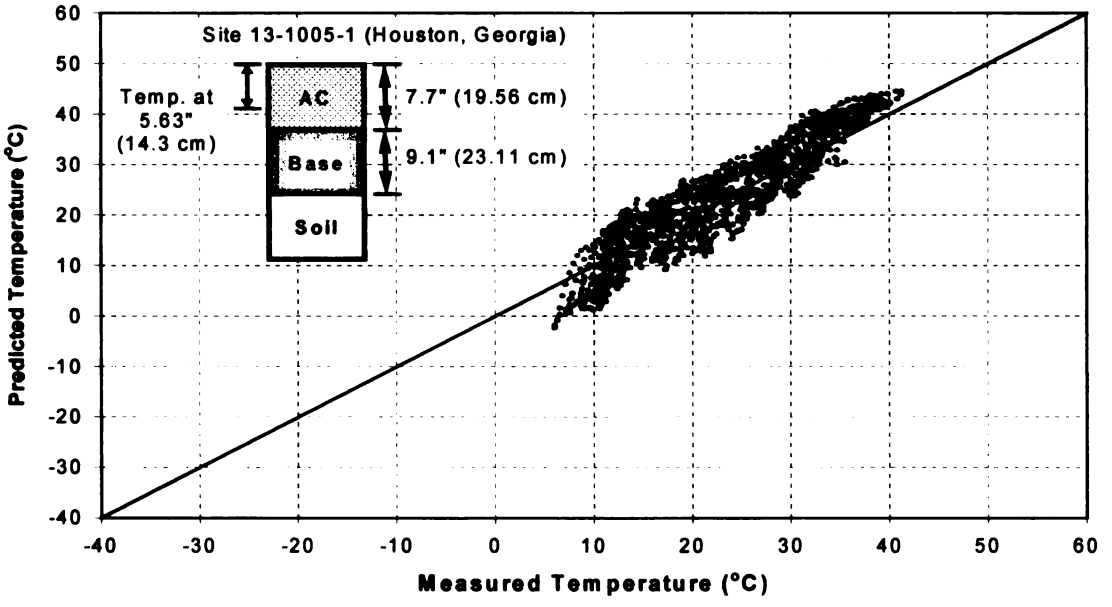


Figure 6-9 (b). Validation: measured temperature vs. predicted temperature at the bottom (site 13-1005-1, Georgia)

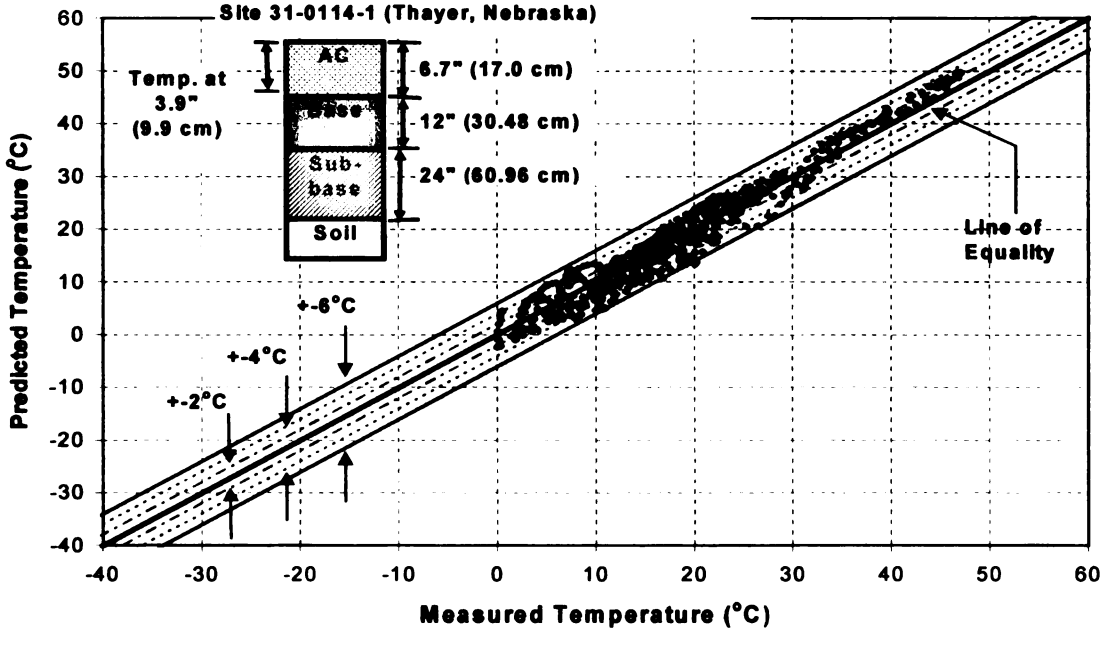


Figure 6-10. Validation: measured temperature vs. predicted temperature at the middepth of 9.9 cm (site 31-0114-1, Nebraska)

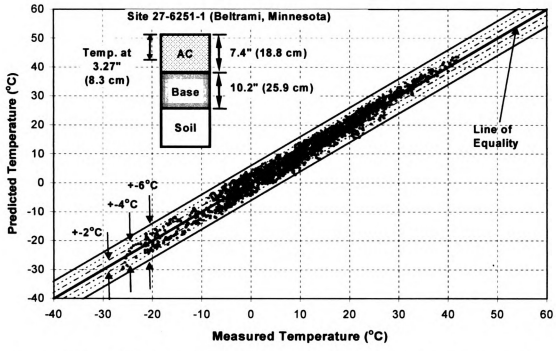


Figure 6-11 (a). Validation: measured temperature vs. predicted temperature at the middepth of 8.3 cm (site 27-6251-1, Minnesota)

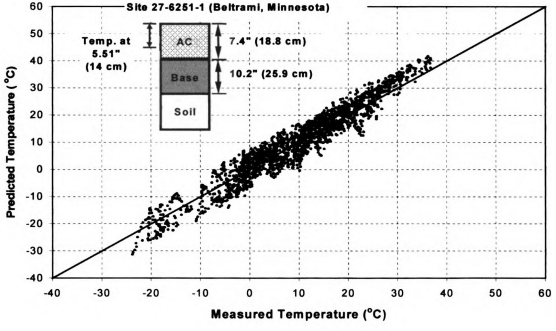


Figure 6-11 (b). Validation: measured temperature vs. predicted temperature at the bottom (site 27-6251-1, Minnesota)

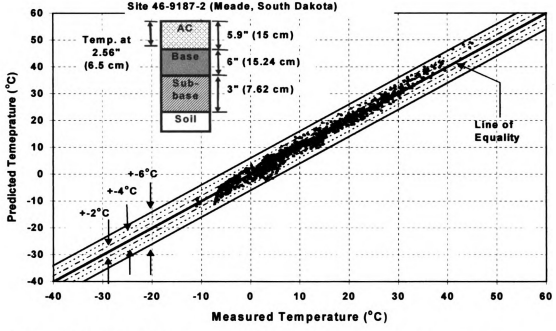


Figure 6-12 (a). Validation: measured temperature vs. predicted temperature at the middepth of 6.5 cm (site 46-9187-2, South Dakota)

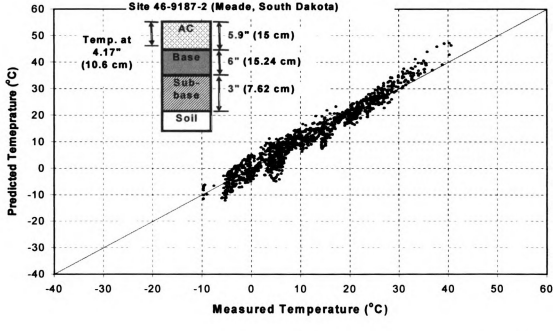


Figure 6-12 (b). Validation: measured temperature vs. predicted temperature at the bottom (site 46-9187-2, South Dakota)

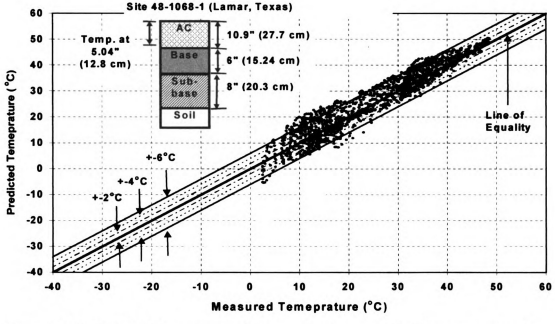


Figure 6-13 (a). Validation: measured temperature vs. predicted temperature at the middepth of 12.8 cm (site 48-1068-1, Texas)

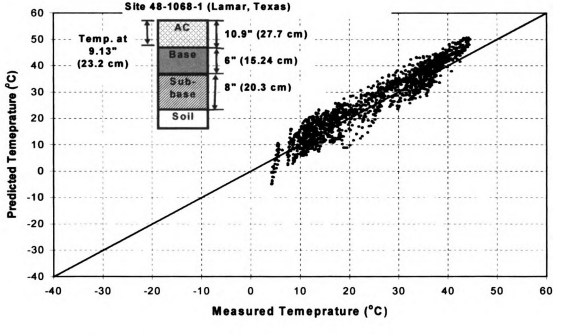


Figure 6-13 (b). Validation: measured temperature vs. predicted temperature at the bottom (site 48-1068-1, Texas)

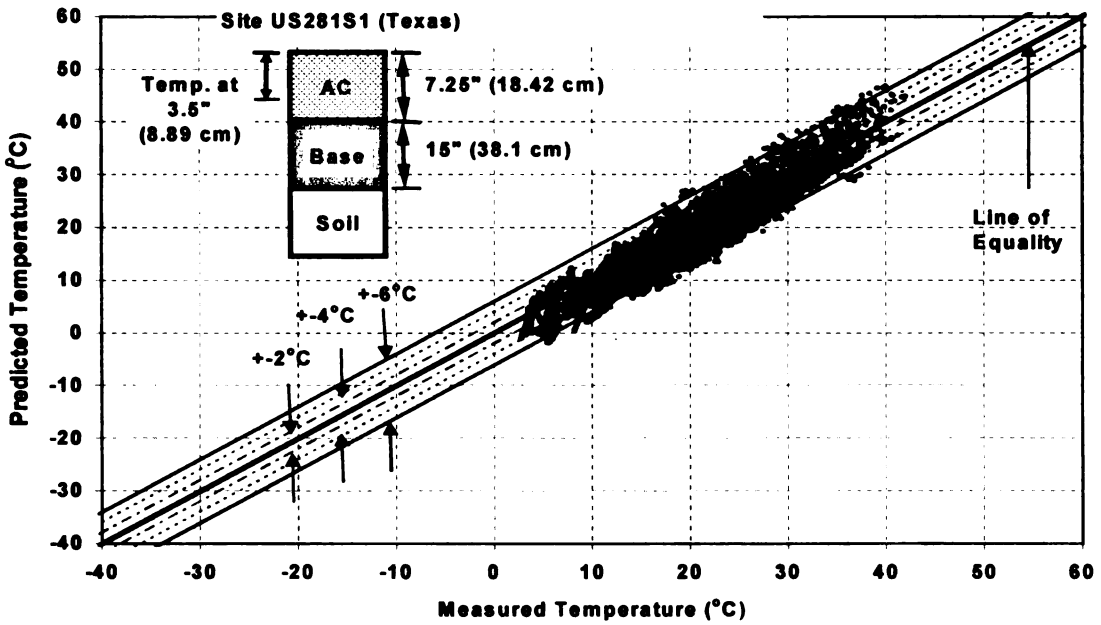


Figure 6-14 (a). Validation: measured temperature vs. predicted temperature at the middepth of 8.89 cm (US281S1, Texas)

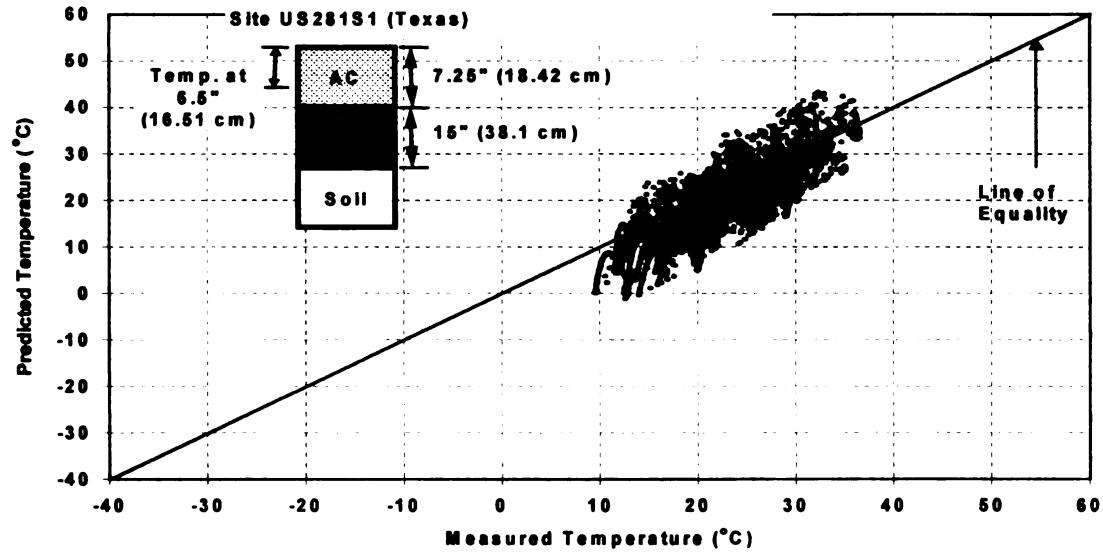


Figure 6-14 (b). Validation: measured temperature vs. predicted temperature at the bottom (US281S1, Texas)

The results from the developed model again overlap the 1:1 or 45° line, indicating that this model has wide-ranging applicability. The newly developed model was comparable to other popular models even though fewer input variables and a simpler procedure was adopted (Figure 6-15).

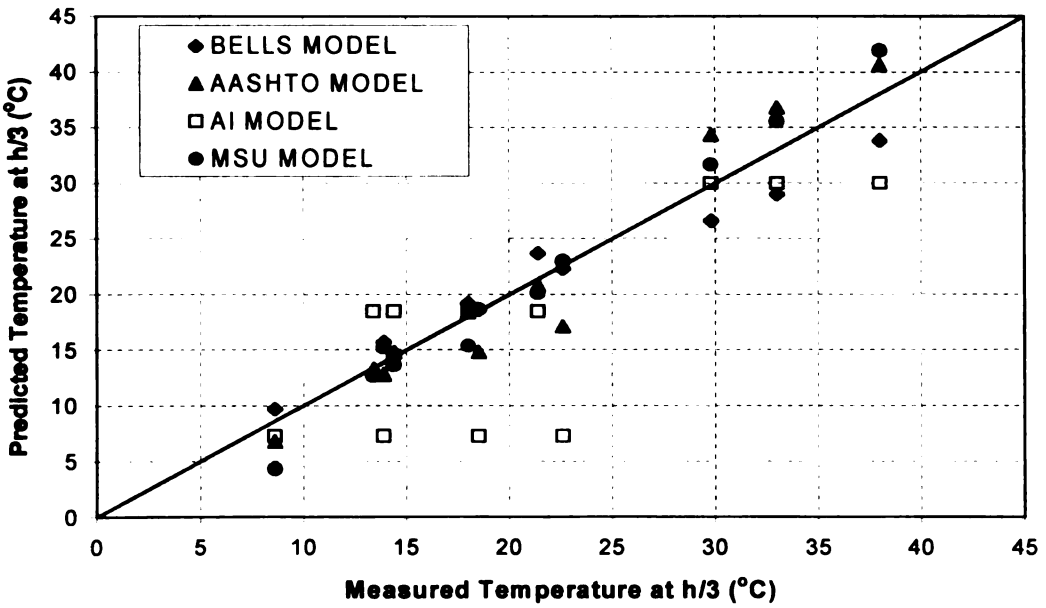


Figure 6-15. Comparison between the MSU model and other models using data from Stubstad et al. (1994). (h/3 represents one third depth of the AC layer)

## 6.4 TEMPERATURE CORRECTION FACTOR FOR AC MODULUS

The deflection profiles and pavement cross-sections were used as inputs to backcalculate the layer moduli for the four test sites (sites 25, 45, 69, 88) and two SPS1 sites (K24, K59). Maximum deflections were measured at a load level of 40 kN (9000

lbs). Figure 6-16 shows the dependence of AC modulus and peak deflection and the independence of base and roadbed modulus on mid-depth AC temperature.

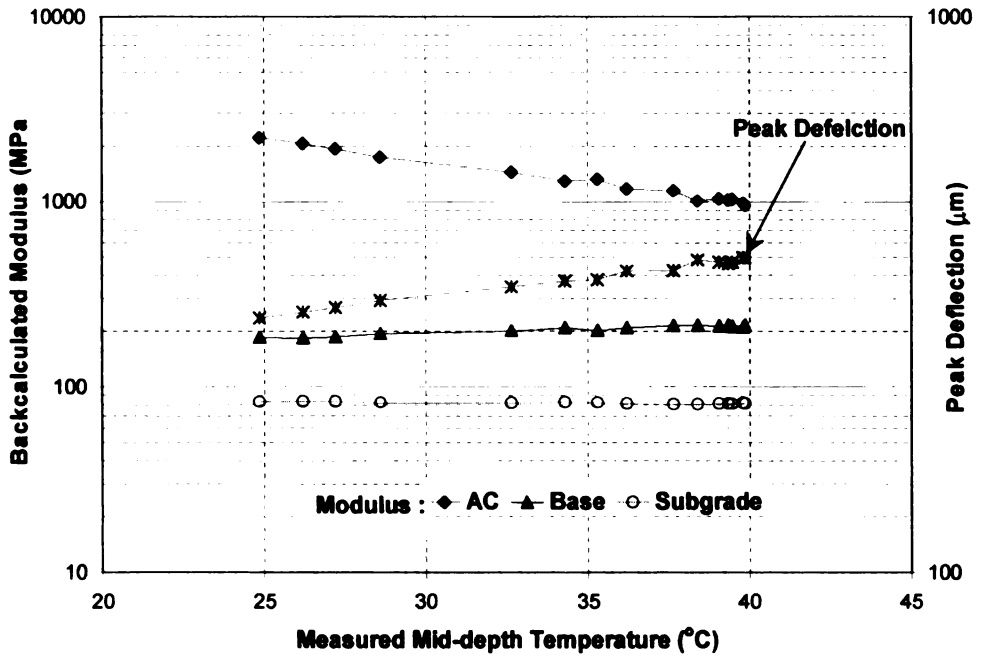


Figure 6-16. Measured mid-depth temperature vs. backcalculated modulus of each layer and peak deflection at site 88 (Deerton, MI)

The backcalculated AC modulus is corrected to a reference pavement temperature $T_r$ (25°C) in accordance with Equation 6-2:

$$E_{Tr} = E_T \times CF \tag{6-2}$$

where:

| | | |
|---|---|---|
| $E_{Tr}$ | = | Corrected AC modulus to the reference temperature $T_r$ such as 25 °C |
| $E_T$ | = | Backcalculated AC modulus at measured middepth temperature T |
| CF | = | Correction factor |

The general relationship between mid-depth temperature and backcalculated AC modulus can be described as follows (e.g., backcalculated AC modulus-middepth temperature data in Figure 16):

$$\log E_T = b + a * T \tag{6-3}$$

where:

| | | |
|---|---|---|
| $E_T$ | = | Backcalculated AC modulus at mid-depth temperature T |
| T | = | Middepth temperature |
| a, b | = | Regression constants |

By substituting Equation 6-3 into Equation 6-2, the correction factor is derived in terms of "a" (regression constant in Equation 6-3):

$$CF = 10^{a(Tr-T)} \tag{6-4}$$

Therefore, the correction factor is determined by the slope, "a", of the linear fit of temperature versus the log of the backcalculated modulus relationship (Kim et al., 1996). Table 6-2 presents the statistical parameters associated with regressions for constant "a". Table 6-3 summarizes the computed values for constant "a" at each site based on measured and predicted mid-depth temperature. Values of "a" obtained using measured and predicted mid-depth temperature at each site are consistent, which also indicates that the temperature prediction and correction procedures were valid.

Table 6-2. Statistical Results of Regression Analysis for Constant "a"

**Site 25 - Regression based on Predicted Mid-depth Temperautre**

| SOURCE | SUM-OF-SQUARES | DF | MEAN-SQUARE | F | p-value |
|---|---|---|---|---|---|
| REGRESSION | 268.47 | 2 | 134.24 | 71174.58 | 1.19952E-42 |
| RESIDUAL | 0.04 | 22 | 0.0019 | | |
| TOTAL | 268.51 | 24 | | | |
| CORRECTED | 0.13 | 23 | | | |

RAW R-SQUARED (1-RESIDUAL/TOTAL) = 0.99985

**Site 25 - Regression based on Measured Mid-depth Temperautre**

| SOURCE | SUM-OF-SQUARES | DF | MEAN-SQUARE | F | p-value |
|---|---|---|---|---|---|
| REGRESSION | 268.50 | 2 | 134.25 | 223005.6 | 4.20349E-48 |
| RESIDUAL | 0.01 | 22 | 0.0006 | | |
| TOTAL | 268.51 | 24 | | | |
| CORRECTED | 0.13 | 23 | | | |

RAW R-SQUARED (1-RESIDUAL/TOTAL) = 0.99995

**Site 45 - Regression based on Predicted Mid-depth Temperautre**

| SOURCE | SUM-OF-SQUARES | DF | MEAN-SQUARE | F | p-value |
|---|---|---|---|---|---|
| REGRESSION | 188.77 | 2 | 94.38 | 38242.825 | 1.49004E-23 |
| RESIDUAL | 0.03 | 12 | 0.0025 | | |
| TOTAL | 188.80 | 14 | | | |
| CORRECTED | 0.03 | 13 | | | |

RAW R-SQUARED (1-RESIDUAL/TOTAL) = 0.99984

Table 6-2. Statistical Results of Regression Analysis for Constant "a" (Continued)

**Site 45 - Regression based on Measured Mid-depth Temperautre**

| SOURCE | SUM-OF-SQUARES | DF | MEAN-SQUARE | F | p-value |
|---|---|---|---|---|---|
| REGRESSION | 188.77 | 2 | 94.38 | 39774.067 | 1.17737E-23 |
| RESIDUAL | 0.03 | 12 | 0.0024 | | |
| TOTAL | 188.80 | 14 | | | |
| CORRECTED | 0.03 | 13 | | | |

RAW R-SQUARED (1-RESIDUAL/TOTAL) = 0.99985

**Site 69 - Regression based on Predicted Mid-depth Temperautre**

| SOURCE | SUM-OF-SQUARES | DF | MEAN-SQUARE | F | p-value |
|---|---|---|---|---|---|
| REGRESSION | 249.06 | 2 | 124.53 | 59272.102 | 4.28486E-35 |
| RESIDUAL | 0.04 | 18 | 0.0021 | | |
| TOTAL | 249.10 | 20 | | | |
| CORRECTED | 0.37 | 19 | | | |

RAW R-SQUARED (1-RESIDUAL/TOTAL) = 0.99985

**Site 88 - Regression based on Predicted Mid-depth Temperautre**

| SOURCE | SUM-OF-SQUARES | DF | MEAN-SQUARE | F | p-value |
|---|---|---|---|---|---|
| REGRESSION | 192.09 | 2 | 96.05 | 60339.324 | 1.83839E-33 |
| RESIDUAL | 0.03 | 17 | 0.0016 | | |
| TOTAL | 192.12 | 19 | | | |
| CORRECTED | 0.49 | 18 | | | |

RAW R-SQUARED (1-RESIDUAL/TOTAL) = 0.99986

Table 6-2. Statistical Results of Regression Analysis for Constant "a" (Continued)

**Site 88 - Regression based on Measured Mid-depth Temperautre**

| SOURCE | SUM-OF-SQUARES | DF | MEAN-SQUARE | F | p-value |
|---|---|---|---|---|---|
| REGRESSION | 145.73 | 2 | 72.87 | 464114.78 | 2.82379E-32 |
| RESIDUAL | 0.00 | 13 | 0.0002 | | |
| TOTAL | 145.73 | 15 | | | |
| CORRECTED | 0.22 | 14 | | | |

RAW R-SQUARED (1-RESIDUAL/TOTAL) = 0.99999

**K24 - Regression based on Predicted Mid-depth Temperautre**

| SOURCE | SUM-OF-SQUARES | DF | MEAN-SQUARE | F | p-value |
|---|---|---|---|---|---|
| REGRESSION | 185.01 | 2 | 92.50 | 22405.577 | 8.59406E-27 |
| RESIDUAL | 0.06 | 15 | 0.0041 | | |
| TOTAL | 185.07 | 17 | | | |
| CORRECTED | 0.50 | 16 | | | |

RAW R-SQUARED (1-RESIDUAL/TOTAL) = 0.99967

**K24 - Regression based on Measured Mid-depth Temperautre**

| SOURCE | SUM-OF-SQUARES | DF | MEAN-SQUARE | F | p-value |
|---|---|---|---|---|---|
| REGRESSION | 185.03 | 2 | 92.51 | 33737.168 | 3.99412E-28 |
| RESIDUAL | 0.04 | 15 | 0.0027 | | |
| TOTAL | 185.07 | 17 | | | |
| CORRECTED | 0.50 | 16 | | | |

RAW R-SQUARED (1-RESIDUAL/TOTAL) = 0.99978

Table 6-2. Statistical Results of Regression Analysis for Constant "a" (Continued)

**K59 - Regression based on Predicted Mid-depth Temperautre**

| SOURCE | SUM-OF-SQUARES | DF | MEAN-SQUARE | F | p-value |
|---|---|---|---|---|---|
| REGRESSION | 138.82 | 2 | 69.41 | 15840.069 | 3.28128E-24 |
| RESIDUAL | 0.06 | 14 | 0.0044 | | |
| TOTAL | 138.88 | 16 | | | |
| CORRECTED | 0.36 | 15 | | | |

RAW R-SQUARED (1-RESIDUAL/TOTAL) = 0.99956

**K59 - Regression based on Measured Mid-depth Temperautre**

| SOURCE | SUM-OF-SQUARES | DF | MEAN-SQUARE | F | p-value |
|---|---|---|---|---|---|
| REGRESSION | 138.86 | 2 | 69.43 | 39657.278 | 5.33199E-27 |
| RESIDUAL | 0.02 | 14 | 0.0018 | | |
| TOTAL | 138.88 | 16 | | | |
| CORRECTED | 0.36 | 15 | | | |

RAW R-SQUARED (1-RESIDUAL/TOTAL) = 0.99982

Table 6-3. Regression Constant "a" at Each Test Site

| Site No. | "a" value | |
|---|---|---|
| | Based on Measured Middepth Temperature | Based on Predicted Middepth Temperature |
| 25 | -0.0230 | -0.0140 |
| 45 | -0.0037 | -0.0039 |
| 69 | | -0.0176 |
| 88 | -0.0231 | -0.0231 |
| K24 | -0.0256 | -0.0265 |
| K59 | -0.0250 | -0.0257 |

## 6.5 INFLUENCE OF TEMPERATURE PREDICTION ON PERFORMANCE PREDICTION

In order to investigate effects of middepth temperature prediction error (ΔT) on performance prediction, a three step procedure was applied. First, AC moduli based on measured and predicted middepth temperatures were backcalculated using MICHBACK and adjusted to a reference pavement temperature (25 °C). Second, these backcalculated moduli were used to compute structural responses using CHEVRONX. Finally, based on these analysis results, rut depths were calculated using the following performance (rut) model (Kim et al., 2000).

$$RD = \left(-0.016H_{AC} + 0.033\ln(SD) + 0.011T_{annual} - 0.01\ln(KV)\right) \cdot \left(-2.703 + 0.657\left(\varepsilon_{v,base}\right)^{0.097} + 0.271\left(\varepsilon_{v,SG}\right)^{0.883} + 0.258\ln(N) - 0.034\ln\left(\frac{E_{AC}}{E_{SG}}\right)\right) \quad (6\text{-}5)$$

where:

| | | |
|---|---|---|
| RD | = | average rut depth along a specified wheel path segment (inch) |
| SD | = | pavement surface deflection (in.), |
| KV | = | kinematic viscosity (centistroke), |
| $T_{annual}$ | = | annual ambient temperature (°F), |
| $H_{AC}$ | = | thickness of asphalt concrete (in.), |
| N | = | cumulative traffic volume (ESAL), |
| $\varepsilon_{v,base}$ | = | vertical compressive strain at the top of base layer ($10^{-3}$), |
| $\varepsilon_{v,SG}$ | = | vertical compressive strain at the top of subgrade ($10^{-3}$), |
| $E_{AC}$ | = | resilient modulus of asphalt concrete (psi), and |
| $E_{SG}$ | = | resilient modulus of subgrade (psi). |

Middepth temperature difference of ±4 °C resulted in a 3% performance (rutting) error in rut prediction (Figure 6-17). The error for temperature corrected AC modulus ranges from 10% to 20% based on a ±2 °C and ±4 °C middepth temperature difference, respectively. These results imply that middepth temperature predictions within ±4 °C

deviation does not significantly affect the performance prediction. This was further investigated statistically, using t-tests performed for the two groups of computed ruts based on measured and predicted middepth temperatures. A temperature deviation of ±4 °C and an α risk value of 0.02 (risk of error) were used. It was concluded that means of two groups are not different with P-value for two-tail tests equal to 0.973. If the p-value is much larger than the specified α risk, it indicates that the means of two groups are not significantly different. This t-test was carried out for corrected AC moduli and structural responses as well, and it was found that a middepth temperature prediction deviation within ±4 °C does not significantly influence them. t-test for temperature prediction deviation within ±2 °C produced similar results. Therefore, ±4 °C of middepth temperature prediction deviation can be used as a criterion for the accuracy of the model. Accordingly, bandwidths of ±2, ±4, and ±6 °C are shown in the validation plots of middepth temperature prediction (Figures 6-6 through 6-14) to illustrate the accuracy of the model. It can be seen that most data resides within ±4 °C bandwidth.

## 6.6 SUMMARY

A practical and accurate subsurface temperature prediction model for asphalt concrete pavements was developed. Temperature correction factors for AC modulus were computed based on measured and predicted mid-depth temperatures, which resulted in consistent values. The form of the new temperature prediction model for AC pavements accounts for the temperature gradients which vary with time of day when FWD profiles are measured. Predicted temperatures at various depths were in good agreement with measured temperatures, demonstrating an acceptable degree of accuracy for the model,

thus promising potential use by state highway agencies. The model's robustness and accuracy were validated using data from SPS1 and SMP sites, and an investigation of the influence of temperature prediction errors on performance prediction was conducted. The validation results confirmed that the model could be adopted in other climatic and geographic regions.

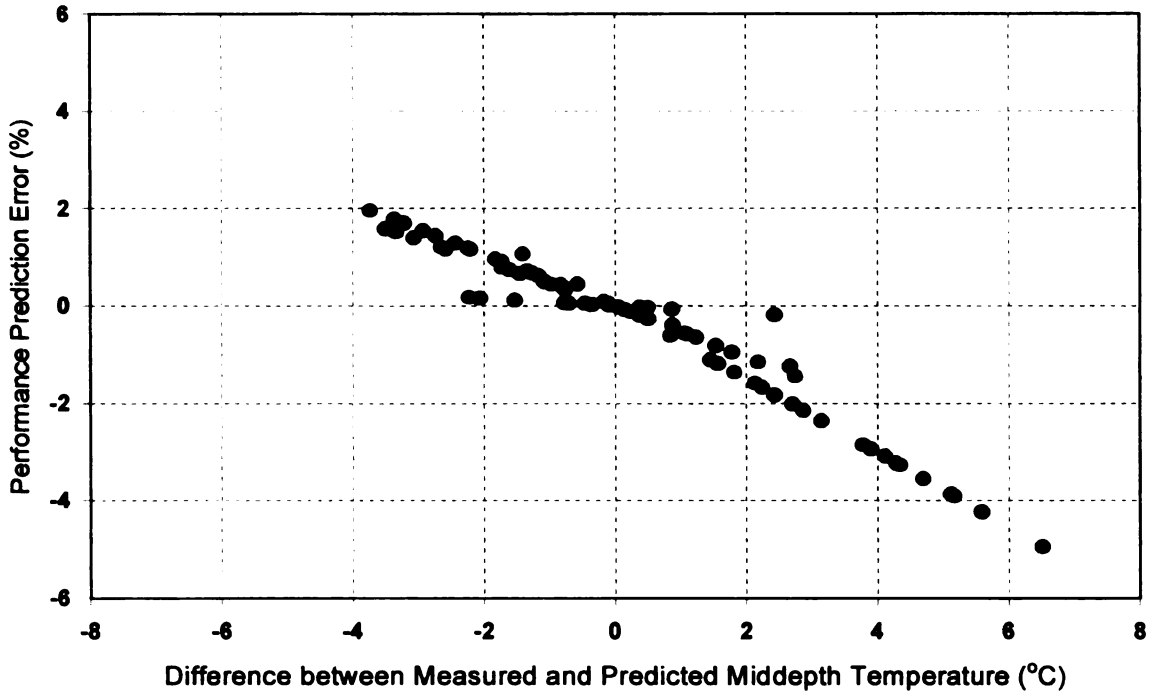


Figure 6-17. Performance (rutting) prediction error caused by middepth temperature prediction deviation

# CHAPTER 7

# RESULTS AND DISCUSSION II – FINITE ELEMENT ANALYSIS

## 7.1 TWO-DIMENSIONAL FINITE ELEMNET (FE) MODEL

The tensile strain at the bottom of AC layer has traditionally been used as a design criterion to assess the number of load applications likely to initiate fatigue cracking. Recently, Briggs and Lukanen (2000) presented the relationship between the number of applications of a given strain level to achieve failure. They concluded that the estimated number of applications to failure was very sensitive to changes in strain. Likewise, the vertical compressive stress/strain on top of AC, base, and subgrade layers has been used to prevent rutting (Figure 7-1).

In an axisymmetric state of stress, only four nonzero stress components, $\sigma_r$, $\sigma_\theta$, $\sigma_z$, and $\tau_{zr}$, exist. Along the axis of symmetry (r = 0), $\tau_{zr} = 0$ and $\sigma_r = \sigma_\theta$. The major and minor principal stresses along the axis of symmetry (r = 0) coincide with either the vertical stress $\sigma_z$ or the horizontal stress $\sigma_r$ (= $\sigma_\theta$) depending on the vertical position z (Figure 3-1). Figures 7-2 and 7-3 show stress plots with time and depth for a case of 18 cm (7") thick AC, base modulus of 345 MPa (50 psi), morning temperature, and uniform FWD load. These plots show typical stress behaviors during FWD loading. Maximum stresses are found at the surface of the AC layer during loading. Bending stresses result in compression in the horizontal direction at the surface of the layer in the vicinity of the load, and tension at the bottom.

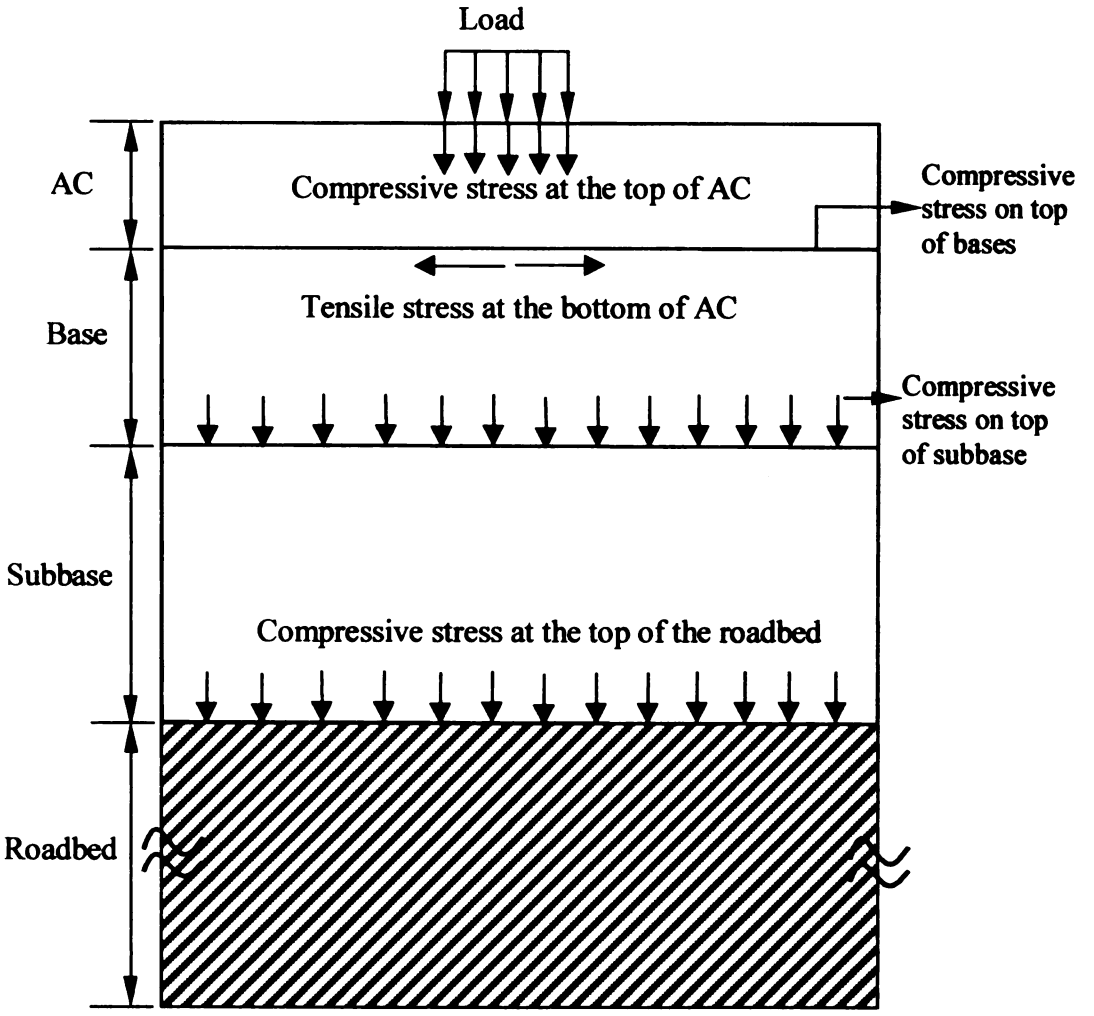


Figure 7-1. Illustration of critical stress/strain locations in a typical pavement structure.

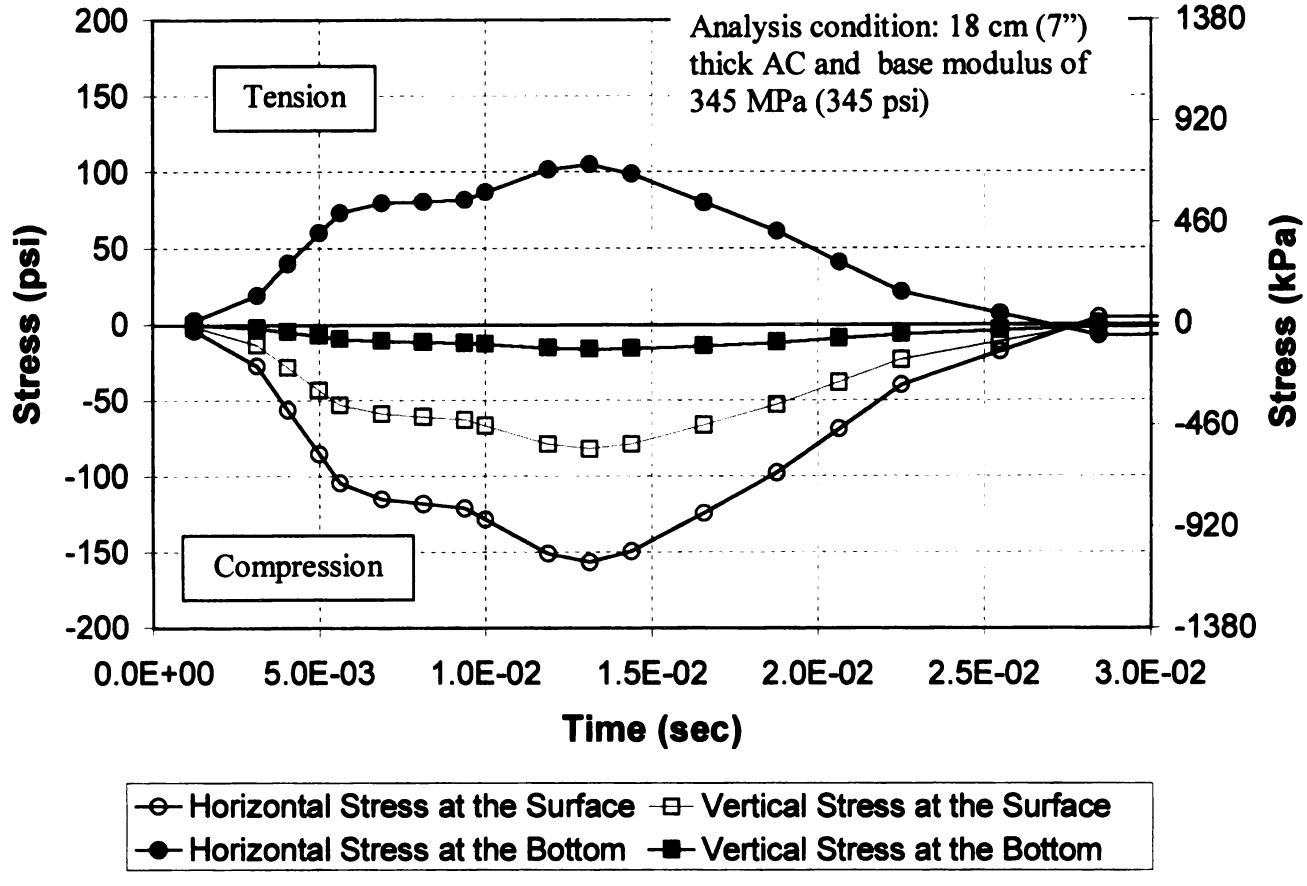


Figure 7-2. Typical stress pulse for morning temperature distribution and uniform load

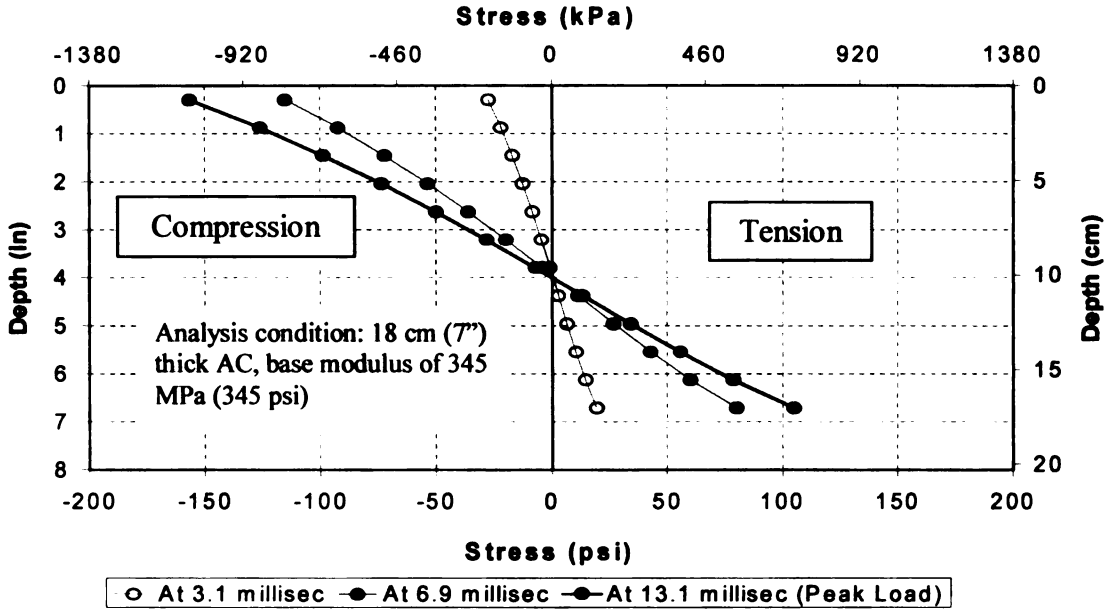


(a) horizontal stress

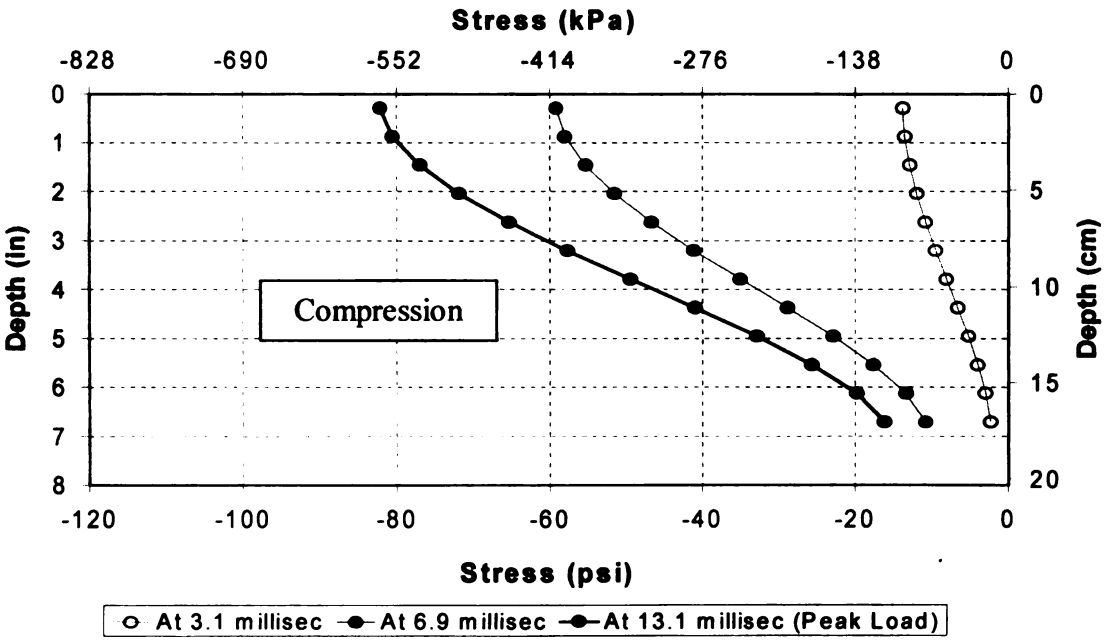


(b) vertical stress

Figure 7-3. Typical example of stresses for uniform temperature and uniform FWD load

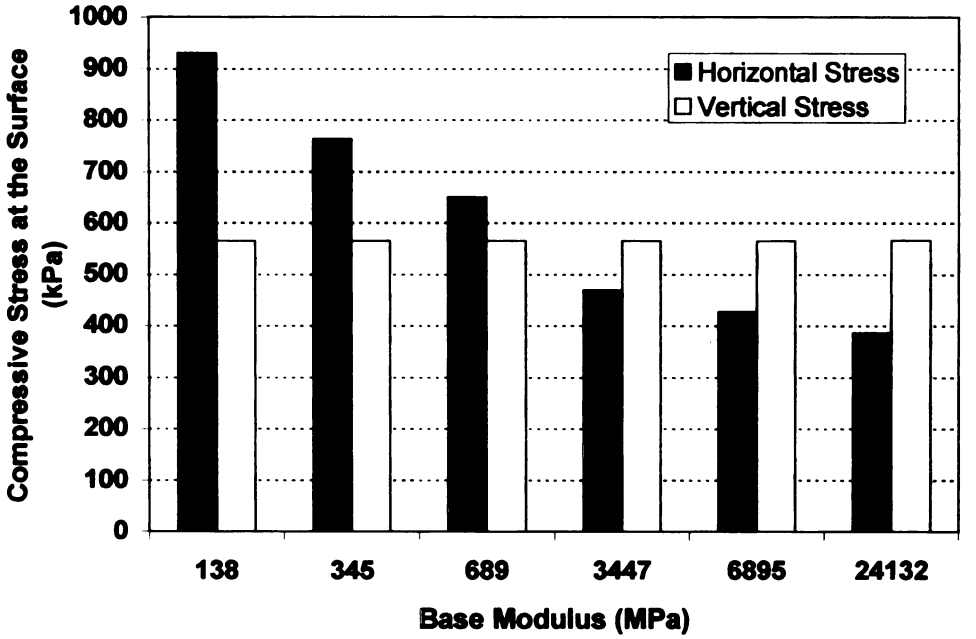


(a) Compressive stress at the surface

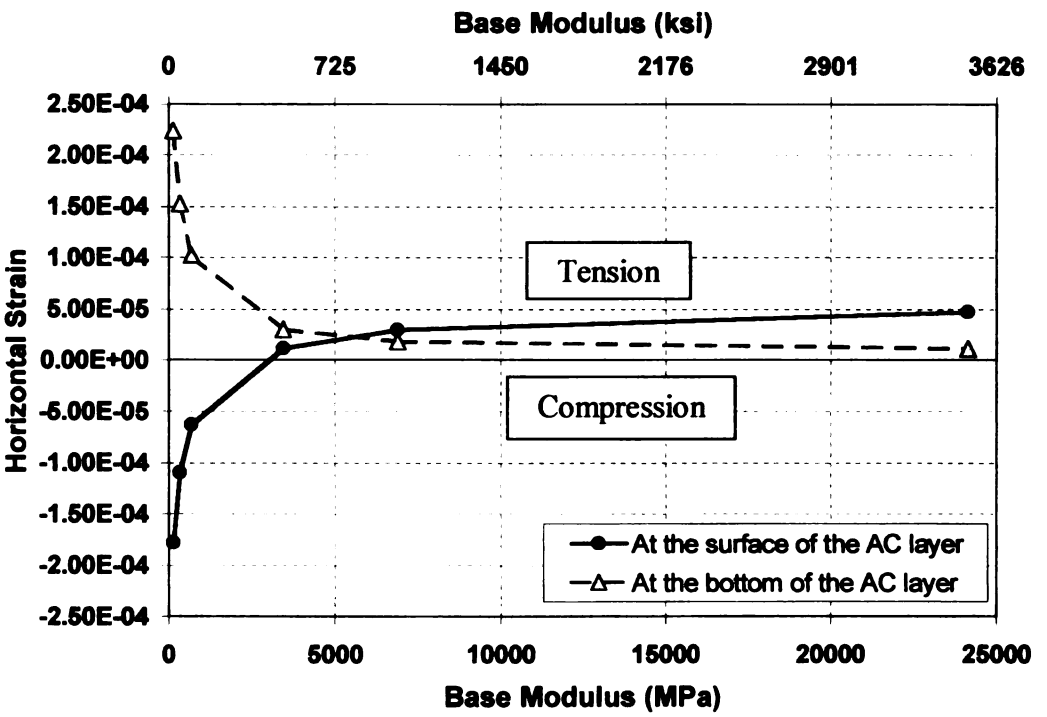


(b) Horizontal strains

Figure 7-4. Effect of base modulus (Analysis condition: 17.8 cm thick AC, day temperature, and uniform load)

However, the high stiffness of the base has the effect of reducing the compressive stresses in the horizontal direction at the top of the AC layer, which eventually causes slight tensile strains at the surface. On the other hand, tensile strains in the horizontal direction at the bottom of the AC layer decreases as base stiffness increases (Figure 7-4).

Distress models are sometimes called transfer functions that relate structural responses to various types of distress such as rutting and fatigue cracking. For fatigue distress models, traditional transfer functions relate tensile strains at the bottom of the AC layer to the allowable number of load repetitions (Huang, 1993). Several agencies presented models that relate the allowable number of load repetitions, $N_f$, to tensile strain, $\varepsilon_t$, at the bottom of the AC layer based on laboratory fatigue tests, for example,

the Asphalt Institute equation for 20% of area cracked is (AI, 1982)

$$N_f = 0.0796\ (\varepsilon_t)^{-3.291}\ (E_1)^{-0.854} \qquad (7\text{-}1)$$

where $E_1$ is the HMA modulus.

According to the concept of design criteria using tensile strain, results from a parametric study indicate that cracking could be initiated at the surface of the pavement where a high stiffness of sublayer is underlain (e.g., asphalt overlaying a concrete pavement).

Typical examples of effects of temperature distributions on horizontal stresses and strains evaluated at the surface and bottom of the AC layer under the load center are plotted in Figures 7-5 and 7-6. The effects of temperature of the AC layer on stress and strain distributions are significant. As temperature increases, stress decreases and strain increases due to the stress relaxation in the AC layer. However, it is noted that strain variations of non-uniform and uniform temperature distributions were close especially at low temperatures, e.g., strains at night and in the morning.

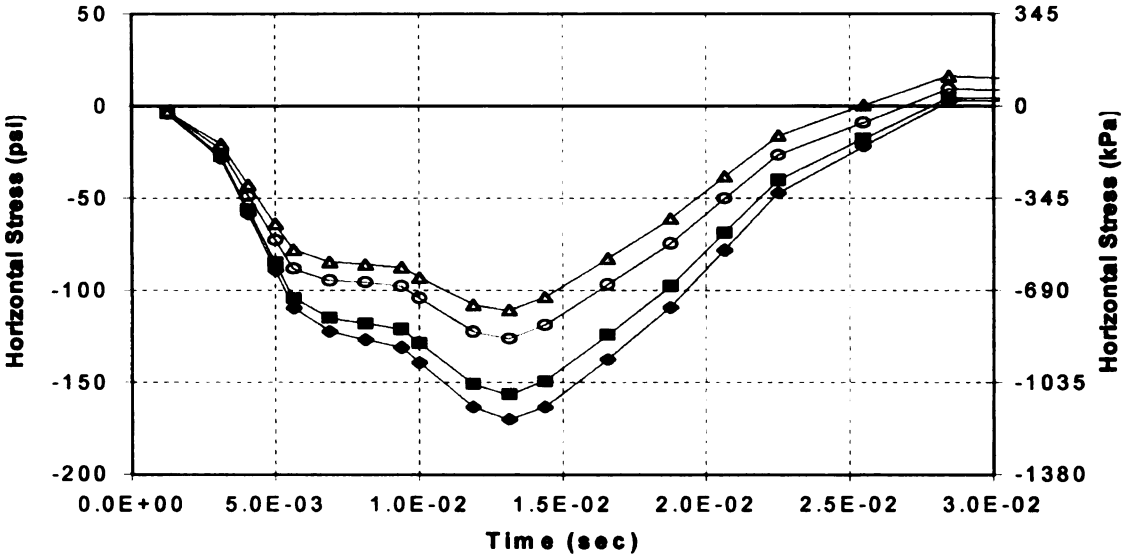


(a) at the surface of the AC layer under the load center

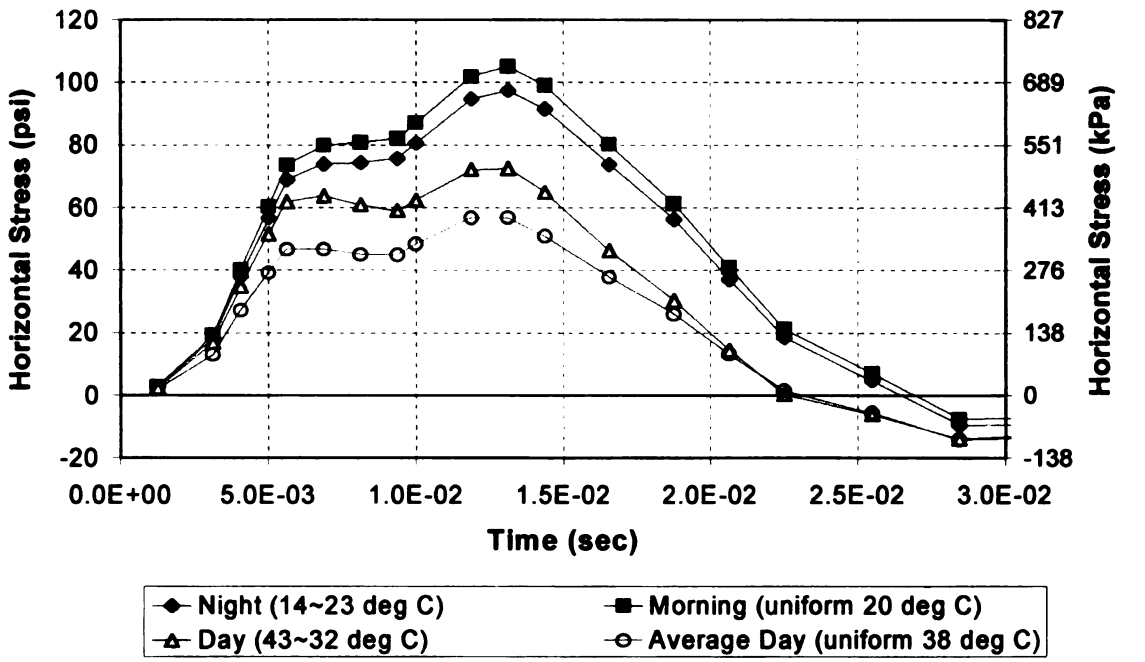


(b) at the bottom of the AC layer under the load center

Figure 7-5. Effects of temperature distributions on horizontal stresses under FWD load

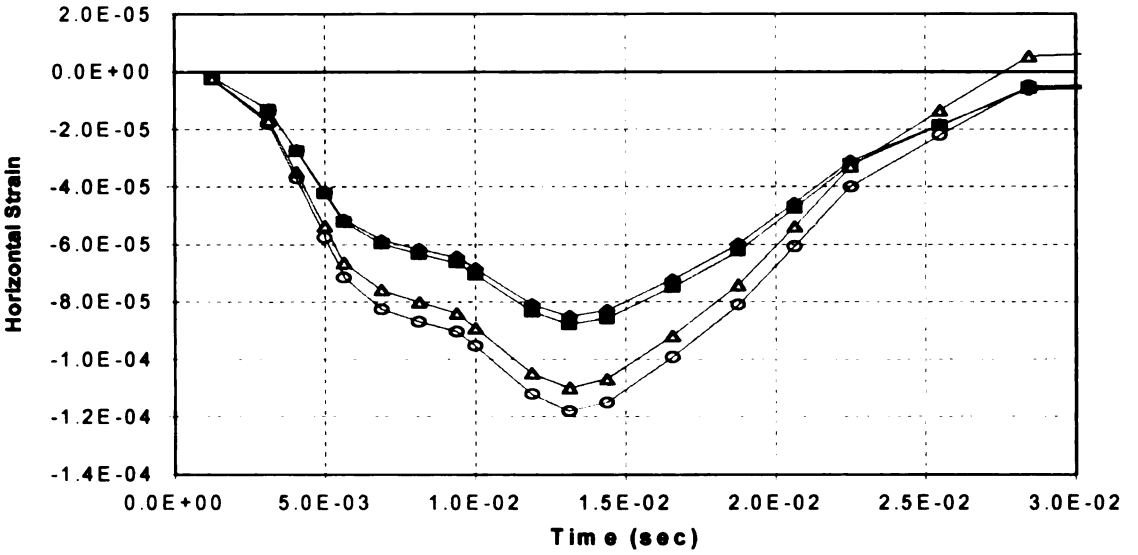


(a) at the surface of the AC layer under the load center

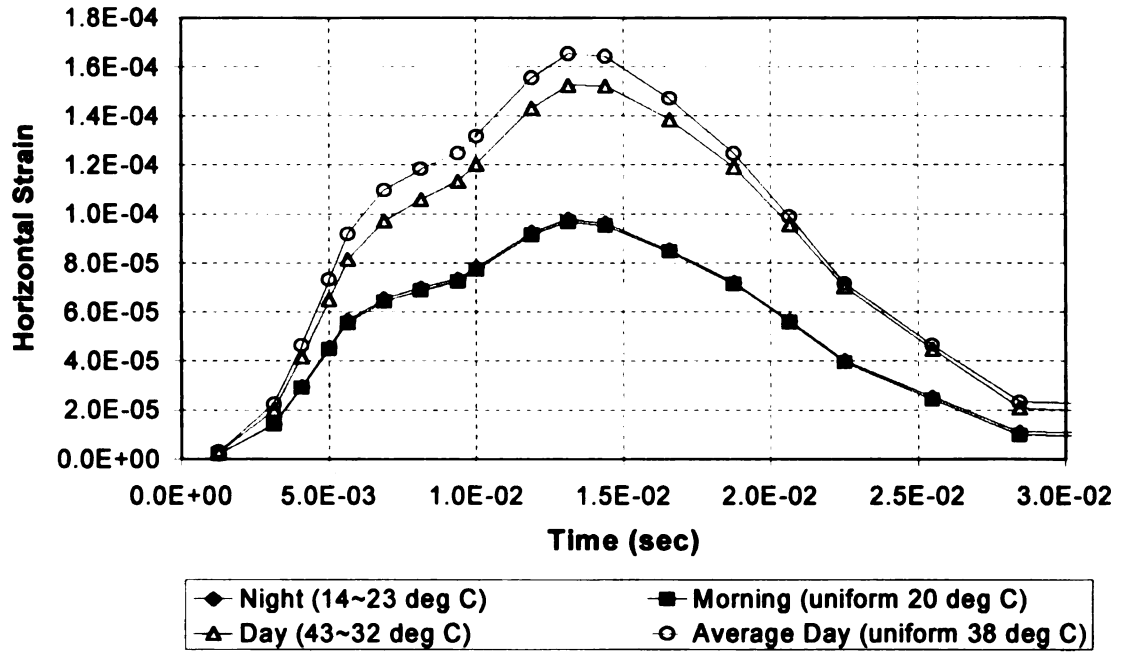


(b) at the bottom of the AC layer under the load center

Figure 7-6. Effects of temperature distributions on horizontal strains under FWD load

The influence of the AC thickness on the structural response was also investigated. As the AC thickness increased, horizontal stresses evaluated at the peak loading time decreased until they reached an asymptotic value. However, vertical stresses did not significantly change (Figure 7-7). Effects of different tire pressure distributions excluding tire tread loads were also investigated. It was found that these had a negligible effect on trends of the stress and strain distributions in the pavement. Effects of tire tread pressure will be discussed in the subsequent sections.

Detailed tables of stress and strain evaluated at the peak loading time are presented in Appendix A.

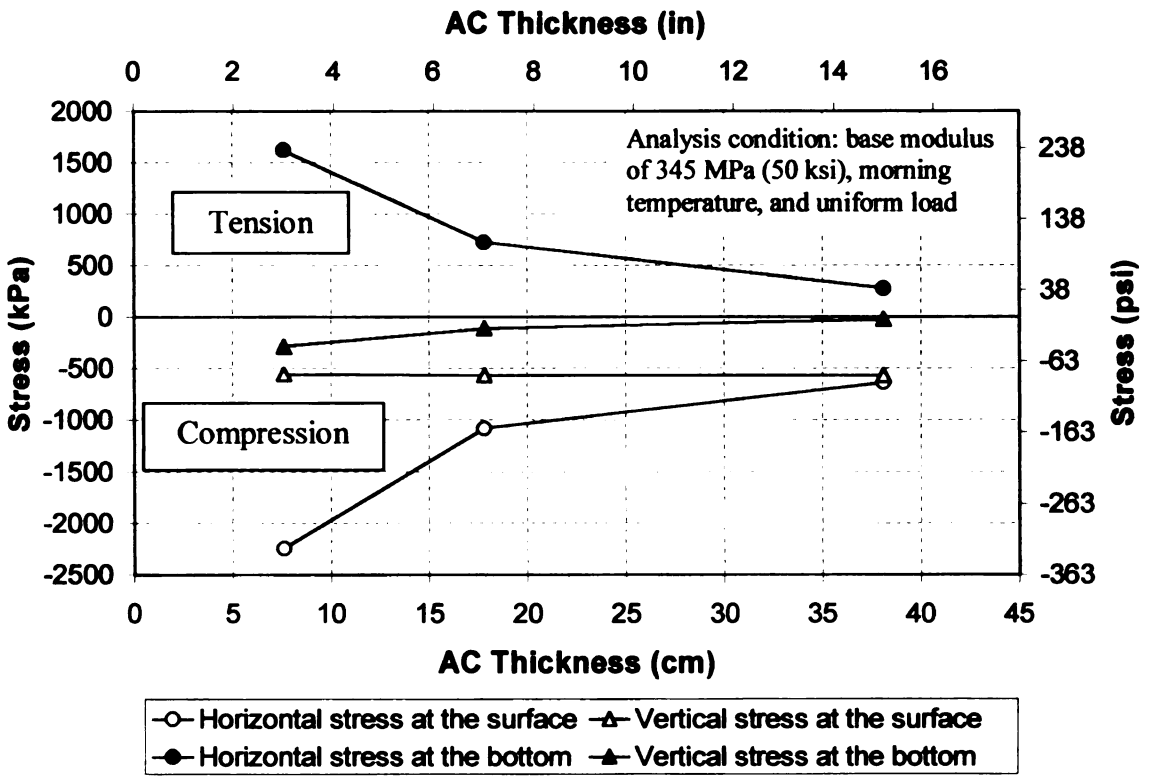


Figure 7-7. Effect of AC thickness on stress response

## 7.2 THREE-DIMENSIONAL FE MODEL

Although the influence of tire contact pressure on the initiation and propagation of pavement distress is significant, very sparse amount of actual data have been reported in the literature (Myers et al., 1998). Hence, effects of more realistic distribution of tire contact pressures are investigated, using tensile strains and dissipated energy.

In order to investigate the effects of temperature distribution and load type, three temperature distribution cases (Morning, Daytime, and Nighttime) were simulated, and three types of load cases were applied:

(a) Load case I: uniform vertical load over the entire load area (no lateral stress),

(b) Load case II: uniform vertical load only under tire treads (no lateral stress), and

(c) Load case III: measured vertical and lateral stresses under tire treads (as measured by Myers et al., 1998).

Dissipated energy is defined as the area within a stress-strain hysteresis loop under cyclic loading and represents the energy lost at a finite location in the AC layer. Figure 7-9 shows typical stress-strain hysteresis loops during a single loading cycle at two different positions (#1 and #2 in Figure 7-8). The dissipated energy per unit volume in the tensile direction was calculated from horizontal tensile stress and strain hysteresis loops (Chatti and Kim, 1996):

$$W_i = \frac{(\sigma_{end} - \sigma_{ini})}{2} \times \frac{(\varepsilon_{end} + \varepsilon_{ini})}{2} + \sum_{i=ini}^{end-1} \left[ \frac{(\sigma_{i+1} - \sigma_i)}{2} \times \frac{(\varepsilon_{i+1} + \varepsilon_i)}{2} \right] \tag{7-2}$$

where:

| | | |
|---|---|---|
| $\sigma_{ini}$, $\varepsilon_{ini}$ | = | initial stress and strain amplitudes |
| $\sigma_{end}$, $\varepsilon_{end}$ | = | ending stress and strain amplitudes |
| $\sigma_i$, $\varepsilon_i$ | = | stress and strain amplitude at a particular time during the cycle |

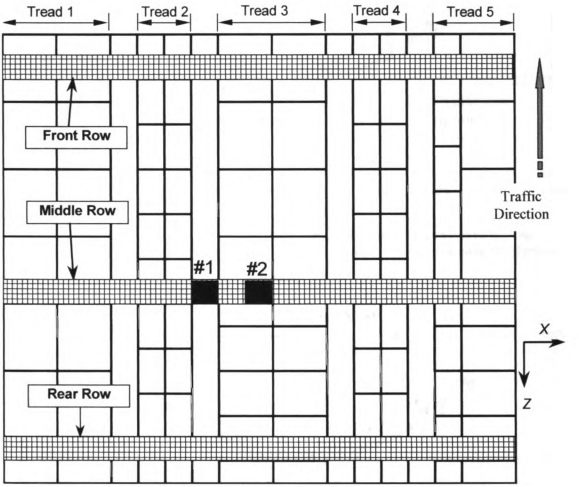


Top View of Loading Area

Figure 7-8. Positions at which pavement responses are evaluated

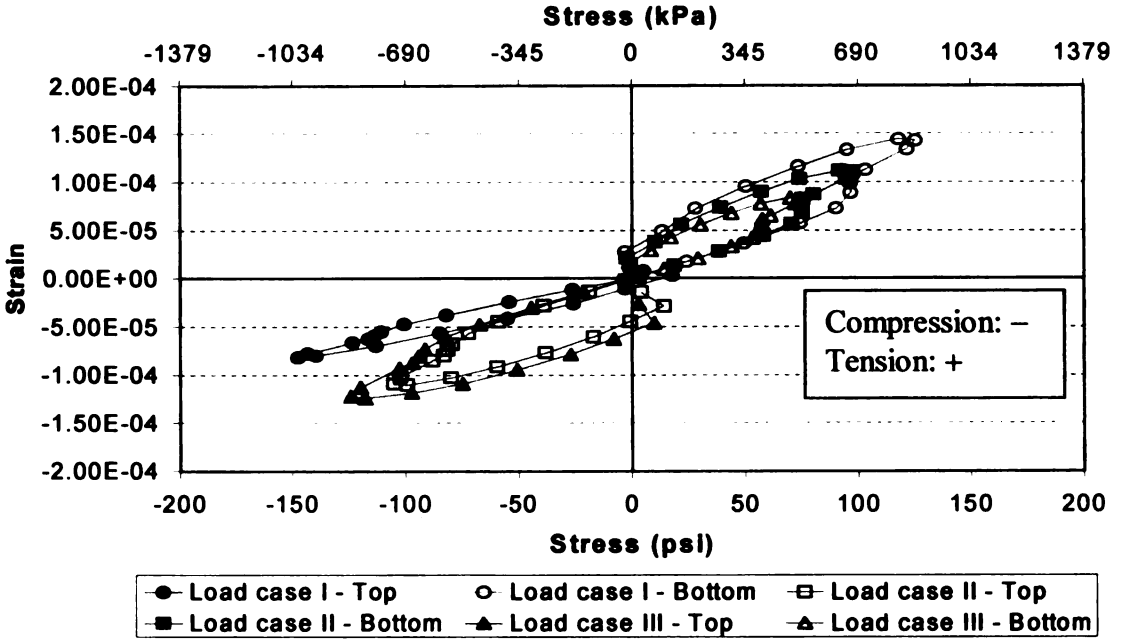


(a) at #1

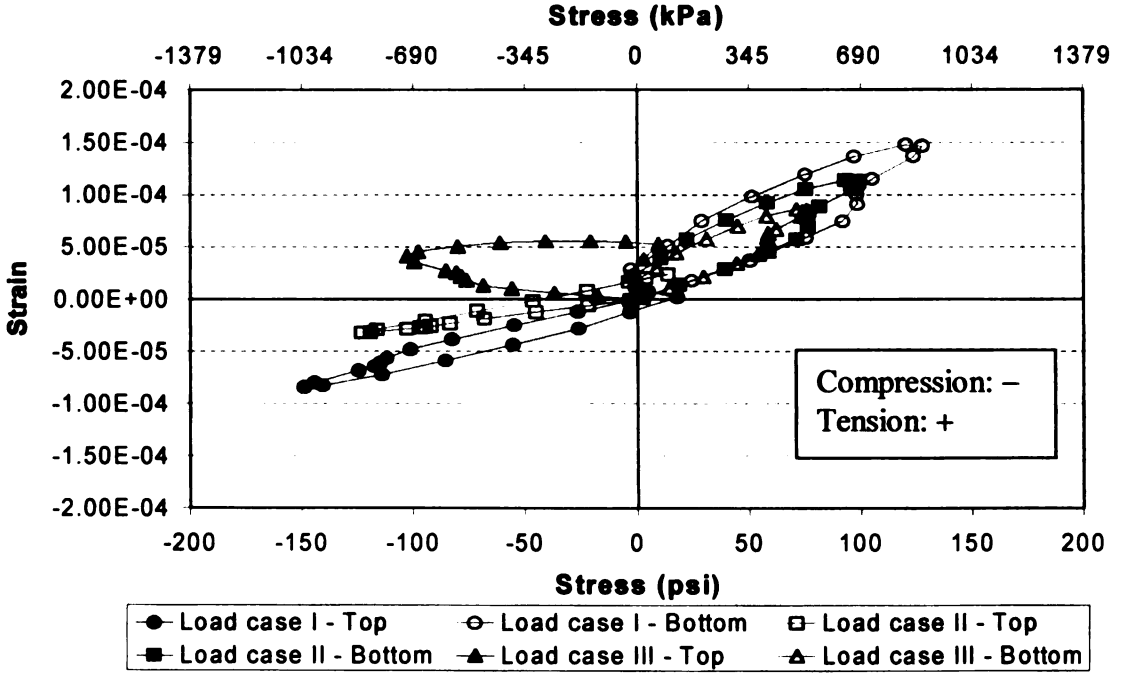


(b) at #2

Figure 7-9. Transverse hysteresis loop for day temperature distribution

Many researchers have applied energy concepts to pavement analysis including the prediction of pavement fatigue life and permanent deformation (Chatti and Kim, 1996; SHRP A-404, 1994; Van Dijk and Visser, 1997; Rowe et al., 1995 and 1997). Fatigue of viscoelastic materials subjected to repeated dynamic loading can be associated with the energy loss such that the fatigue life can be related to the total energy dissipated during the period before failure.

SHRP (1994) established a relationship between dissipated energy and fatigue life, $N_f$:

$$N_f = 2.365\exp^{0.069VFB} (w_o)^{-1.882} \quad (7\text{-}3)$$

where:

VFB = percentage of voids filled with asphalt
$w_o$ = initial dissipated energy per cycle, psi
with $R^2 = 0.76$

The fatigue life, $N_f$, decreases with increasing initial dissipated energy per cycle.

For load cases I and II, tensile stresses and strains in the horizontal direction at the bottom of the AC layer and compressive stresses and strains at the surface were always present. It should be noted that tensile strain at the surface of the AC layer occurred for the load case III (measured vertical and lateral stresses under tire treads) and day temperature distribution (Figure 7-9). Similarly, Myers et al. (1998) reported transverse tensile stresses induced by radial truck tires at the tire-pavement interface from elastic analysis. The authors concluded that these tensile stresses appeared to provide the most viable mechanism of surface-initiated longitudinal wheel path cracks, perhaps combined with thermal stresses during cooling.

Results from 3-D analyses for load cases I and II were consistent with those from 2-D analyses. The peak value of dissipated energy generally occurred at the bottom of the AC layer under the uniform load. At high temperature, the dissipated energy increased especially at the bottom of the AC layer (Figure 7-10). According to the concept of the viscoelastic theory/dissipated energy, as the amount of dissipated energy increases, the fatigue life is expected to decrease. Similar analyses were reported by Rowe and Brown (1997); as temperature was increased, fatigue life decreased. Cracking could be initiated at the bottom under uniform loading since the peak value of dissipated energy occurs at the bottom. For high temperature and tire tread loads (load case II and III), dissipated energy at the surface became higher than at the bottom at certain positions (Figures 7-11 and 7-12). These results from load cases II and III indicate that these surface conditions can become critical so that cracking could be initiated at the surface as explained in the earlier section. Detailed plots of dissipated energy are presented in Appendix A.

Figures 7-13 and 7-14 show horizontal stress distributions under the load area for the load case I. The stress distribution follows typical bending stress distribution with compression at the surface and tension at the bottom. However, for load case II (uniform vertical load only under tire treads), peak compressions at the surface were localized under tire treads, and tension at the bottom was similar to that for load case I. The influence of the tire tread load on stress distribution is significant at the surface of the AC layer and reduced with depth. (Figures 7-15 and 7-16). No unusual peak stresses were observed due to the numerical formulation.

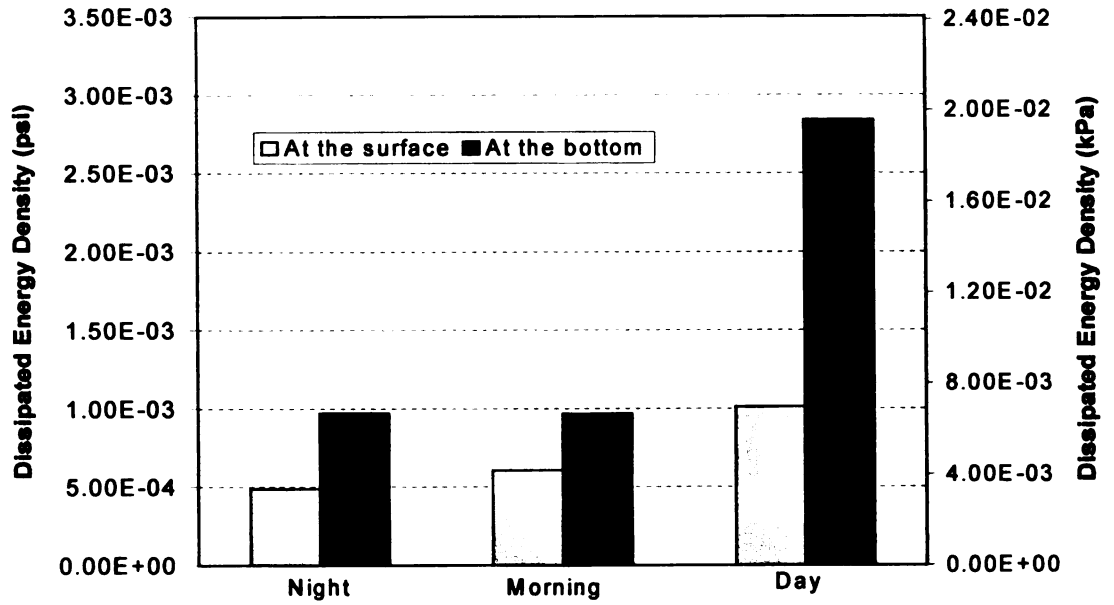


(a) at #1

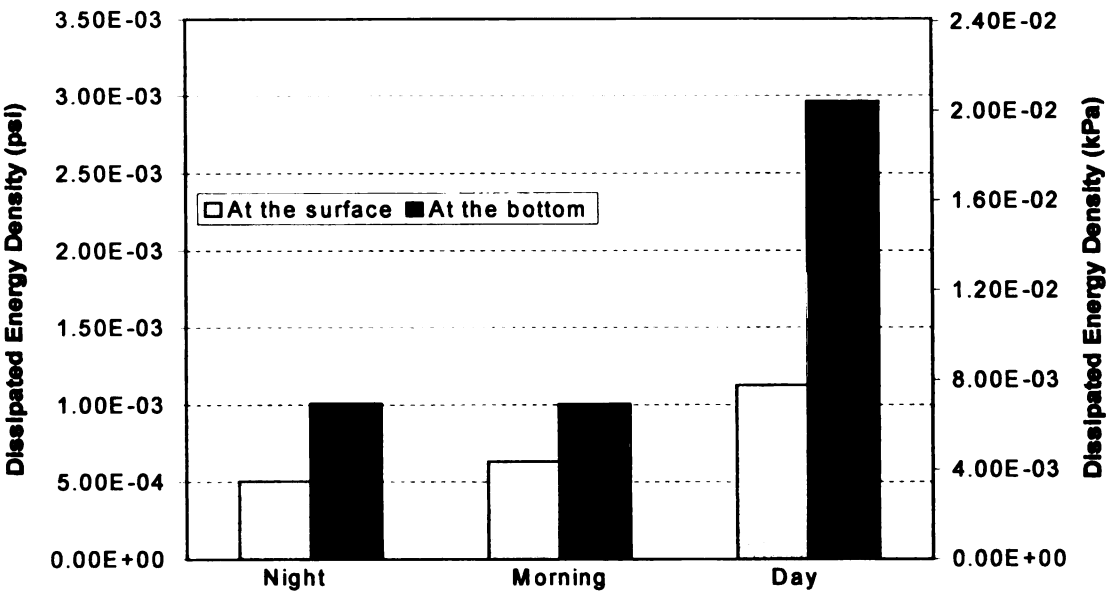


(b) at #2

Figure 7-10. Calculated dissipated energy for the load case I

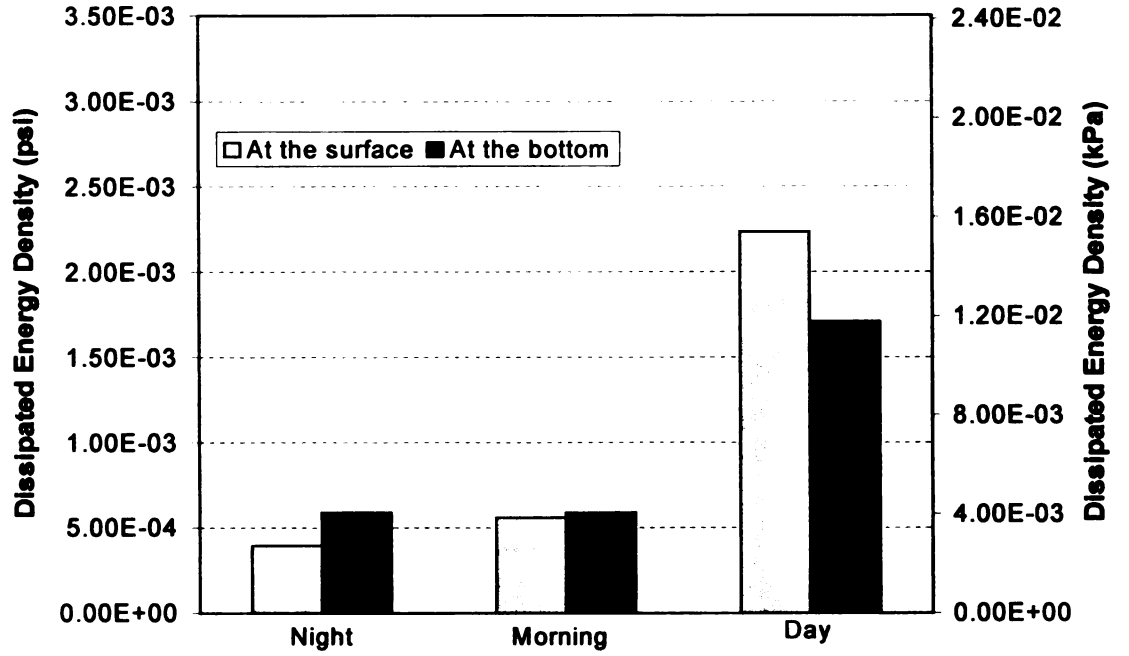


(a) at #1

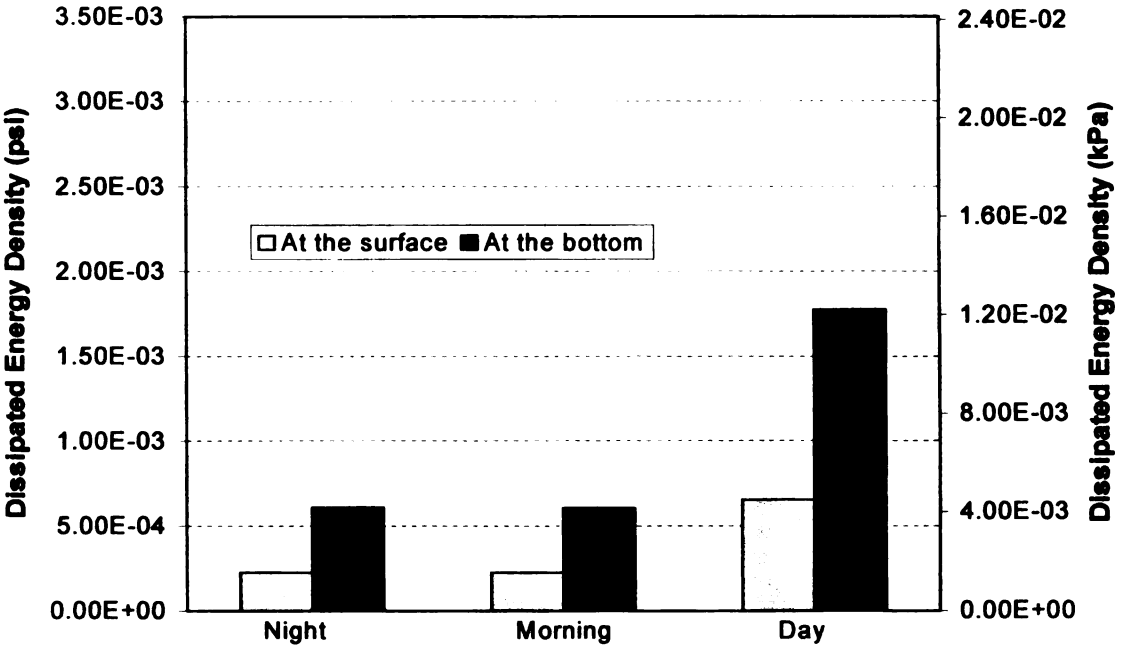


(b) at #2

Figure 7-11. Calculated dissipated energy for the load case II

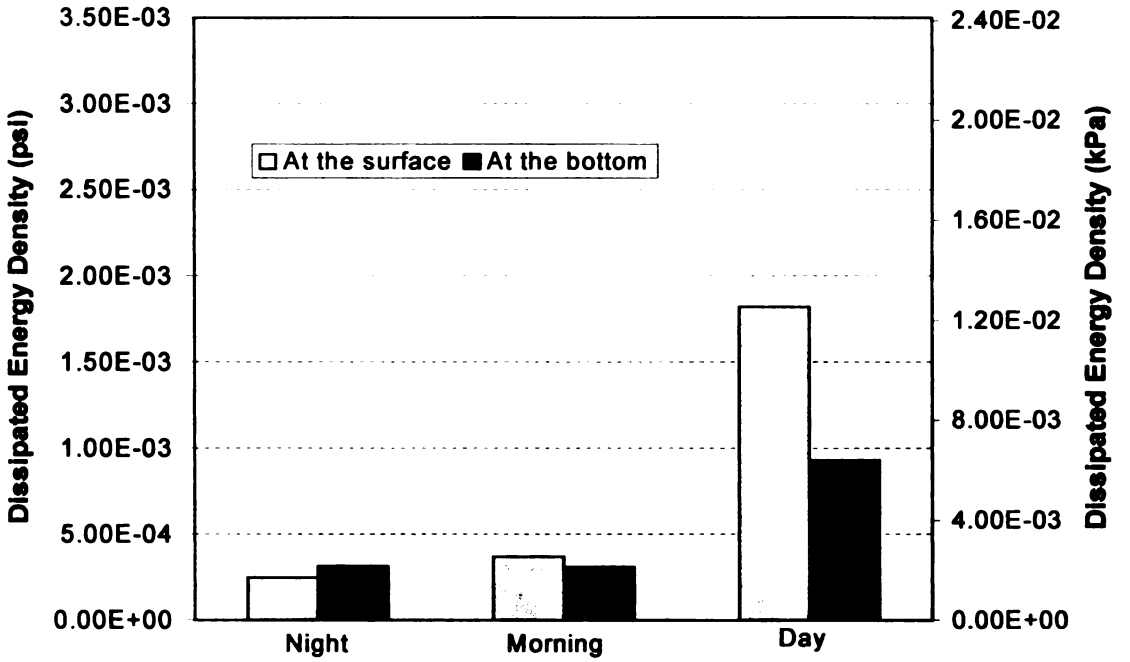


(a) at #1

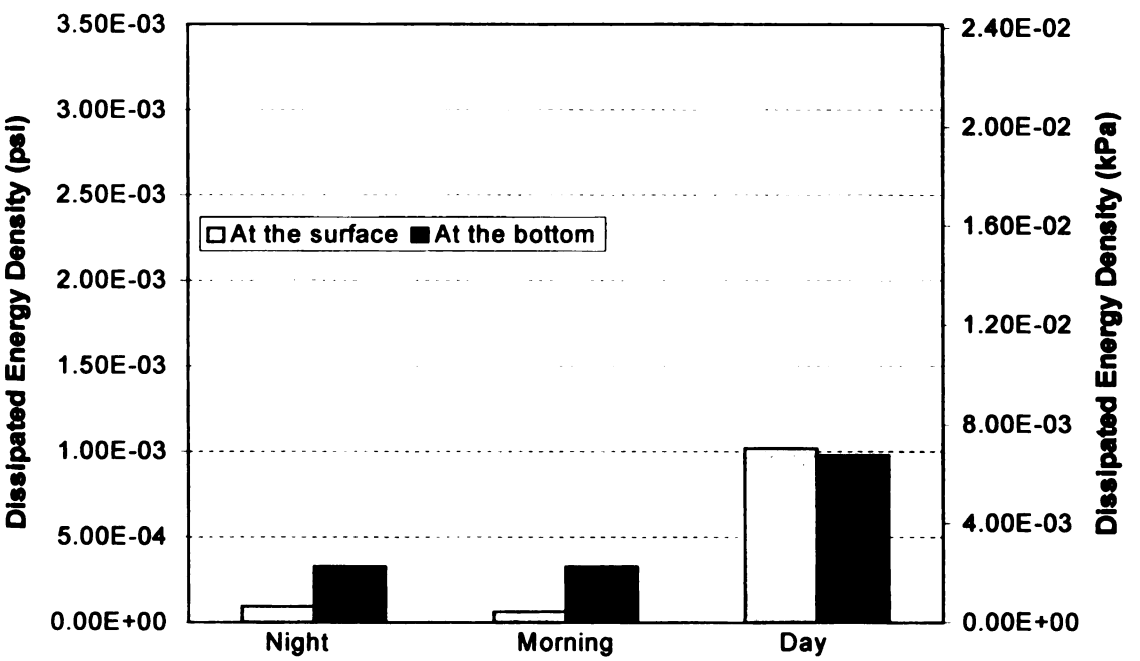


(b) at #2

Figure 7-12. Calculated dissipated energy for the load case III

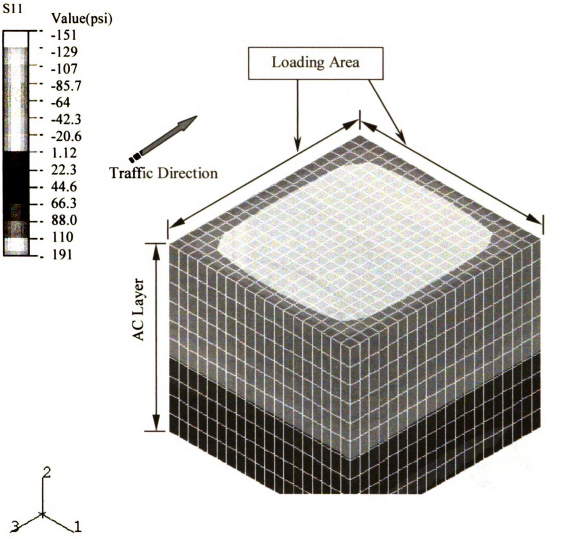


Figure 7-13. Typical contour lines of the horizontal stress under the load for the load case I and day temperature distribution

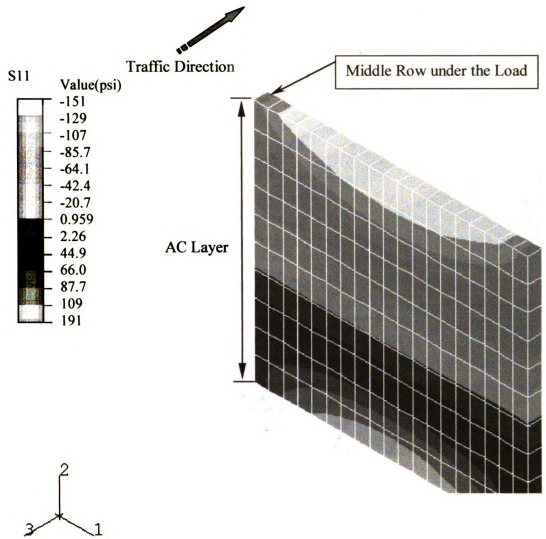


Figure 7-14. Typical contour lines of the horizontal stress under the middle row for the load case I and day temperature distribution

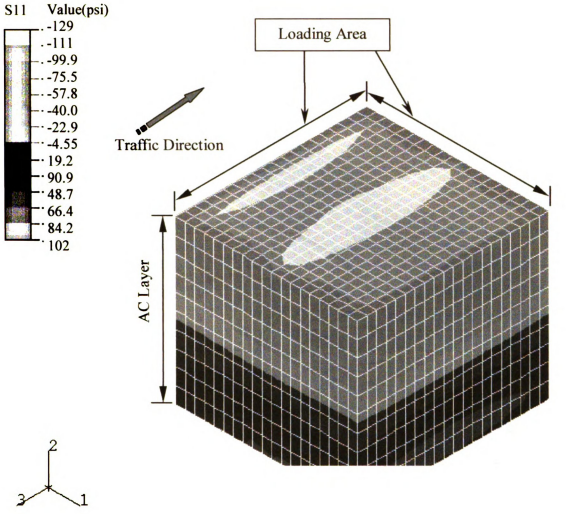


Figure 7-15. Typical contour lines of the horizontal stress under the load for the load case II and day temperature distribution

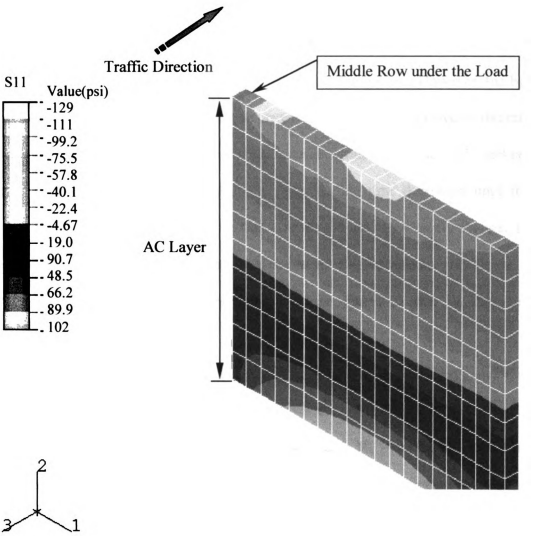


Figure 7-16. Typical contour lines of the horizontal stress under the middle row for the load case II and day temperature distribution

## 7.3 SUMMARY

Parametric study (AC thickness, base stiffness, loading condition, and temperature distribution across the AC layer) was conducted with a 2-D axisymmetric FE model. Bending stresses resulted in compression in the transverse direction at the surface of the AC layer in the vicinity of the load, and tension at the bottom. However, the base stiffness had the effect of decreasing the compressive stresses in the transverse direction at the surface and eventually induced slight tensile strains. As the AC thickness increased, horizontal stresses evaluated at the peak loading time decreased until they reached an asymptotic value. However, vertical stresses did not significantly change. The effects of temperature of the AC layer on stress and strain distributions are significant. As temperature increased, stresses decreased and strains increased due to the stress relaxation in the AC layer.

Effects of three temperature distributions (night, morning, and day) and three loading types (load case I - uniform vertical load over the entire load area, load case II - uniform vertical load only under tire treads, and load case III - measured vertical and lateral stresses under tire treads) on the structural response were investigated with the 3-D FE model. For most cases of loading, compressive stresses and strains in the transverse direction at the surface of the AC layer and tensile stresses and strains at the bottom were always present. However, for the load case III, tensile strain at the surface of the AC layer occurred at high temperature. For the load case I, higher dissipated energy was magnitudes resulted at the bottom of the AC layer than at the surface. As temperature increased, the dissipated energy increased especially at the bottom of the AC layer.

However, for load cases II and III, as temperature increased, dissipated energy also increased at both the surface and the bottom of the AC layer, and dissipated energy became greater at the surface than at the bottom in some locations. This could explain the occurrence of top-down cracking in AC pavements under certain conditions.

# CHAPTER 8

# SUMMARY, CONCLUSIONS, AND RECOMMENDATIONS

## 8.1 SUMMARY AND CONCLUSIONS

The objectives of this research were to:

- Develop a practical, but fundamentally sound model to predict the effective temperature in the AC layer and temperature correction factor for backcalculated AC moduli.
- Investigate temperature effects on structural analysis and performance evaluation.
- Simulate selected AC pavements based on the viscoelasticity/elasticity composite layer system.
- Better understand stress-strain behaviors of flexible pavements subjected to FWD load pulse and various temperature distributions across the AC layer.

A comprehensive literature review regarding flexible pavement temperature prediction model and correction factors, structural analysis of flexible pavements, applications of temperature correction procedure and structural analysis to the field was presented. Axisymmetric finite element model and viscoelasticity were also overviewed.

Based on the field data collected from in-service flexible pavements in Michigan, a practical and accurate subsurface temperature prediction model for asphalt concrete pavements was developed. Temperature correction factors for AC modulus were computed based on measured and predicted mid-depth temperatures, which resulted in consistent values. Temperature data points (317) and deflection profiles (656) were collected from the six in-service test sites in Michigan. Temperature data points (197)

from three of the test sites were used to develop the temperature prediction model, and data from the remaining sites were used for validation. The developed temperature prediction model has a $R^2$ greater than 90% and an F-statistic significantly greater than 1.0. The form of the new temperature prediction model for AC pavements accounts for the temperature gradients which vary with time of day when FWD profiles are measured. Predicted temperatures at various depths were in good agreement with measured temperatures, demonstrating an acceptable degree of accuracy for the model, thus promising potential use by state highway agencies. For further validation of the temperature prediction model, temperature data points (18444) from seven Seasonal Monitoring Program (SMP) sites (Colorado, Connecticut, Georgia, Nebraska, Minnesota, South Dakota, Texas) were obtained from the DATAPAVE 2.0 (LTPP Database). The validation results suggested that the model could be adopted to all seasons and other climatic and geographic regions. The major improvements over existing models are (a) the model does not require temperatures for the previous 5 days (b) it takes into account temperature gradients due to diurnal heating and cooling cycles (c) it needs fewer parameters than other published models and (d) the effect of temperature prediction error on the performance prediction were also investigated.

Middepth temperature difference of ±4 °C resulted in a 3% performance (rutting) error in rut prediction. The error for temperature corrected AC modulus ranges from 10% to 20% based on a ±2 °C and ±4 °C middepth temperature difference, respectively. These results imply that middepth temperature predictions within ±4 °C deviation does not significantly affect the performance prediction. This was further investigated statistically, using t-tests performed for the two groups of computed ruts based on measured and

predicted middepth temperatures, and it was concluded that the means of two groups are equal. Accordingly, bandwidths of ±2, ±4, and ±6 °C were applied to the validation plots of middepth temperature prediction, and most data resided within ±4 °C bandwidth.

The developed temperature prediction and correction procedure have been incorporated into revised versions of the programs MICHPAVE and MICHPACK.

Parametric study (AC thickness, base stiffness, loading condition, and temperature distribution across the AC layer) was conducted with a 2-D axisymmetric FE model. Bending stresses resulted in compression in the transverse direction at the surface of the AC layer in the vicinity of the load, and tension at the bottom. However, the base stiffness had the effect of decreasing the compressive stresses in the transverse direction at the surface and eventually induced slight tensile strains. As the AC thickness increased, horizontal stresses evaluated at the peak loading time decreased until they reached an asymptotic value. However, vertical stresses did not significantly change. The effects of temperature of the AC layer on stress and strain distributions are significant. As temperature increased, stresses decreased and strains increased due to the stress relaxation in the AC layer.

Effects of three temperature distributions (night, morning, and day) and three loading types (load case I - uniform vertical load over the entire load area, load case II - uniform vertical load only under tire treads, and load case III - measured vertical and lateral stresses under tire treads) on the structural response were investigated with the 3-D FE model. The evaluations from 2-D and 3-D analyses were consistent. For most cases of loading, compressive stresses and strains in the transverse direction at the surface of the

AC layer and tensile stresses and strains at the bottom were always present. However, for the load case III, tensile strain at the surface of the AC layer occurred at high temperature. For the load case I, higher dissipated energy was magnitudes resulted at the bottom of the AC layer than at the surface. As temperature increased, the dissipated energy increased especially at the bottom of the AC layer. However, for load cases II and III, as temperature increased, dissipated energy also increased at both the surface and the bottom of the AC layer, and dissipated energy became greater at the surface than at the bottom in some locations. This results could explain the occurrence of top-down cracking in AC pavements under certain conditions, and contribute to the development of an improved performance model and/or asphalt pavement design program based on advanced material characterization and dynamic FWD.

## 8.2 RECOMMEDATIONS FOR FUTURE RESEARCH

- In order to achieve higher suitability for various site and environmental conditions, the calibration work for the pavement temperature prediction model and correction factors for AC modulus should be continued with updated version of the LTPP database.
- The influence of temperature prediction error on the shape of the deflection basin should be studied.
- The effect of repeated cyclic loads on the structural analysis needs to be investigated based on viscoelasticity, realistic temperature distribution, and dynamic loads.
- An attempt needs to be made to implement the flexible pavement analysis for pavement designs and performance models.

- Discontinued flexible pavement (e.g., pavement with cracks) should be simulated to study the influence of viscoelasticity, temperature distribution, and dynamic loads.

# APPENDICES

# APPENDIX A

## ADDITIONAL FIGURES AND TABLES IN CHAPTER 7

Additional tables and figures for the chapter 7 are here presented. Table A-1 shows stresses and strains evaluated at the peak loading from the parametric study. Figures A-1 through A-9 present calculated dissipated energy at various locations for different types of loading and temperature distributions form the 3-D analysis.

Table A-1. Parametric study: stresses and strains at the peak load

(a) S11 (Horizontal Stress) at the top element under the load center (kPa)

| AC Thickness (cm) | | 7.6 | | | | 17.8 | | | | 38.1 | | |
|---|---|---|---|---|---|---|---|---|---|---|---|---|
| Base Modulus (MPa) | | 138 | 345 | 689 | 6895 | 138 | 345 | 689 | 6895 | 138 | 345 | 689 |
| Loading Condition | | | | | | | | | | | | |
| Temperature Condition | | | | | | | | | | | | |
| Day (43 ~ °C) | Uniform | -1950.5 | -1315.5 | -963.9 | -451.7 | -930.8 | -763.9 | -649.6 | -428.2 | -571.6 | -546.4 | -521.9 |
| | High Center | -1816.1 | -1244.5 | -922.5 | -440.3 | -870.8 | -724.0 | -623.2 | -427.0 | -552.5 | -530.6 | -509.2 |
| | High Egde | -1596.8 | -1057.0 | -764.6 | -350.3 | -758.4 | -612.9 | -513.6 | -322.4 | -447.7 | -425.6 | -404.0 |
| Average Day (41, 38, 34°C) | Uniform | -2074.0 | -1387.2 | -1005.3 | -436.0 | -1079.0 | -870.8 | -725.3 | -434.6 | -679.7 | -640.1 | -602.1 |
| | High Center | -1930.5 | -1312.8 | -961.8 | -425.9 | -1004.6 | -821.9 | -694.3 | -436.2 | -650.4 | -616.0 | -582.8 |
| | High Egde | -1698.9 | -1115.6 | -797.0 | -337.1 | -883.2 | -701.2 | -575.6 | -324.3 | -539.0 | -504.3 | -470.8 |
| Night (13 ~ °C) | Uniform | -3310.9 | -2421.5 | -1816.8 | -607.6 | -1392.1 | -1172.1 | -994.2 | -531.5 | -741.9 | -708.8 | -672.0 |
| | High Center | -3015.8 | -2230.5 | -1692.0 | -588.8 | -1275.5 | -1083.9 | -927.4 | -519.3 | -701.9 | -673.6 | -641.4 |
| | High Egde | -2777.9 | -2007.1 | -1487.9 | -474.4 | -1160.4 | -968.0 | -812.2 | -410.8 | -596.0 | -567.1 | -534.6 |
| Morning (20 °C) | Uniform | -3105.4 | -2245.6 | -1674.7 | -579.4 | -1283.1 | -1080.4 | -918.4 | -508.2 | -664.5 | -638.5 | -608.7 |
| | High Center | -2835.1 | -2075.3 | -1565.1 | -562.3 | -1178.3 | -1001.8 | -859.1 | -497.4 | -632.9 | -610.3 | -584.4 |
| | High Egde | -2598.7 | -1854.7 | -1365.9 | -451.6 | -1066.6 | -889.4 | -748.1 | -392.0 | -529.9 | -507.0 | -480.9 |

(b) S22 (Vertical Stress) at the top element under the load center (kPa)

| AC Thickness (cm) | | 7.6 | | | | 17.8 | | | | 38.1 | | |
|---|---|---|---|---|---|---|---|---|---|---|---|---|
| Base Modulus (MPa) | | 138 | 345 | 689 | 6895 | 138 | 345 | 689 | 6895 | 138 | 345 | 689 |
| Loading Condition | | | | | | | | | | | | |
| Temperature Condition | | | | | | | | | | | | |
| Day (43 ~ °C) | Uniform | -556.3 | -560.4 | -562.8 | -565.2 | -565.5 | -565.5 | -565.6 | -566.2 | -565.1 | -565.1 | -565.2 |
| | High Center | -555.9 | -559.9 | -562.3 | -565.4 | -565.6 | -565.6 | -565.7 | -565.7 | -565.0 | -565.0 | -565.0 |
| | High Egde | -417.6 | -420.9 | -422.6 | -423.7 | -424.1 | -424.1 | -424.2 | -424.6 | -424.0 | -424.0 | -424.0 |
| Average Day (41, 38, 34°C) | Uniform | -555.6 | -560.1 | -562.8 | -565.4 | -566.0 | -566.0 | -566.1 | -566.7 | -564.8 | -564.8 | -564.9 |
| | High Center | -555.1 | -559.4 | -562.1 | -565.6 | -565.9 | -565.9 | -566.1 | -566.7 | -564.5 | -564.5 | -564.6 |
| | High Egde | -417.2 | -420.7 | -422.6 | -423.8 | -424.5 | -424.5 | -424.6 | -425.1 | -423.8 | -423.9 | -423.9 |
| Night (13 ~ °C) | Uniform | -549.9 | -553.8 | -557.2 | -564.9 | -567.2 | -566.8 | -566.6 | -566.9 | -564.3 | -564.4 | -564.5 |
| | High Center | -549.7 | -553.3 | -556.5 | -564.5 | -567.0 | -566.6 | -566.5 | -566.8 | -564.1 | -564.1 | -564.1 |
| | High Egde | -412.6 | -415.8 | -418.6 | -424.0 | -425.6 | -425.3 | -425.1 | -425.3 | -423.6 | -423.7 | -423.7 |
| Morning (20 °C) | Uniform | -550.8 | -554.8 | -558.1 | -565.0 | -566.5 | -566.3 | -566.1 | -566.5 | -564.8 | -564.8 | -564.8 |
| | High Center | -550.6 | -554.3 | -557.5 | -564.8 | -566.4 | -566.2 | -566.1 | -566.5 | -564.5 | -564.5 | -564.6 |
| | High Egde | -413.3 | -416.6 | -419.3 | -423.9 | -425.0 | -424.7 | -424.7 | -424.9 | -423.8 | -423.9 | -423.9 |

Note. Compression is negative and tension positive.

Table A-1. Parametric study: stresses and strains at the peak load (continued)

(c) E11 (Horizontal Strain) at the top element under the load center

| AC Thickness (cm) | | 7.6 | | | | 17.8 | | | | 38.1 | | |
|---|---|---|---|---|---|---|---|---|---|---|---|---|
| Base Modulus (MPa) | | 138 | 345 | 689 | 6895 | 138 | 345 | 689 | 6895 | 138 | 345 | 689 |
| Loading Condition | | | | | | | | | | | | |
| Temperature Condition | | | | | | | | | | | | |
| | Uniform | -3.83E-04 | -2.17E-04 | -1.25E-04 | 1.21E-05 | -1.78E-04 | -1.10E-04 | -6.29E-05 | 2.97E-05 | -1.74E-05 | -1.11E-05 | -4.96E-06 |
| Day | High Center | -3.48E-04 | -1.99E-04 | -1.14E-04 | 1.50E-05 | -1.53E-04 | -9.33E-05 | -5.19E-05 | 3.02E-05 | -1.27E-05 | -7.18E-06 | -1.79E-06 |
| (43 ~ °C) | High Egde | -3.23E-04 | -1.82E-04 | -1.05E-04 | 6.10E-06 | -1.58E-04 | -9.91E-05 | -5.83E-05 | 2.17E-05 | -1.79E-05 | -1.23E-05 | -6.88E-06 |
| Average Day | Uniform | -3.64E-04 | -2.08E-04 | -1.20E-04 | 1.22E-05 | -1.80E-04 | -1.18E-04 | -7.46E-05 | 1.34E-05 | -3.38E-05 | -2.77E-05 | -2.18E-05 |
| | High Center | -3.31E-04 | -1.90E-04 | -1.10E-04 | 1.45E-05 | -1.58E-04 | -1.03E-04 | -6.50E-05 | 1.29E-05 | -2.92E-05 | -2.40E-05 | -1.88E-05 |
| (41, 38, 34°C) | High Egde | -3.06E-04 | -1.73E-04 | -9.97E-05 | 6.81E-06 | -1.57E-04 | -1.03E-04 | -6.55E-05 | 1.04E-05 | -2.99E-05 | -2.46E-05 | -1.94E-05 |
| | Uniform | -1.86E-04 | -1.31E-04 | -9.37E-05 | -1.85E-05 | -1.07E-04 | -8.50E-05 | -6.75E-05 | -2.19E-05 | -2.67E-05 | -2.47E-05 | -2.24E-05 |
| Night | High Center | -1.68E-04 | -1.19E-04 | -8.60E-05 | -1.74E-05 | -9.52E-05 | -7.63E-05 | -6.09E-05 | -2.06E-05 | -2.42E-05 | -2.25E-05 | -2.05E-05 |
| (13 ~ °C) | High Egde | -1.58E-04 | -1.10E-04 | -7.80E-05 | -1.51E-05 | -9.15E-05 | -7.25E-05 | -5.72E-05 | -1.76E-05 | -2.24E-05 | -2.07E-05 | -1.87E-05 |
| Morning | Uniform | -2.10E-04 | -1.45E-04 | -1.01E-04 | -1.71E-05 | -1.12E-04 | -8.78E-05 | -6.82E-05 | -1.84E-05 | -2.33E-05 | -2.13E-05 | -1.91E-05 |
| | High Center | -1.90E-04 | -1.32E-04 | -9.27E-05 | -1.58E-05 | -9.95E-05 | -7.82E-05 | -6.10E-05 | -1.70E-05 | -2.09E-05 | -1.92E-05 | -1.73E-05 |
| (20 °C) | High Egde | -1.78E-04 | -1.21E-04 | -8.42E-05 | -1.41E-05 | -9.68E-05 | -7.55E-05 | -5.83E-05 | -1.51E-05 | -1.99E-05 | -1.81E-05 | -1.62E-05 |

(d) E22 (Vertical Strain) at the top element under the load center

| AC Thickness (cm) | | 7.6 | | | | 17.8 | | | | 38.1 | | |
|---|---|---|---|---|---|---|---|---|---|---|---|---|
| Base Modulus (MPa) | | 138 | 345 | 689 | 6895 | 138 | 345 | 689 | 6895 | 138 | 345 | 689 |
| Loading Condition | | | | | | | | | | | | |
| Temperature Condition | | | | | | | | | | | | |
| | Uniform | 6.41E-04 | 3.45E-04 | 1.80E-04 | -6.53E-05 | 2.47E-04 | 1.26E-04 | 4.24E-05 | -1.23E-04 | -1.29E-05 | -2.41E-05 | -3.51E-05 |
| Day | High Center | 5.77E-04 | 3.12E-04 | 1.60E-04 | -7.06E-05 | 2.02E-04 | 9.64E-05 | 2.26E-05 | -1.24E-04 | -2.15E-05 | -3.12E-05 | -4.08E-05 |
| (43 ~ °C) | High Egde | 5.44E-04 | 2.93E-04 | 1.54E-04 | -4.37E-05 | 2.30E-04 | 1.24E-04 | 5.17E-05 | -9.11E-05 | -1.19E-06 | -1.10E-05 | -2.07E-05 |
| Average Day | Uniform | 5.96E-04 | 3.22E-04 | 1.67E-04 | -6.46E-05 | 2.38E-04 | 1.33E-04 | 5.89E-05 | -9.08E-05 | 1.38E-05 | 3.83E-06 | -5.84E-06 |
| | High Center | 5.38E-04 | 2.91E-04 | 1.50E-04 | -6.87E-05 | 2.00E-04 | 1.08E-04 | 4.25E-05 | -9.02E-05 | 6.23E-06 | -2.40E-06 | -1.08E-05 |
| (41, 38, 34°C) | High Egde | 5.05E-04 | 2.72E-04 | 1.43E-04 | -4.44E-05 | 2.16E-04 | 1.25E-04 | 6.05E-05 | -6.88E-05 | 1.78E-05 | 9.10E-06 | 5.98E-07 |
| | Uniform | 1.72E-04 | 1.11E-04 | 7.00E-05 | -1.28E-05 | 6.36E-05 | 4.01E-05 | 2.09E-05 | -2.90E-05 | -3.98E-06 | -6.18E-06 | -8.65E-06 |
| Night | High Center | 1.52E-04 | 9.82E-05 | 6.15E-05 | -1.40E-05 | 5.11E-05 | 3.05E-05 | 1.37E-05 | -3.04E-05 | -6.63E-06 | -8.54E-06 | -1.07E-05 |
| (13 ~ °C) | High Egde | 1.49E-04 | 9.63E-05 | 6.09E-05 | -8.34E-06 | 6.03E-05 | 3.96E-05 | 2.29E-05 | -2.05E-05 | -3.44E-07 | -2.27E-06 | -4.45E-06 |
| Morning | Uniform | 2.31E-04 | 1.48E-04 | 9.26E-05 | -1.41E-05 | 8.44E-05 | 5.37E-05 | 2.90E-05 | -3.39E-05 | -6.43E-06 | -8.88E-06 | -1.17E-05 |
| | High Center | 2.05E-04 | 1.31E-04 | 8.20E-05 | -1.57E-05 | 6.84E-05 | 4.16E-05 | 1.99E-05 | -3.56E-05 | -9.42E-06 | -1.16E-05 | -1.40E-05 |
| (20 °C) | High Egde | 1.99E-04 | 1.27E-04 | 8.00E-05 | -8.92E-06 | 7.94E-05 | 5.25E-05 | 3.09E-05 | -2.37E-05 | -1.83E-06 | -3.98E-06 | -6.46E-06 |

Note. Compression is negative and tension positive.

Table A-1. Parametric study: stresses and strains at the peak load (continued)

(e) S11 (Horizontal Stress) at the bottom element under the load center (kPa)

| AC Thickness (cm) | | 7.6 | | | | 17.8 | | | | 38.1 | | |
|---|---|---|---|---|---|---|---|---|---|---|---|---|
| Base Modulus (MPa) | | 138 | 345 | 689 | 6895 | 138 | 345 | 689 | 6895 | 138 | 345 | 689 |
| Loading Condition | | | | | | | | | | | | |
| Temperature Condition | | | | | | | | | | | | |
| Day (43 ~ °C) | Uniform | 1541.0 | 628.7 | 137.0 | -403.3 | 864.6 | 500.0 | 237.6 | -231.0 | 384.4 | 309.3 | 231.3 |
| | High Center | 1442.4 | 616.4 | 160.0 | -377.7 | 774.3 | 452.1 | 218.4 | -206.2 | 336.5 | 271.0 | 202.8 |
| | High Egde | 1254.2 | 483.8 | 79.8 | -328.1 | 739.1 | 423.0 | 197.3 | -198.0 | 336.1 | 270.2 | 201.8 |
| Average Day (41, 38, 34°C) | Uniform | 1423.1 | 559.1 | 92.5 | -419.8 | 715.0 | 391.6 | 157.1 | -267.5 | 292.0 | 225.3 | 156.9 |
| | High Center | 1332.1 | 549.5 | 115.9 | -395.3 | 639.7 | 354.1 | 145.2 | -239.7 | 255.6 | 197.5 | 137.7 |
| | High Egde | 1158.3 | 428.9 | 45.9 | -339.4 | 611.0 | 331.2 | 129.8 | -228.5 | 255.3 | 196.8 | 136.9 |
| Night (13 ~ °C) | Uniform | 2722.8 | 1713.4 | 1023.2 | -204.6 | 942.5 | 672.2 | 443.1 | -135.5 | 283.3 | 242.3 | 194.0 |
| | High Center | 2477.3 | 1583.7 | 966.7 | -175.1 | 837.7 | 600.3 | 398.3 | -118.9 | 247.9 | 212.1 | 169.9 |
| | High Egde | 2287.7 | 1414.1 | 824.6 | -182.9 | 812.2 | 576.1 | 377.0 | -118.2 | 247.9 | 211.9 | 169.5 |
| Morning (20 °C) | Uniform | 2658.6 | 1620.3 | 928.0 | -235.0 | 1014.9 | 724.6 | 480.4 | -121.3 | 319.2 | 277.8 | 228.4 |
| | High Center | 2425.6 | 1505.1 | 883.2 | -204.8 | 902.5 | 647.6 | 432.4 | -105.9 | 279.3 | 243.2 | 200.1 |
| | High Egde | 2227.7 | 1331.4 | 741.2 | -206.5 | 873.6 | 620.3 | 408.3 | -106.5 | 279.3 | 243.0 | 199.6 |

(f) S22 (Vertical Stress) at the bottom element under the load center (kPa)

| AC Thickness (cm) | | 7.6 | | | | 17.8 | | | | 38.1 | | |
|---|---|---|---|---|---|---|---|---|---|---|---|---|
| Base Modulus (MPa) | | 138 | 345 | 689 | 6895 | 138 | 345 | 689 | 6895 | 138 | 345 | 689 |
| Loading Condition | | | | | | | | | | | | |
| Temperature Condition | | | | | | | | | | | | |
| Day (43 ~ °C) | Uniform | -311.9 | -404.4 | -461.0 | -523.2 | -117.6 | -182.4 | -239.8 | -378.3 | -20.5 | -33.7 | -49.5 |
| | High Center | -284.5 | -374.0 | -432.1 | -510.2 | -104.7 | -163.1 | -215.5 | -344.4 | -18.0 | -29.5 | -43.4 |
| | High Egde | -261.2 | -333.8 | -374.6 | -405.5 | -101.1 | -156.0 | -204.1 | -317.6 | -18.0 | -29.5 | -43.3 |
| Average Day (41, 38, 34°C) | Uniform | -310.5 | -404.0 | -461.5 | -527.0 | -117.7 | -183.4 | -242.6 | -393.2 | -21.3 | -35.5 | -52.4 |
| | High Center | -283.2 | -373.6 | -432.6 | -514.7 | -104.7 | -164.0 | -218.1 | -357.5 | -18.6 | -31.1 | -45.9 |
| | High Egde | -260.3 | -333.5 | -375.0 | -407.6 | -101.3 | -156.9 | -206.6 | -330.7 | -18.7 | -31.1 | -45.8 |
| Night (13 ~ °C) | Uniform | -183.2 | -265.3 | -337.2 | -511.5 | -65.1 | -108.2 | -155.1 | -341.5 | -13.8 | -22.6 | -34.2 |
| | High Center | -165.5 | -241.0 | -308.7 | -488.5 | -57.7 | -96.3 | -138.4 | -308.8 | -12.1 | -19.8 | -30.0 |
| | High Egde | -155.1 | -223.3 | -281.4 | -406.7 | -56.1 | -93.1 | -132.9 | -288.9 | -12.1 | -19.8 | -29.9 |
| Morning (20 °C) | Uniform | -197.9 | -283.3 | -355.5 | -515.0 | -67.3 | -111.8 | -159.3 | -341.2 | -13.3 | -21.6 | -32.5 |
| | High Center | -179.0 | -257.9 | -326.3 | -493.5 | -59.8 | -99.5 | -142.3 | -308.8 | -11.7 | -18.9 | -28.5 |
| | High Egde | -167.3 | -237.9 | -295.8 | -407.9 | -58.0 | -96.0 | -136.4 | -288.2 | -11.7 | -18.9 | -28.5 |

Note. Compression is negative and tension positive.

Table A-1. Parametric study: stresses and strains at the peak load (continued)

(g) E11 (Horizontal Strain) at the bottom element under the load center

| AC Thickness (cm) | | 7.6 | | | | 17.8 | | | | 38.1 | | |
|---|---|---|---|---|---|---|---|---|---|---|---|---|
| Base Modulus (MPa) | | 138 | 345 | 689 | 6895 | 138 | 345 | 689 | 6895 | 138 | 345 | 689 |
| Loading Condition | | | | | | | | | | | | |
| Temperature Condition | | | | | | | | | | | | |
| | Uniform | 3.70E-04 | 2.01E-04 | 1.11E-04 | 1.01E-05 | 2.24E-04 | 1.52E-04 | 1.02E-04 | 1.81E-05 | 4.10E-05 | 3.44E-05 | 2.76E-05 |
| Day | High Center | 3.44E-04 | 1.93E-04 | 1.10E-04 | 1.30E-05 | 2.01E-04 | 1.37E-04 | 9.30E-05 | 1.74E-05 | 3.59E-05 | 3.01E-05 | 2.42E-05 |
| (43 ~ °C) | High Egde | 3.02E-04 | 1.59E-04 | 8.38E-05 | 4.65E-06 | 1.92E-04 | 1.29E-04 | 8.59E-05 | 1.43E-05 | 3.58E-05 | 3.00E-05 | 2.41E-05 |
| Average Day | Uniform | 3.88E-04 | 2.11E-04 | 1.16E-04 | 1.02E-05 | 2.45E-04 | 1.65E-04 | 1.10E-04 | 2.05E-05 | 4.86E-05 | 4.02E-05 | 3.18E-05 |
| | High Center | 3.62E-04 | 2.03E-04 | 1.15E-04 | 1.33E-05 | 2.19E-04 | 1.49E-04 | 1.00E-04 | 1.97E-05 | 4.26E-05 | 3.52E-05 | 2.79E-05 |
| (41, 38, 34°C) | High Egde | 3.18E-04 | 1.67E-04 | 8.79E-05 | 4.53E-06 | 2.09E-04 | 1.40E-04 | 9.26E-05 | 1.62E-05 | 4.25E-05 | 3.51E-05 | 2.77E-05 |
| | Uniform | 1.97E-04 | 1.31E-04 | 8.56E-05 | 7.21E-06 | 1.29E-04 | 9.77E-05 | 7.18E-05 | 1.19E-05 | 2.79E-05 | 2.46E-05 | 2.08E-05 |
| Night | High Center | 1.79E-04 | 1.21E-04 | 8.04E-05 | 8.30E-06 | 1.15E-04 | 8.72E-05 | 6.44E-05 | 1.13E-05 | 2.44E-05 | 2.15E-05 | 1.82E-05 |
| (13 ~ °C) | High Egde | 1.66E-04 | 1.08E-04 | 6.94E-05 | 4.32E-06 | 1.11E-04 | 8.38E-05 | 6.12E-05 | 9.63E-06 | 2.44E-05 | 2.15E-05 | 1.82E-05 |
| Morning | Uniform | 2.12E-04 | 1.37E-04 | 8.83E-05 | 7.09E-06 | 1.28E-04 | 9.66E-05 | 7.07E-05 | 1.16E-05 | 2.49E-05 | 2.21E-05 | 1.89E-05 |
| | High Center | 1.93E-04 | 1.27E-04 | 8.34E-05 | 8.35E-06 | 1.14E-04 | 8.63E-05 | 6.35E-05 | 1.10E-05 | 2.17E-05 | 1.94E-05 | 1.66E-05 |
| (20 °C) | High Egde | 1.78E-04 | 1.13E-04 | 7.11E-05 | 4.06E-06 | 1.10E-04 | 8.27E-05 | 6.02E-05 | 9.31E-06 | 2.18E-05 | 1.94E-05 | 1.65E-05 |

(h) E22 (Vertical Strain) at the bottom element under the load center

| AC Thickness (cm) | | 7.6 | | | | 17.8 | | | | 38.1 | | |
|---|---|---|---|---|---|---|---|---|---|---|---|---|
| Base Modulus (MPa) | | 138 | 345 | 689 | 6895 | 138 | 345 | 689 | 6895 | 138 | 345 | 689 |
| Loading Condition | | | | | | | | | | | | |
| Temperature Condition | | | | | | | | | | | | |
| | Uniform | -6.61E-04 | -3.78E-04 | -2.27E-04 | -5.74E-05 | -3.76E-04 | -2.68E-04 | -1.94E-04 | -7.37E-05 | -6.10E-05 | -5.24E-05 | -4.37E-05 |
| Day | High Center | -6.15E-04 | -3.62E-04 | -2.23E-04 | -6.14E-05 | -3.36E-04 | -2.41E-04 | -1.76E-04 | -6.86E-05 | -5.34E-05 | -4.59E-05 | -3.83E-05 |
| (43 ~ °C) | High Egde | -5.42E-04 | -3.01E-04 | -1.74E-04 | -3.91E-05 | -3.22E-04 | -2.28E-04 | -1.63E-04 | -6.04E-05 | -5.33E-05 | -4.58E-05 | -3.82E-05 |
| Average Day | Uniform | -7.05E-04 | -4.02E-04 | -2.40E-04 | -5.87E-05 | -4.31E-04 | -3.03E-04 | -2.17E-04 | -8.24E-05 | -8.15E-05 | -6.88E-05 | -5.62E-05 |
| | High Center | -6.56E-04 | -3.84E-04 | -2.36E-04 | -6.31E-05 | -3.85E-04 | -2.73E-04 | -1.97E-04 | -7.67E-05 | -7.13E-05 | -6.03E-05 | -4.93E-05 |
| (41, 38, 34°C) | High Egde | -5.78E-04 | -3.20E-04 | -1.84E-04 | -3.96E-05 | -3.69E-04 | -2.58E-04 | -1.83E-04 | -6.75E-05 | -7.13E-05 | -6.01E-05 | -4.91E-05 |
| | Uniform | -2.47E-04 | -1.73E-04 | -1.23E-04 | -4.02E-05 | -1.77E-04 | -1.40E-04 | -1.11E-04 | -5.12E-05 | -4.02E-05 | -3.63E-05 | -3.17E-05 |
| Night | High Center | -2.25E-04 | -1.59E-04 | -1.15E-04 | -4.01E-05 | -1.58E-04 | -1.25E-04 | -9.94E-05 | -4.69E-05 | -3.52E-05 | -3.17E-05 | -2.78E-05 |
| (13 ~ °C) | High Egde | -2.08E-04 | -1.43E-04 | -1.00E-04 | -3.03E-05 | -1.53E-04 | -1.20E-04 | -9.46E-05 | -4.27E-05 | -3.52E-05 | -3.17E-05 | -2.77E-05 |
| Morning | Uniform | -2.81E-04 | -1.92E-04 | -1.34E-04 | -4.18E-05 | -1.69E-04 | -1.33E-04 | -1.06E-04 | -4.92E-05 | -3.22E-05 | -2.93E-05 | -2.60E-05 |
| | High Center | -2.56E-04 | -1.78E-04 | -1.26E-04 | -4.20E-05 | -1.50E-04 | -1.19E-04 | -9.47E-05 | -4.51E-05 | -2.82E-05 | -2.57E-05 | -2.28E-05 |
| (20 °C) | High Egde | -2.36E-04 | -1.58E-04 | -1.09E-04 | -3.11E-05 | -1.45E-04 | -1.14E-04 | -8.99E-05 | -4.10E-05 | -2.82E-05 | -2.56E-05 | -2.27E-05 |

Note. Compression is negative and tension positive.

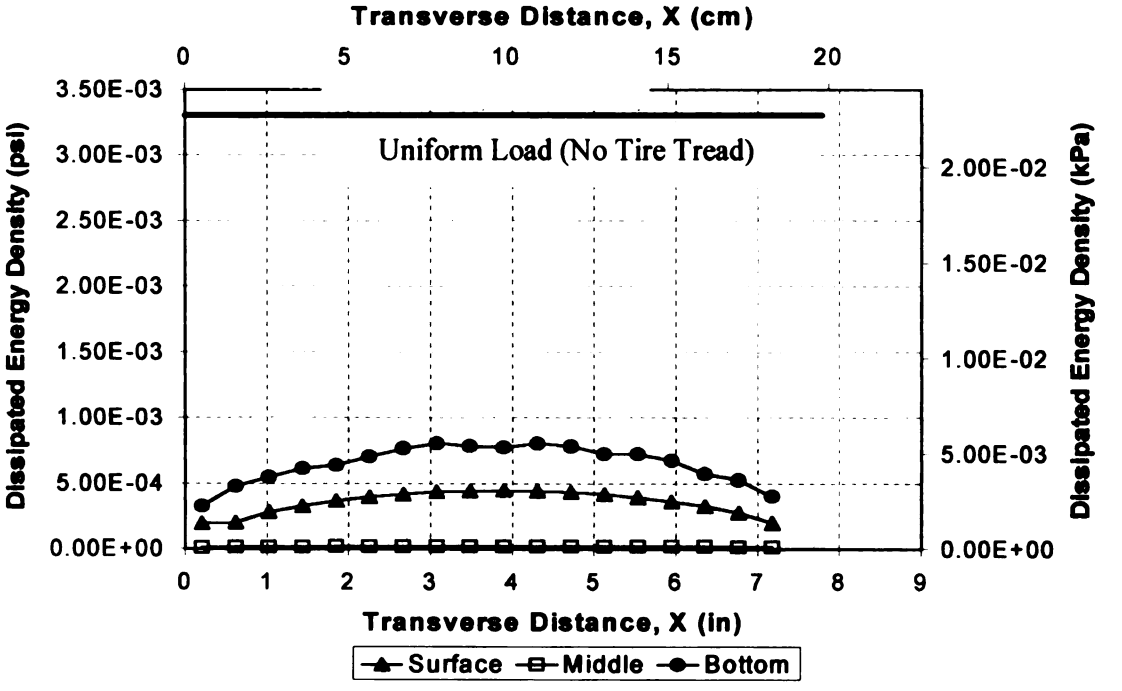


(a) at the front row

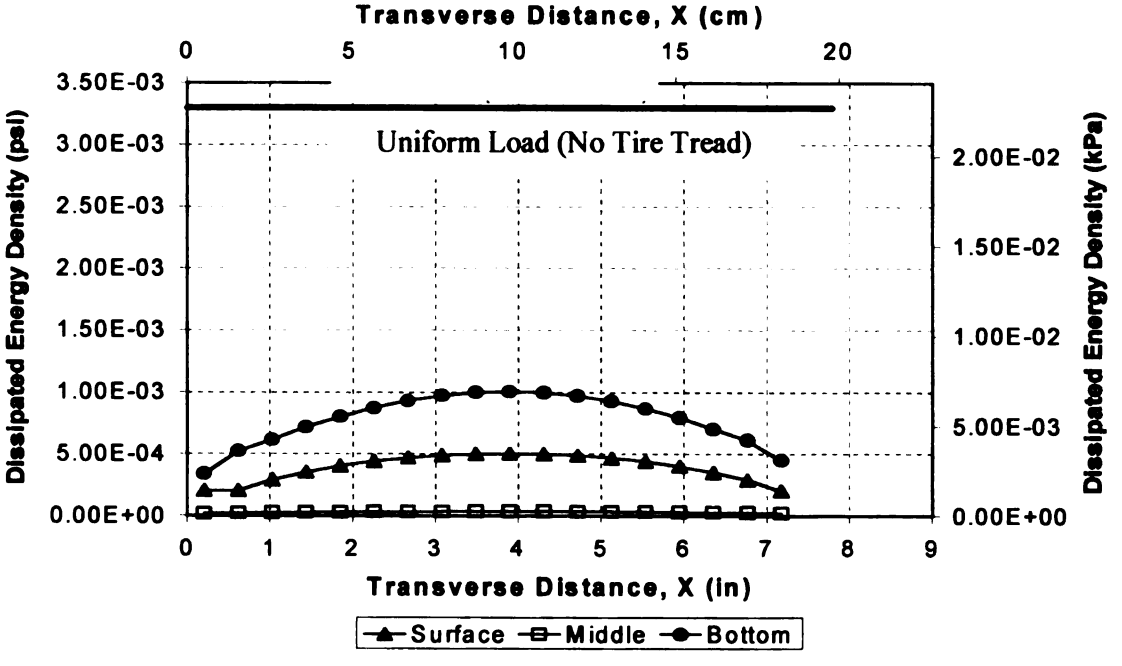


(b) at the middle row

Figure A-1. Calculated dissipated energy for the load case I and night temperature distribution

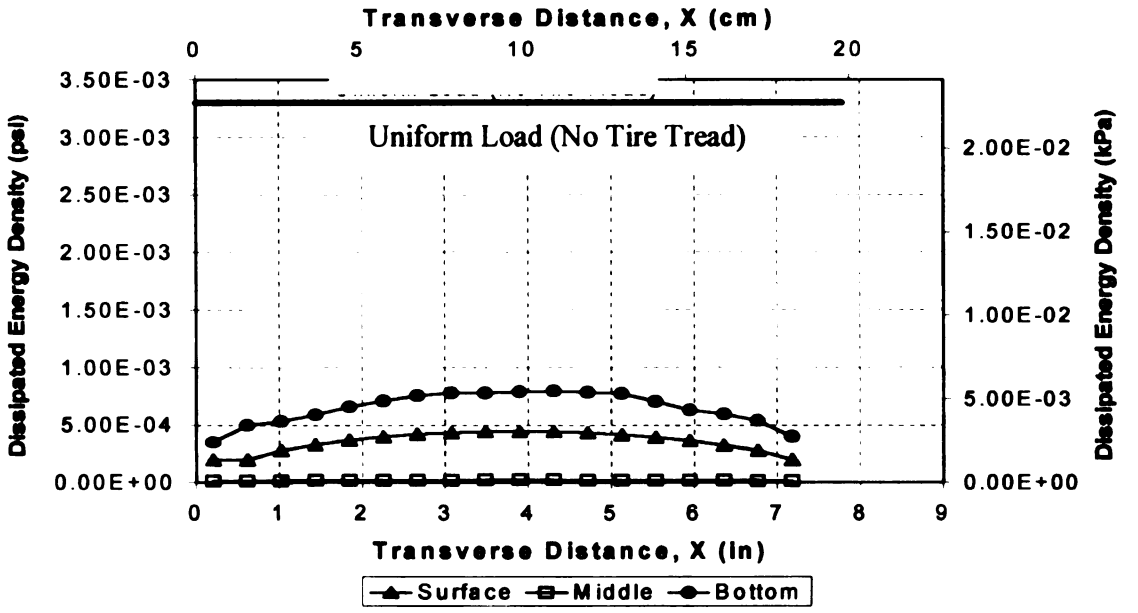


(c) at the rear row

Figure A-1. Calculated dissipated energy for the load case I and night temperature distribution (continued)

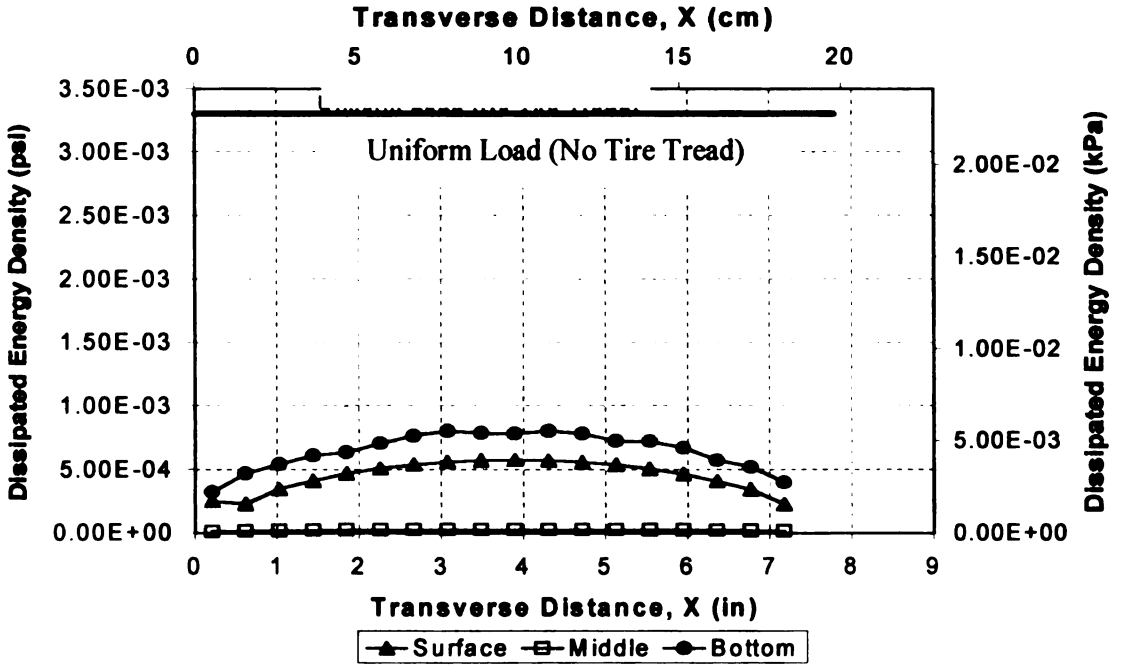


(a) at the front row

Figure A-2. Calculated dissipated energy for the load case I and morning temperature distribution

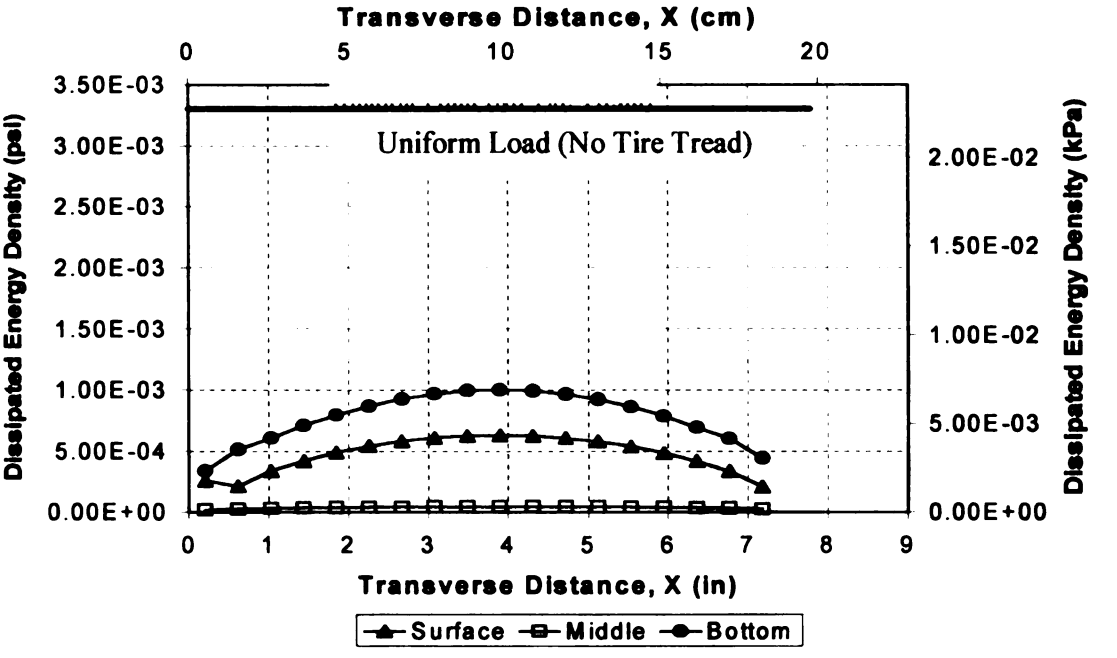


(b) at the middle row

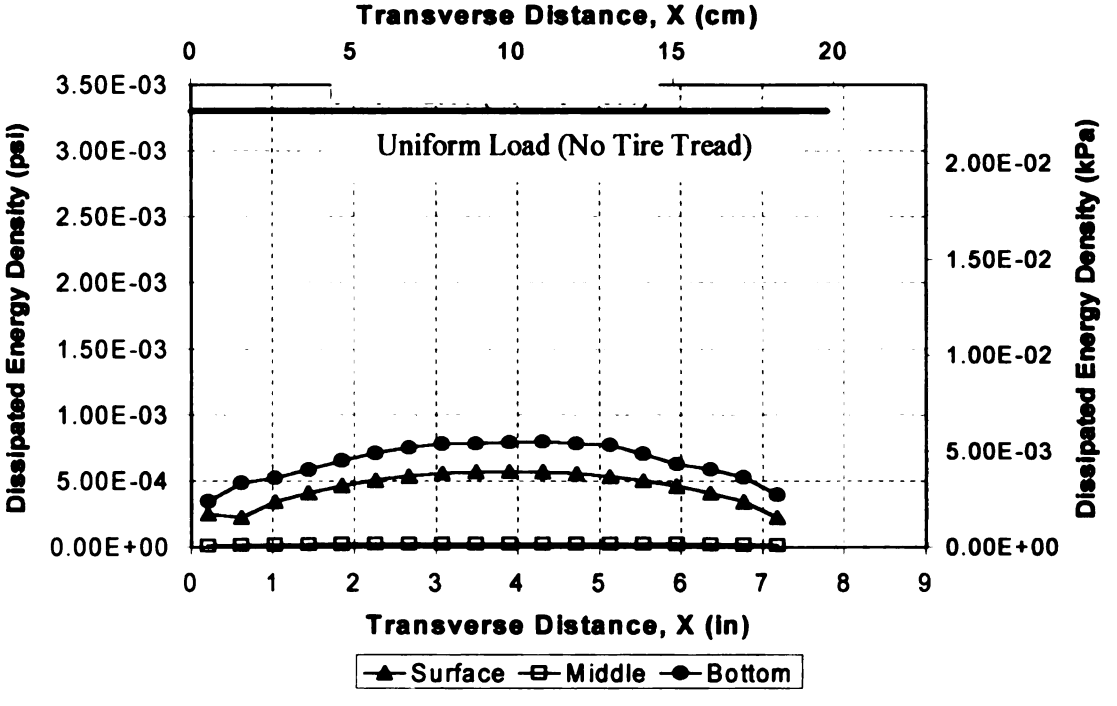


(c) at the rear row

Figure A-2. Calculated dissipated energy for the load case I and morning temperature distribution (continued)

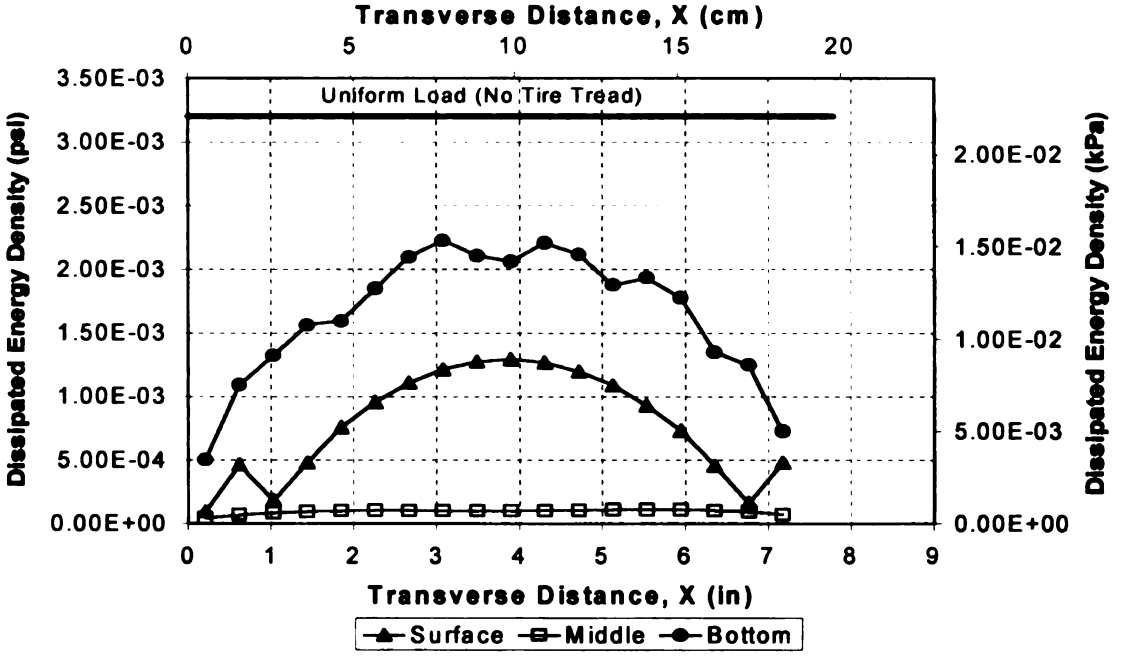


(a) at the front row

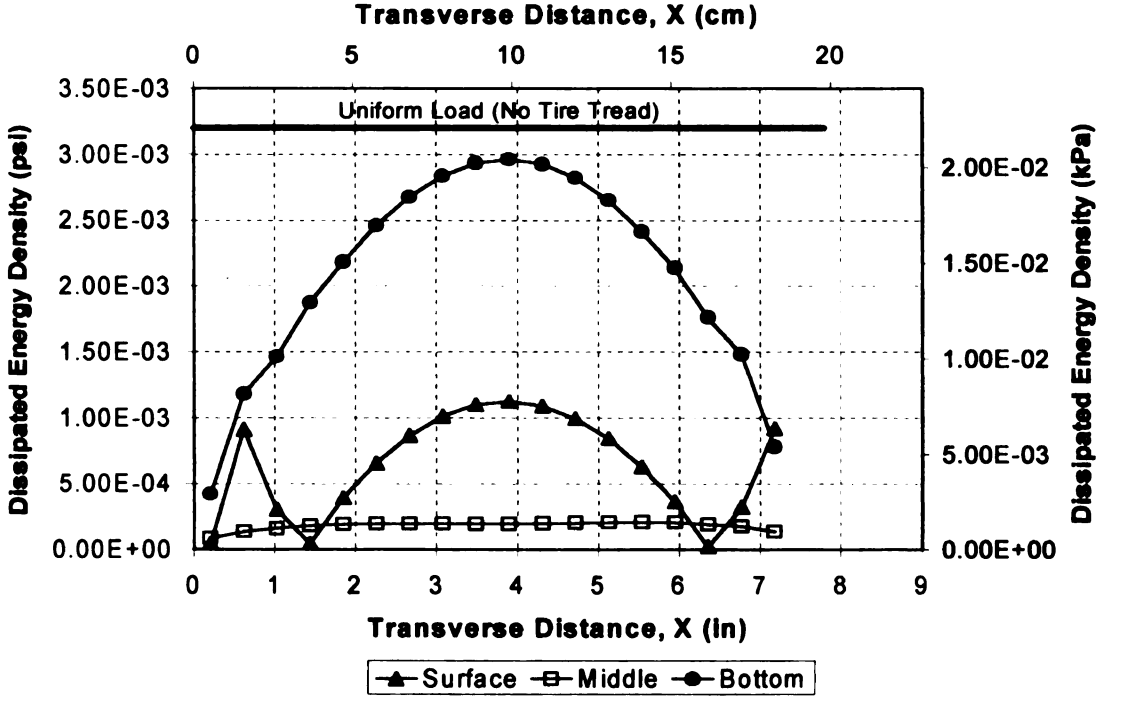


(b) at the middle row

Figure A-3. Calculated dissipated energy for the load case I and day temperature distribution

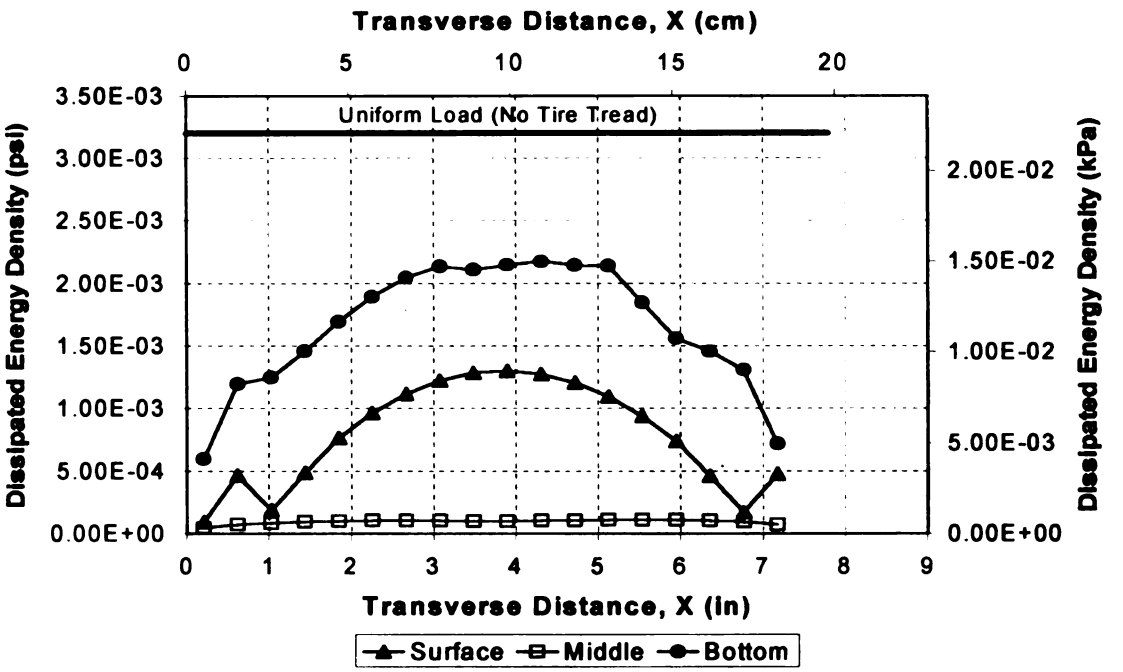


(c) at the rear row

Figure A-3. Calculated dissipated energy for the load case I and day temperature distribution (continued)

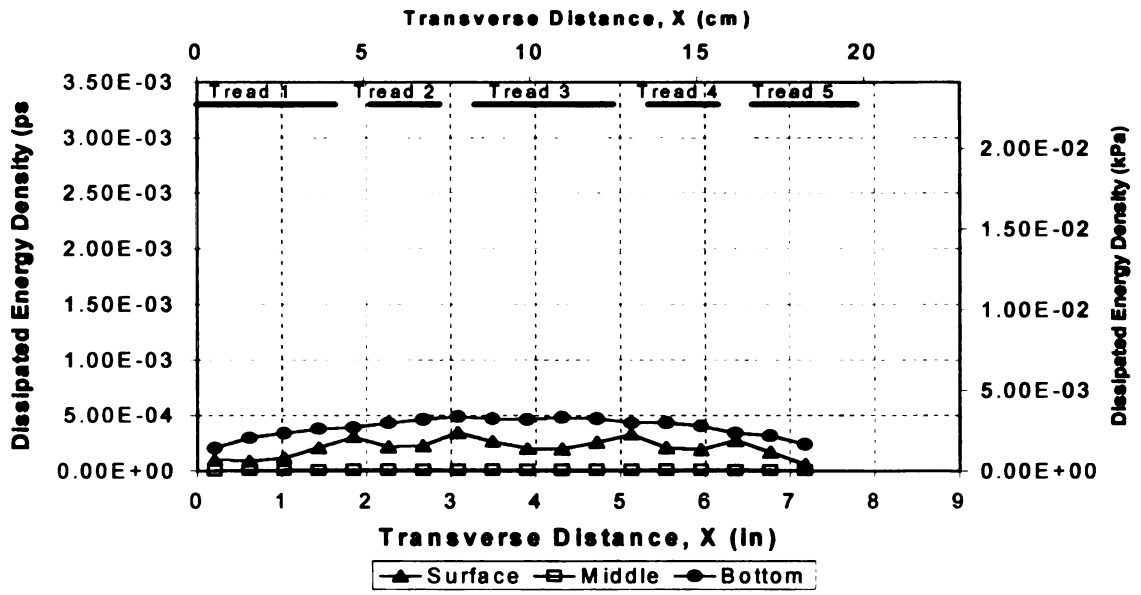


(a) at the front row

Figure A-4. Calculated dissipated energy for the load case II and night temperature distribution

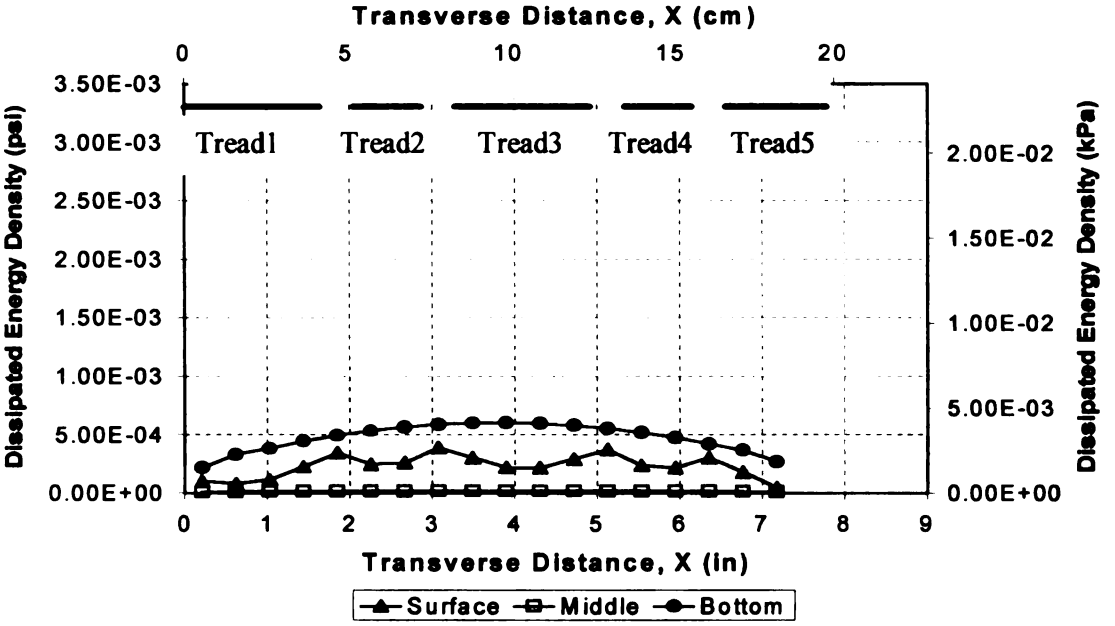


(b) at the middle row

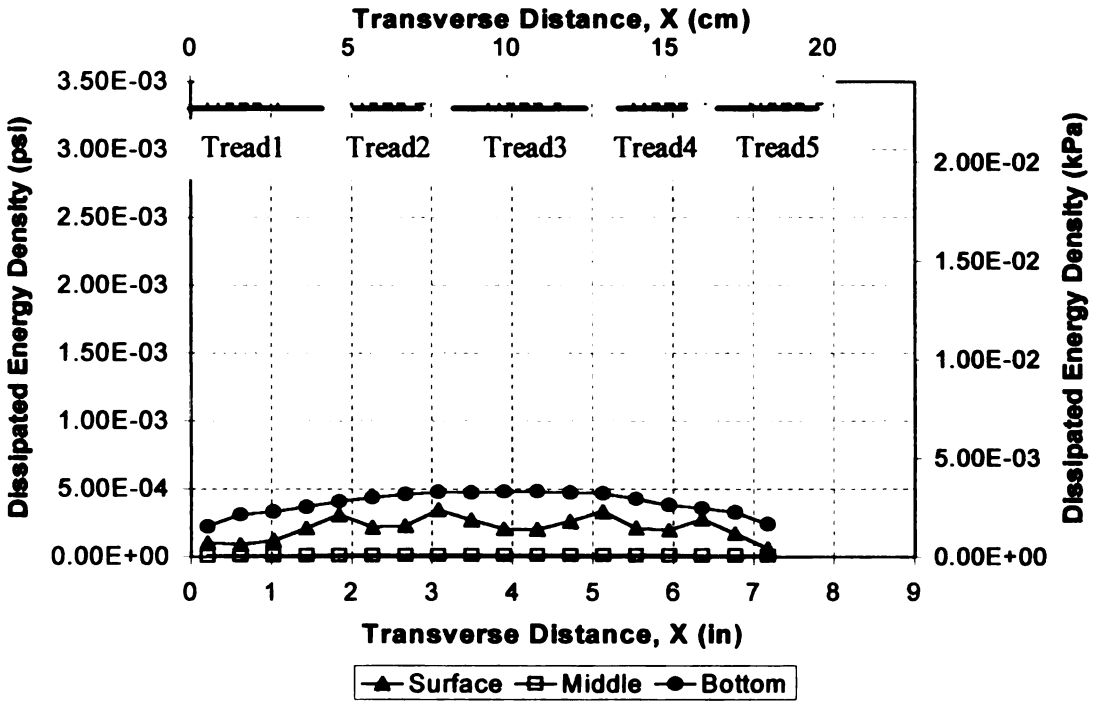


(c) at the rear row

Figure A-4. Calculated dissipated energy for the load case II and night temperature distribution (continued)

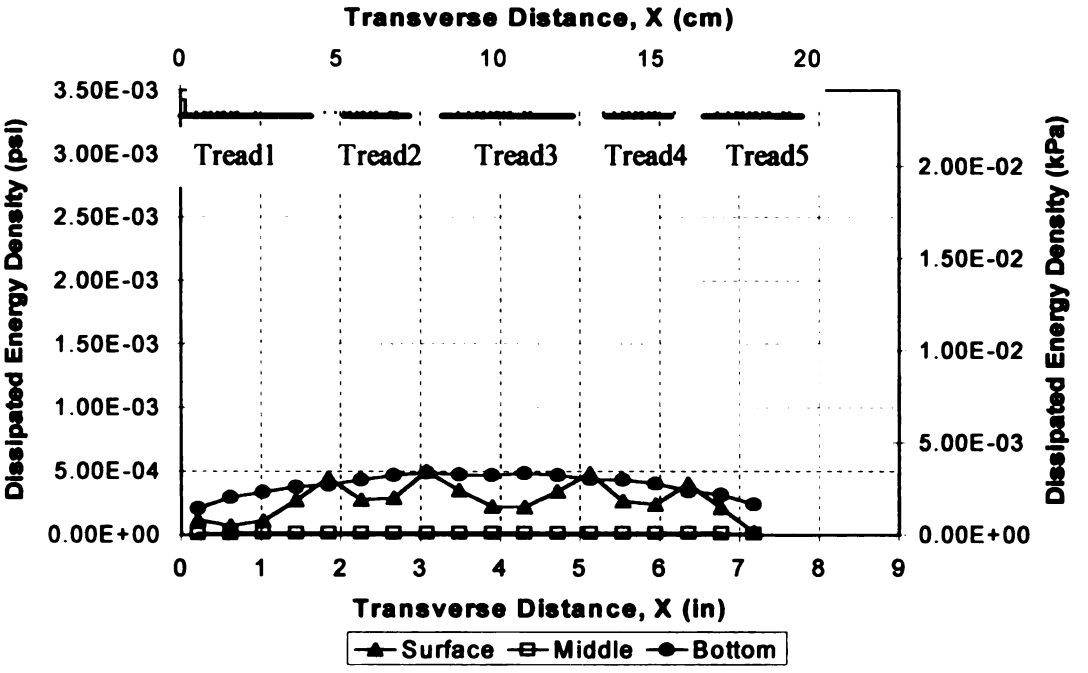


(a) at the front row

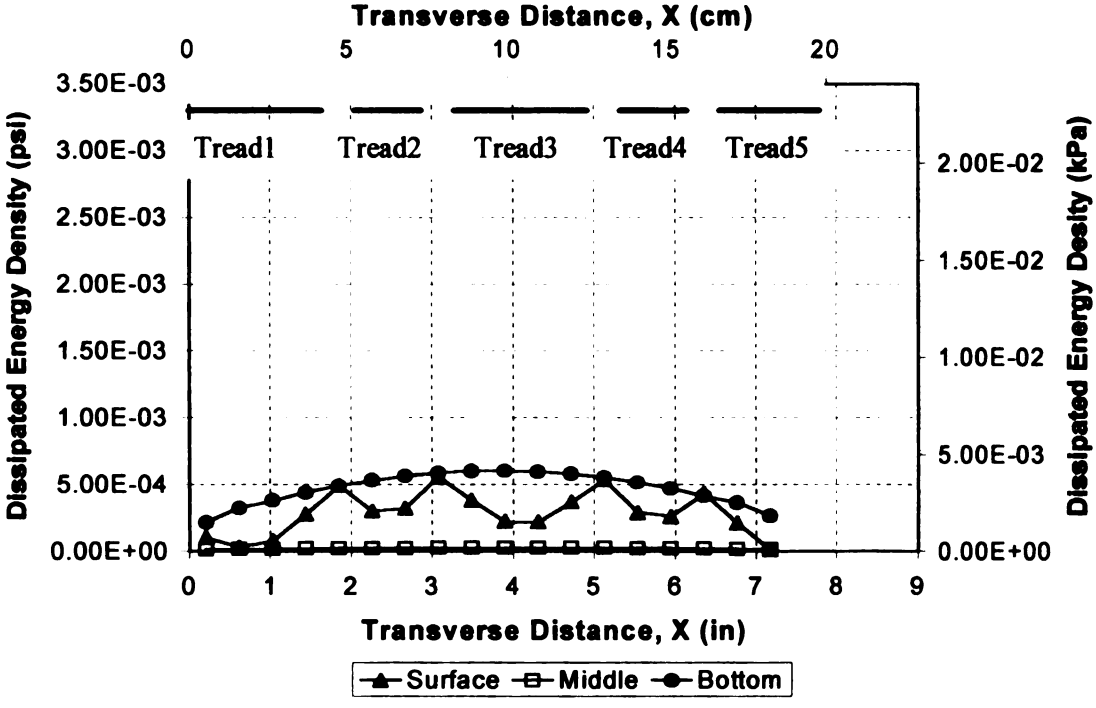


(b) at the middle row

Figure A-5. Calculated dissipated energy for the load case II and morning temperature distribution

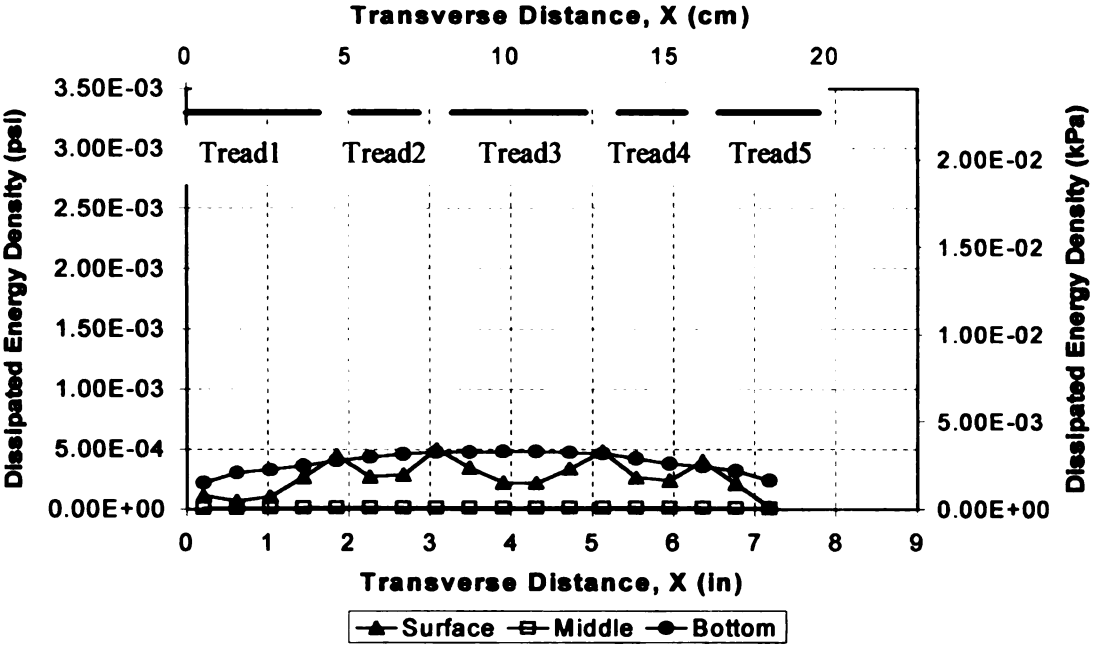


(c) at the rear row

Figure A-5. Calculated dissipated energy for the load case II and morning temperature distribution (continued)

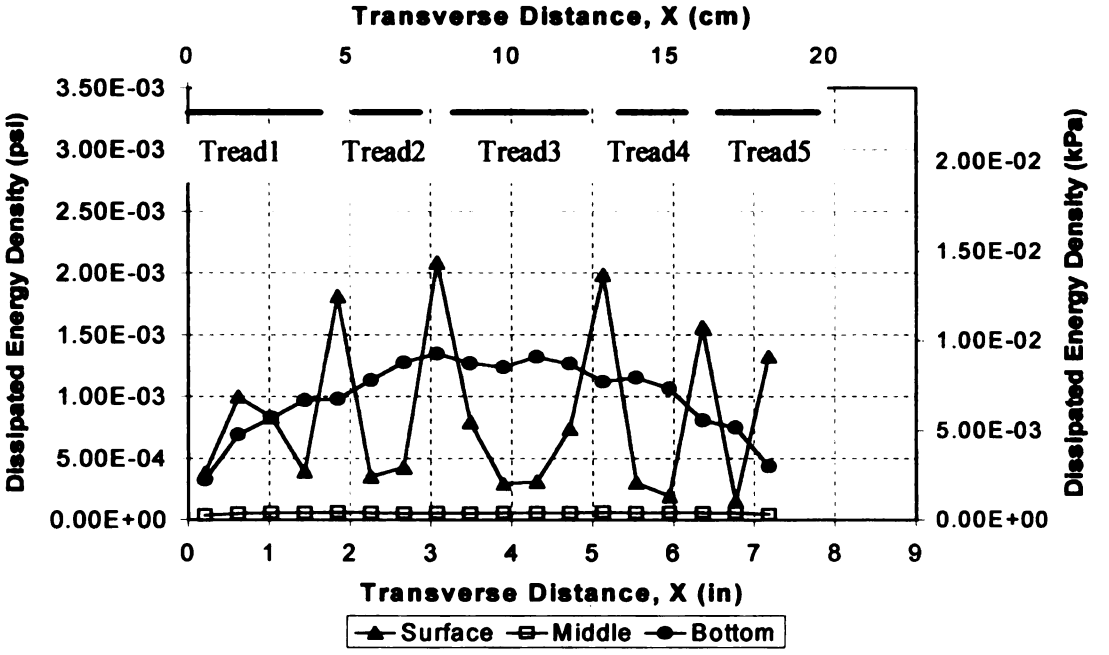


(a) at the front row

Figure A-6. Calculated dissipated energy for the load case II and day temperature distribution

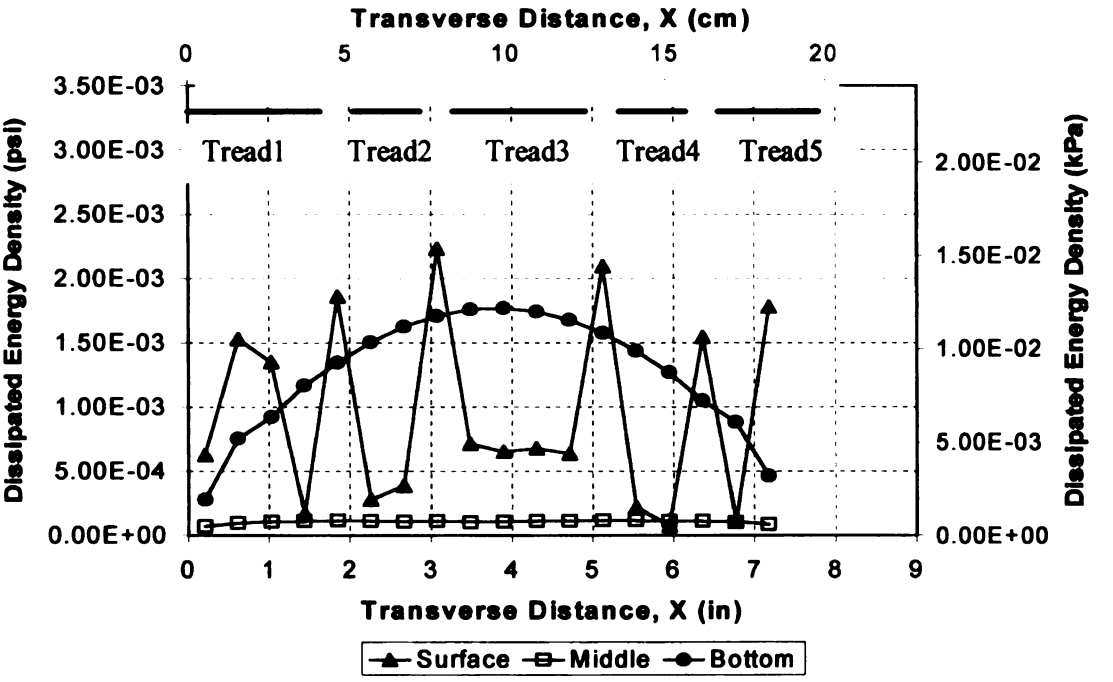


(b) at the middle row

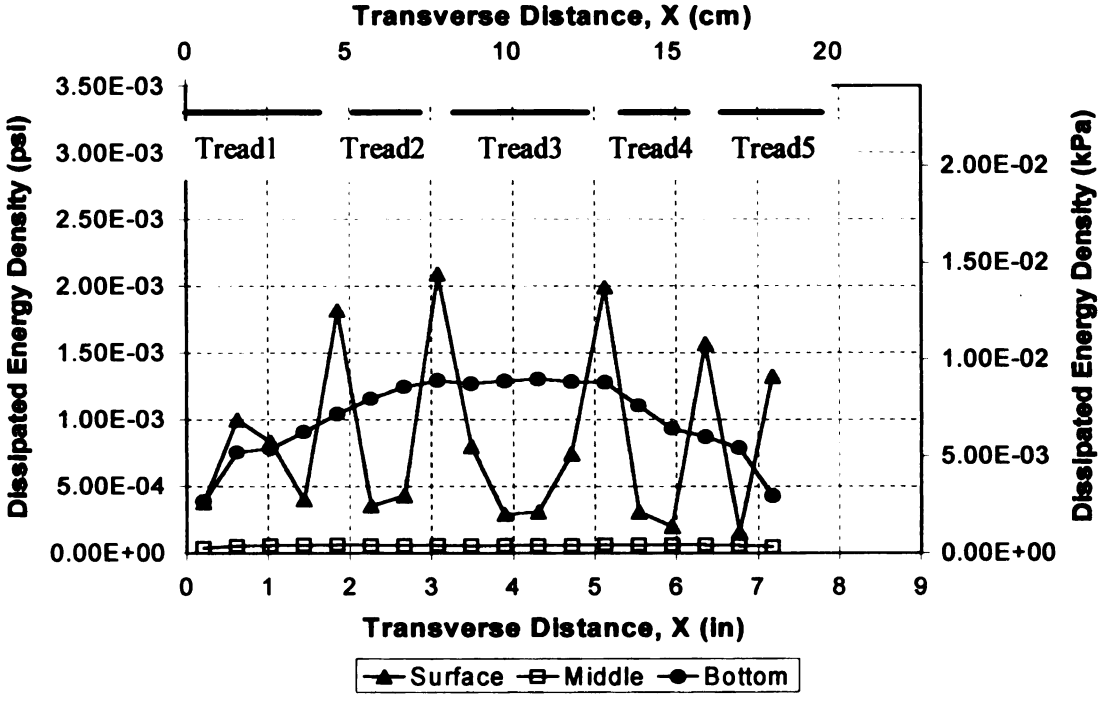


(c) at the rear row

Figure A-6. Calculated dissipated energy for the load case II and day temperature distribution (continued)

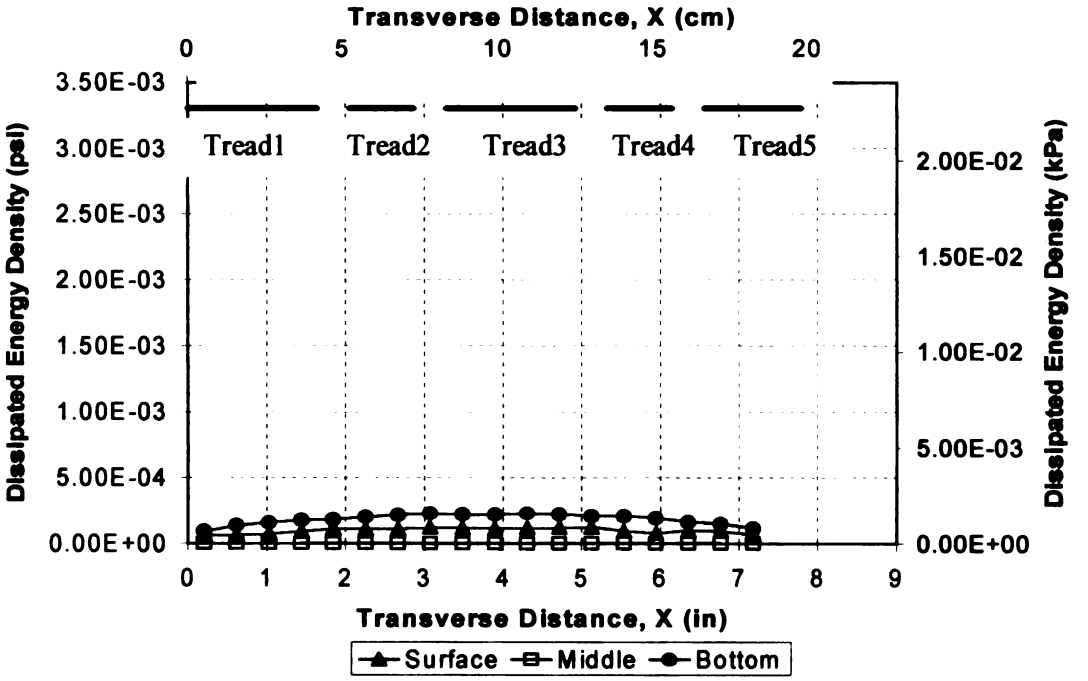


(a) at the front row

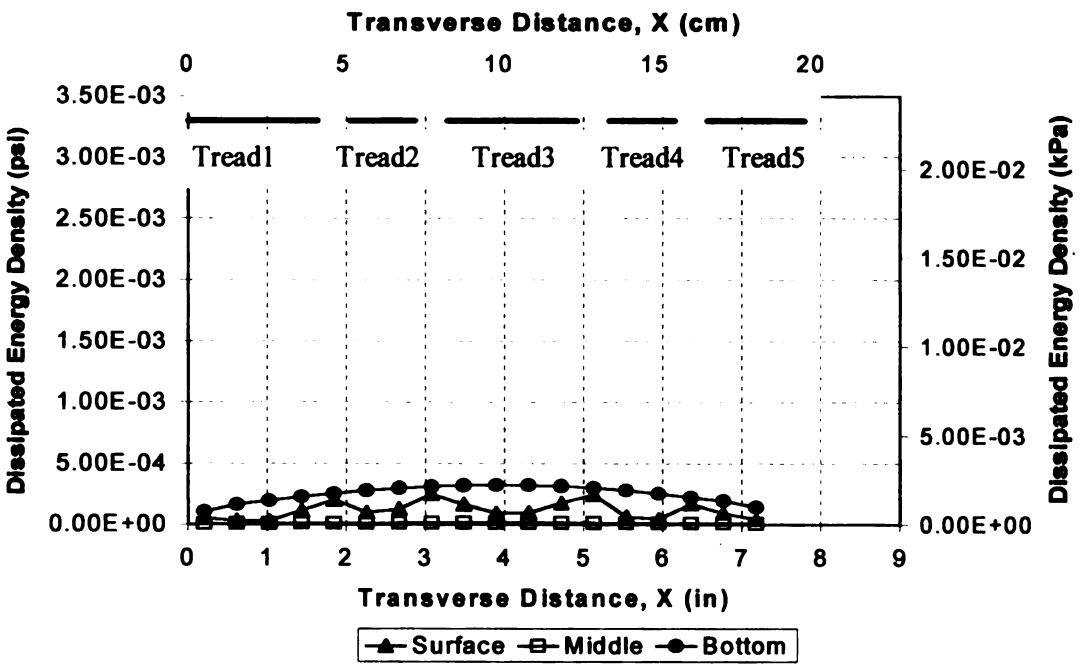


(b) at the middle row

Figure A-7. Calculated dissipated energy for the load case III and night temperature distribution

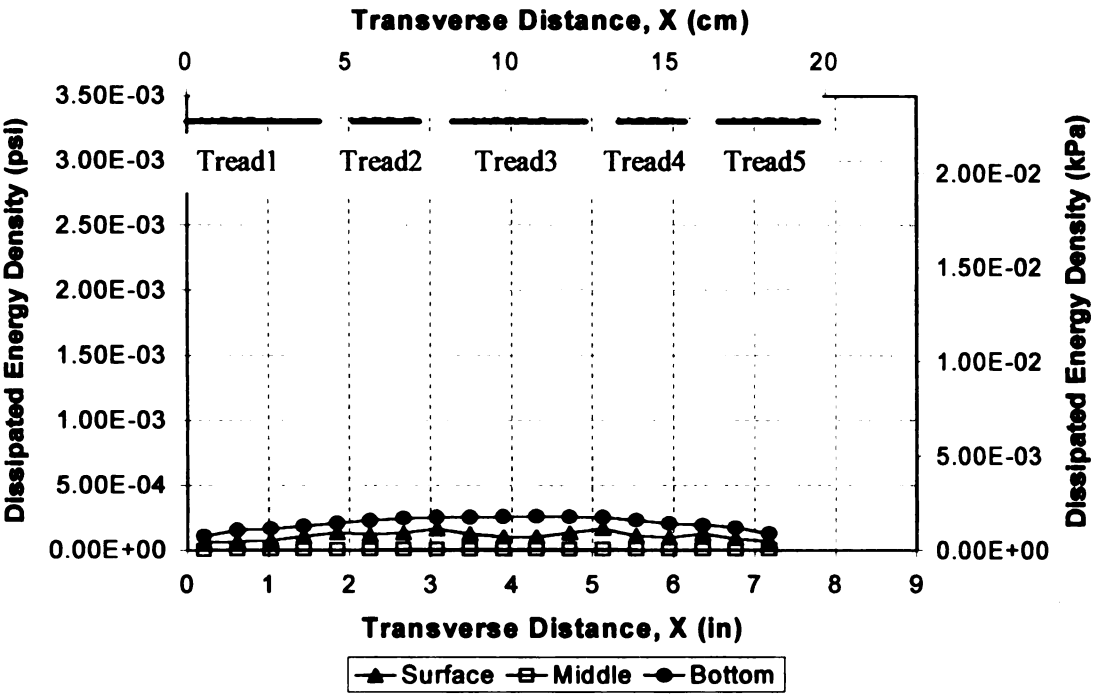


(c) at the rear row

Figure A-7. Calculated dissipated energy for the load case III and night temperature distribution (continued)

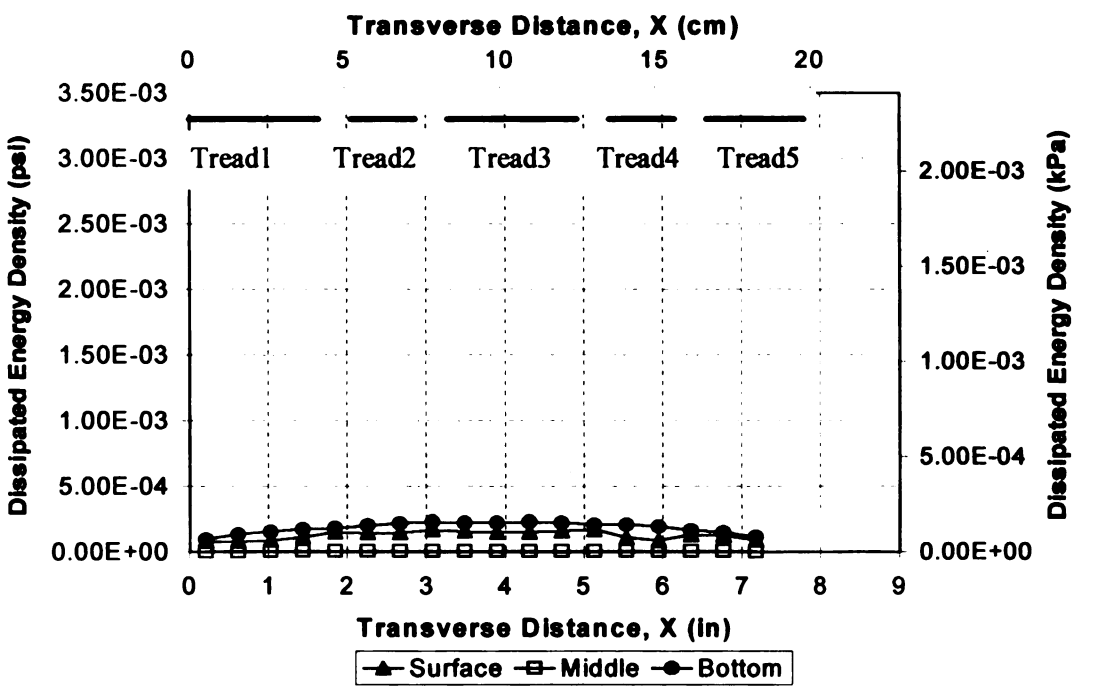


(a) at the front row

Figure A-8. Calculated dissipated energy for the load case III and morning temperature distribution

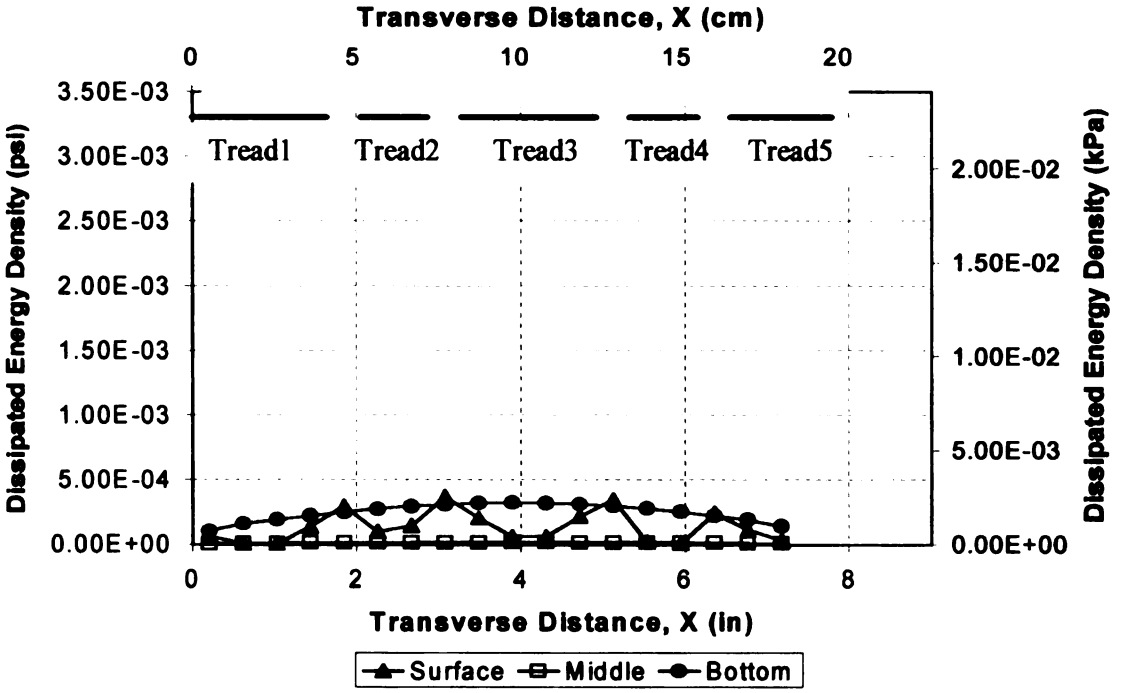


(b) at the middle row

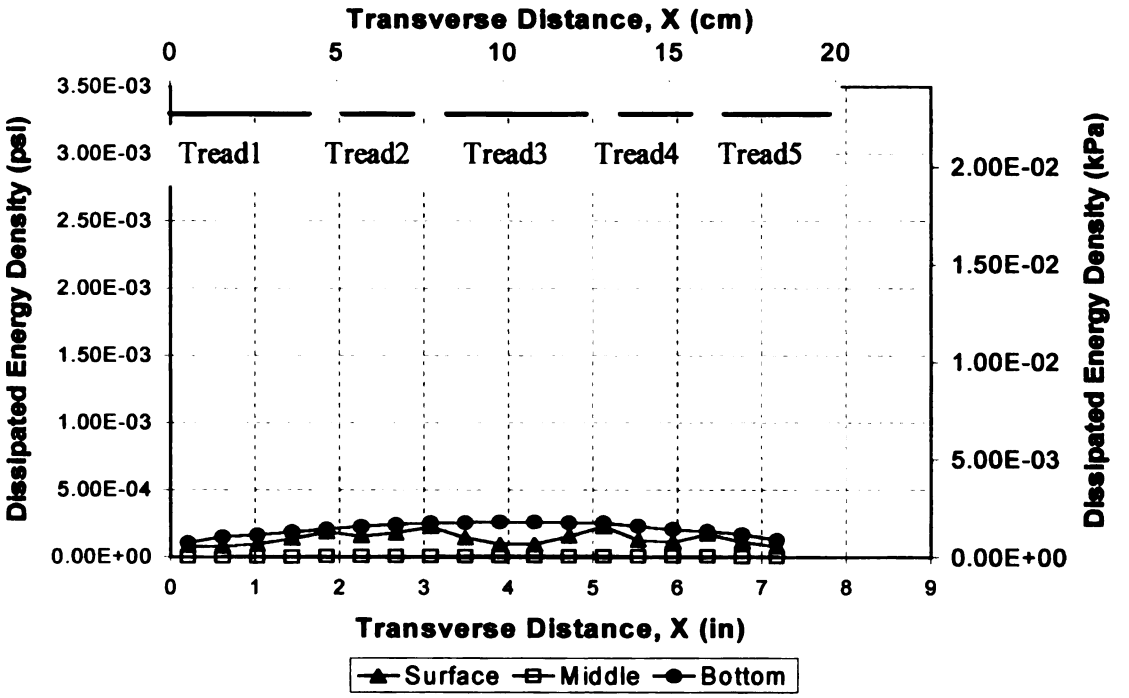


(c) at the rear row

Figure A-8. Calculated dissipated energy for the load case III and morning temperature distribution (continued)

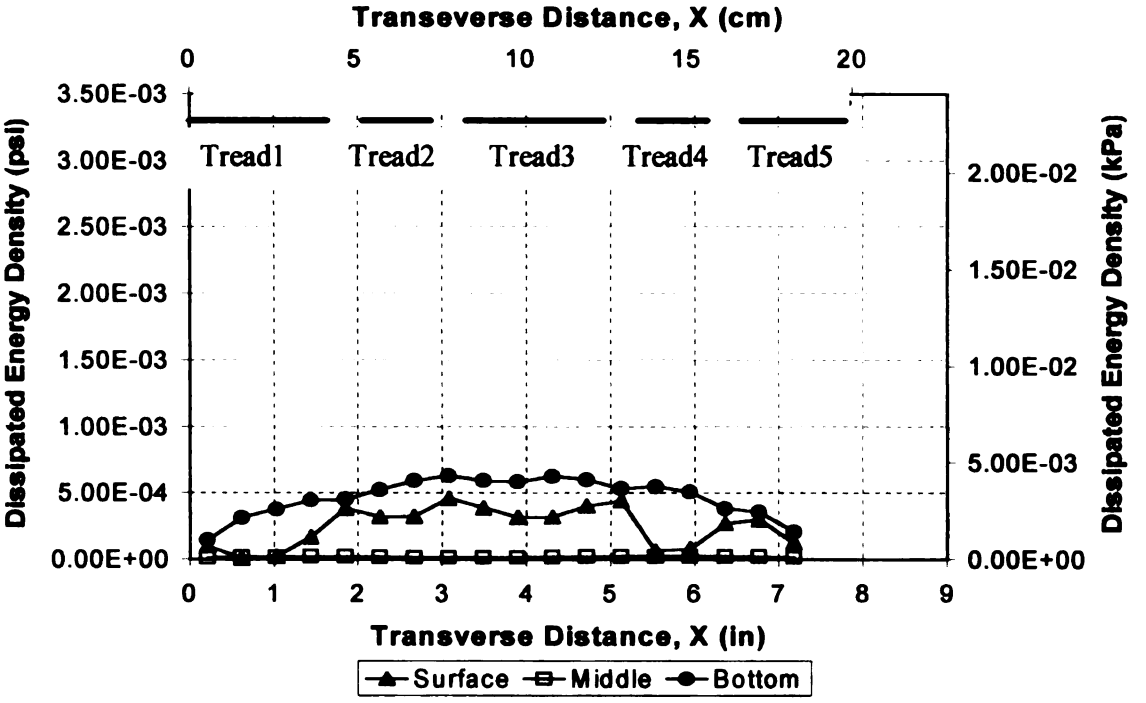


(a) at the front row

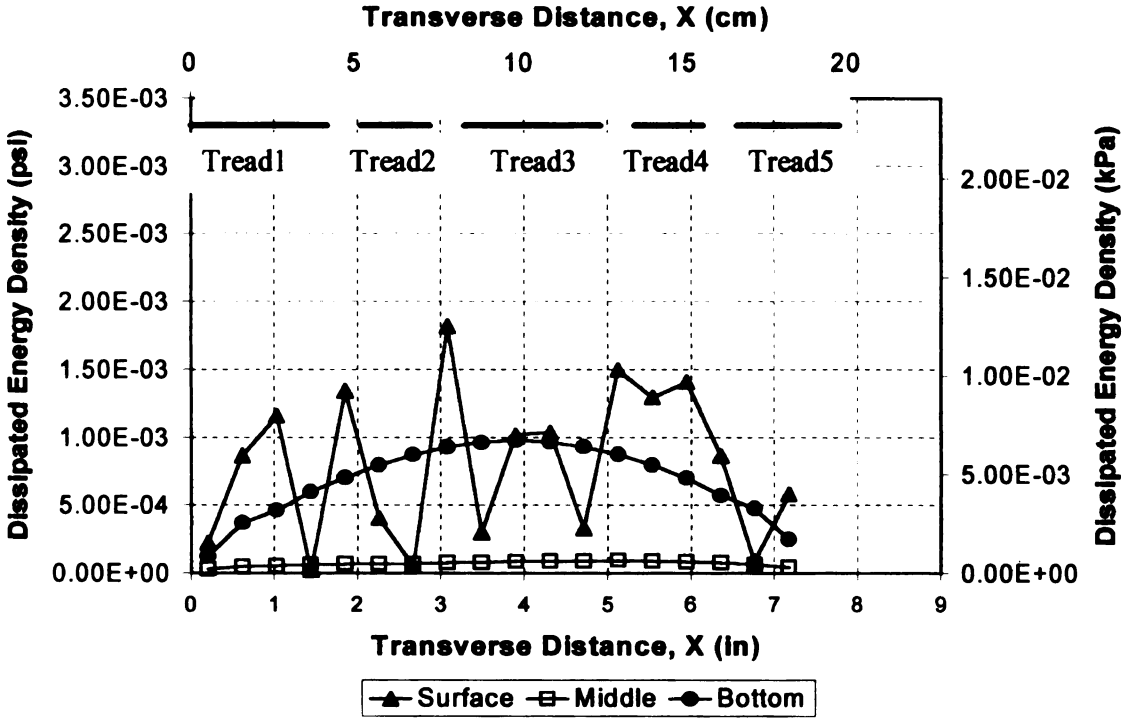


(b) at the middle row

Figure A-9. Calculated dissipated energy for the load case III and day temperature distribution

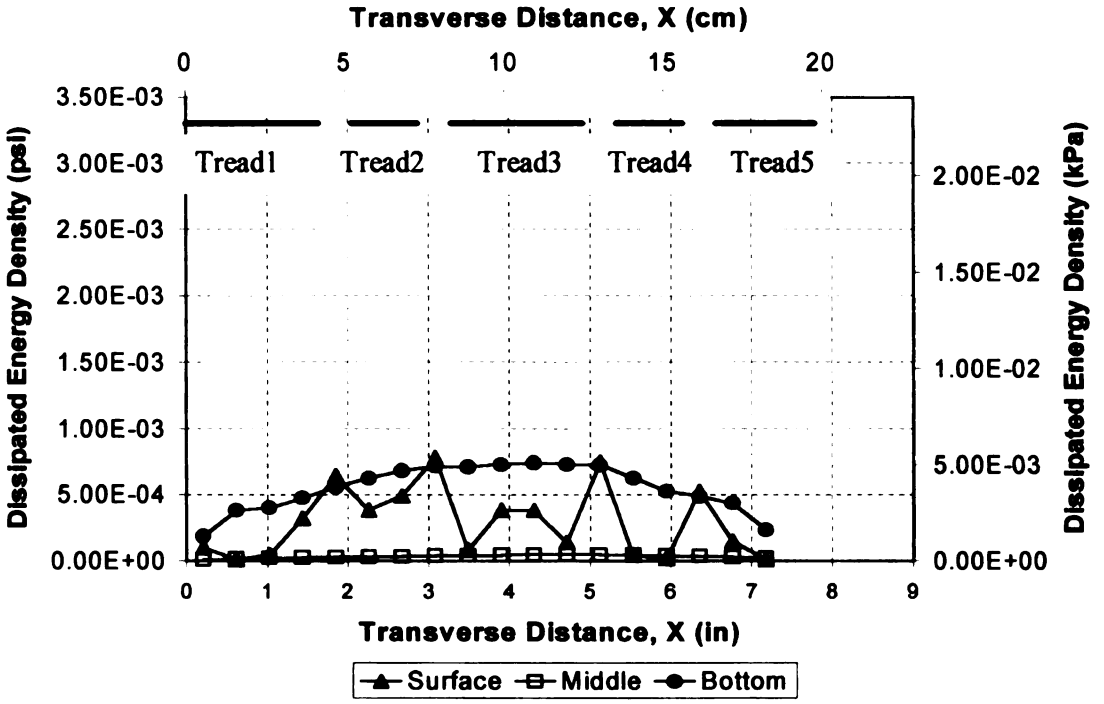


(c) at the rear row

Figure A-9. Calculated dissipated energy for the load case III and day temperature distribution (continued)

## APPENDIX B

## EXAMPLE OF A FINITE ELEMENT ANALYSIS INPUT FILE

An example ABAQUS input file of a 3-D analysis is here presented. Mesh and elements were generated and imported from I-DAES. Because the generated input model defines nodes with each nodal coordinates instead of keyword commands, node and element definition in the input file therefore are huge. Due to the space limitations, some parts skip.

Note. Lines starting with multiple * are comment lines.

```
**************************************************************
*HEADING
SDRC I-DEAS ABAQUS FILE TRANSLATOR
*** This input file is for the 3-D model: uniform load and day temperature distribution.
*** Detailed geometry is presented in Chapter 5.
**************************************************************
*** Node Definition
**************************************************************
*NODE, SYSTEM=R
      1, 5.0000000E+00, 2.4650000E+02,-5.0000000E+00
      2, 5.0000000E+00, 2.4650000E+02,-4.5900000E+00
      3, 5.0000000E+00, 2.4650000E+02,-4.1800000E+00
      4, 5.0000000E+00, 2.4650000E+02,-3.7700000E+00
      5, 5.0000000E+00, 2.4650000E+02,-3.3600000E+00
      6, 5.0000000E+00, 2.4650000E+02,-2.9500000E+00
      7, 5.0000000E+00, 2.4650000E+02,-2.5400000E+00
      8, 5.0000000E+00, 2.4650000E+02,-2.1300000E+00
      9, 5.0000000E+00, 2.4650000E+02,-1.7200000E+00
     10, 5.0000000E+00, 2.4650000E+02,-1.3100000E+00
******************************
**** skip due to the space limitations
******************************
```

```
    34970, 6.3050468E+00, 2.3820433E+02, 5.7219956E-01
    34971,-4.4805292E+01, 2.3950000E+02, 2.8351542E+01
**************************************************************
*** Element Definition
**************************************************************
*ELEMENT,TYPE=C3D4   ,ELSET=BASE
21149,26693,26698,26713,26162
21150,25496,28901,25472,28633
21151,31028,31033,9265,33168
*******************************
**** skip due to the space limitations
*******************************
73789,28262,28267,30763,28322
*ELEMENT,TYPE=C3D4   ,ELSET=SOILT
20021,24241,24317,24244,24240
20022,24241,24244,24317,24243
20023,24237,24278,24238,24243
20024,24237,24238,24278,24255
20025,24226,24224,24273,24277
*******************************
**** skip due to the space limitations
*******************************
21147,24240,24244,24311,24317
21148,24244,24317,24243,24238
*ELEMENT,TYPE=C3D8   ,ELSET=AC
1,1,2,23,22,442,443,464,463
2,2,3,24,23,443,444,465,464
3,3,4,25,24,444,445,466,465
4,4,5,26,25,445,446,467,466
5,5,6,27,26,446,447,468,467
6,6,7,28,27,447,448,469,468
*******************************
**** skip due to the space limitations
*******************************
19997,23556,23557,8838,8837,23997,23998,9279,9278
19998,23557,23558,8839,8838,23998,23999,9280,9279
19999,23558,23559,8840,8839,23999,24000,9281,9280
20000,23559,23560,8841,8840,24000,24001,9282,9281
*ELEMENT,TYPE=C3D8   ,ELSET=SOIL
20001,24002,24003,24006,24005,24011,24012,24015,24014
20002,24003,24004,24007,24006,24012,24013,24016,24015
20003,24005,24006,24009,24008,24014,24015,24018,24017
*******************************
**** skip due to the space limitations
*******************************
20019,24041,24042,24045,24044,24050,24051,24054,24053
```

```
20020,24042,24043,24046,24045,24051,24052,24055,24054
**********************************************************
****El sets and Node sets for analysis
**********************************************************
*NSET, NSET=NDTOPMID, GENERATE
10,409,21
*ELSET, ELSET=ELTOP, GENERATE
2,362,20
10,370,20
12,372,20
13,373,20
19,379,20
*ELSET, ELSET=ELMIDDLE, GENERATE
1602,1962,20
1610,1970,20
1612,1972,20
1613,1973,20
1619,1979,20
*ELSET, ELSET=ELBTTM, GENERATE
3602,3962,20
3612,3972,20
3614,3974,20
3615,3975,20
3619,3979,20
*ELSET, ELSET=ELANLY
ELTOP,ELMIDDLE,ELBTTM,
*ELSET, ELSET=ELTOTALTOP, GENERATE
1,380,1
*ELSET, ELSET=ELTREAD1, GENERATE
1,60,1
*ELSET, ELSET=ELTREAD2, GENERATE
81,120,1
*ELSET, ELSET=ELTREAD3, GENERATE
141,220,1
*ELSET, ELSET=ELTREAD4, GENERATE
241,280,1
*ELSET, ELSET=ELTREAD5, GENERATE
301,380,1
*ELSET, ELSET=ELTREAD
ELTREAD1,ELTREAD2,ELTREAD3,ELTREAD4,ELTREAD5
*******
*ELSET, ELSET=ACALL, GENERATE
1,3980,1
*ELSET, ELSET=ACCROSS, GENERATE
12,372,20
412,772,20
```

```
812,1172,20
1212,1572,20
1612,1972,20
2012,2372,20
2412,2772,20
2812,3172,20
3212,3572,20
3612,3972,20
********
*ELSET, ELSET=V1, GENERATE
1,3,1
21,23,1
*ELSET, ELSET=V2, GENERATE
4,6,1
24,26,1
******************************
**** skip due to the space limitations
******************************
*ELSET, ELSET=S91, GENERATE
100356,100358,1
100376,100378,1
*ELSET, ELSET=S92, GENERATE
100359,100360,1
100379,100380,1
************************************************************
****Membrane Element for lateral stress applications
***The membrane elements have negligible stiffness
************************************************************
*ELEMENT,TYPE=M3D4,ELSET=MEMB1
100001,22,23,2,1
*ELGEN, ELSET=ALLMEMB
100001,20,1,1,19,21,20
************************************************************
***Material Definition
************************************************************
**************************
*MEMBRANE SECTION, ELSET=ALLMEMB, MATERIAL=MEMBRANE1
1
*MATERIAL,NAME=MEMBRANE1
*ELASTIC,TYPE=ISOTROPIC
0.000001
**************************
*SOLID SECTION,ELSET=BASE,MATERIAL=BASE
*MATERIAL,NAME=BASE
*ELASTIC,TYPE=ISOTROPIC
5.0E+4, 0.35
```

```
*** psi
*SOLID SECTION,ELSET=SOILT,MATERIAL=SOIL
*MATERIAL,NAME=SOIL
*ELASTIC,TYPE=ISOTROPIC
1.0E+04, 4.500E-01
*SOLID SECTION,ELSET=SOIL,MATERIAL=SOIL
*SOLID SECTION,ELSET=AC,MATERIAL=AC
*MATERIAL,NAME=AC
*ELASTIC,TYPE=ISOTROPIC
2071851, 0.3
****psi
*VISCOELASTIC,TIME=PRONY
0.1546401,,1.1447957
0.3099463,,0.0006052
0.3118353,,0.0173438
0.1846149,,0.0000131
**********
*TRS
25.,47.8,392
**degree C
**********************************************
*** Boundary Condition
*** Temperature is specified to each node or node sets.
*** It is assumed that temperature varies only with depth (Y-direction).
**********************************************
*INITIAL CONDITION, TYPE=TEMPERATURE
***** unit degree C
1,43.00
2,43.00
3,43.00
4,43.00
5,43.00
6,43.00
********************************
**** skip due to the space limitations
********************************
34941,34.22
34946,34.22
34951,34.22
34956,34.22
34961,34.22
34966,34.22
34971,34.22
***************
*BOUNDARY
4872,1
```

```
5292,1
5313,1
5733,1
******************************
**** skip due to the space limitations
******************************
9766,3
9745,3
9724,3
9703,3
**************************************************
*** Apply Load
**************************************************
*RESTART,WRITE,FREQ=10000
***************
******STEP 1
*STEP,INC=10,AMPLITUDE=RAMP
*VISCO,CETOL=0.1
0.001,0.001250
*DLOAD
ELTOTALTOP,P1,2.76
*ELPRINT,ELSET=ELANLY,TOTALS=YES,POSITION=CENTROIDAL,FREQ=100
00
S11,S22,S33,E11,E22,E33,S13,E13,S23
*NODE PRINT,NSET=NDTOPMID,TOTALS=YES,FREQ=10000
U,RF
*NODE FILE, NSET=NDTOPMID, FREQ=1
U,RF
*END STEP
***********
*****STEP 2
*STEP,INC=10,AMPLITUDE=RAMP
*VISCO,CETOL=0.1
0.001,0.001875
*DLOAD
ELTOTALTOP,P1,19.32
*ELPRINT,ELSET=ELANLY,TOTALS=YES,POSITION=CENTROIDAL,FREQ=100
00
S11,S22,S33,E11,E22,E33,S13,E13,S23
*NODE PRINT,NSET=NDTOPMID,TOTALS=YES,FREQ=10000
U,RF
*NODE FILE, NSET=NDTOPMID, FREQ=1
U,RF
*END STEP
***********
******************************
```

```
**** skip due to the space limitations
*******************************
*************
*****STEP 18
*STEP,INC=10,AMPLITUDE=RAMP
*VISCO,CETOL=0.1
0.001,0.002969
*DLOAD
ELTOTALTOP,P1,0
*ELPRINT,ELSET=ELANLY,TOTALS=YES,POSITION=CENTROIDAL,FREQ=100
00
S11,S22,S33,E11,E22,E33,S13,E13,S23
*NODE PRINT,NSET=NDTOPMID,TOTALS=YES,FREQ=10000
U,RF
*NODE FILE, NSET=NDTOPMID, FREQ=1
U,RF
*END STEP
***********
*****STEP 19
*STEP,INC=10
*VISCO,CETOL=0.1
0.1,0.0228437
*ELPRINT,ELSET=ELANLY,TOTALS=YES,POSITION=CENTROIDAL,FREQ=100
00
S11,S22,S33,E11,E22,E33,S13,E13,S23
*NODE PRINT,NSET=NDTOPMID,TOTALS=YES,FREQ=10000
U,RF
*NODE FILE, NSET=NDTOPMID, FREQ=1
U,RF
*END STEP
***********
************************************************************
```

# REFERENCES

## References


*AASHTO Guide for Design of Pavement Structures,* American Association of State Highway and Transportation Officials, Washington, D.C., 1986

*AASHTO Guide for Design of Pavement Structures,* American Association of State Highway and Transportation Officials, Washington, D.C., 1993

ABAQUS *User Manual*, Version 5.5, Hibbitt, Karlsson and Sorensen, Inc., 1993.

Acum, W.E.A. and Fox, L., *Computation of Road Stresses in a Three-layer Elastic System*, Geotechnique, 2, 1951, pp. 293-300.

AI, *Research and Development of The Asphalt Institute's Thickness Design Manual (MS-1),* 9th ed., Research Report 82-2, Asphalt Institute, 1982

Baladi, G.Y., *Integrated Material and Structural Design Method for Flexible Pavements*, Volume 1: Technical Report, Federal Highway Administration, Washington, D.C., 1988

Baladi, G.Y., and Snyder, M., *Highway Pavements*, A Four Week Course Developed for the FHWA, January, 1989.

Balzer, S. and Jansen, J.M., *Temperature Correction of Asphalt Moduli for FWD Measurements*, Proceedings, 4th International Conference on the Bearing Capacity of Roads and Airfields, Minneapolis, Minnesota, 1994

Bonnaure, F., A. Gravois, and J. Udron, *A New Method for Predicting the Fatigue Life of Bituminous Mixes*, Proc., Association of Aspahlt paving Technologists, 1980

Briggs, R.C. and Lukanen, E.O., *Variations in Backcalculated Pavement Layer Moduli in LTPP Seasonal Monitoring Sites*, Nondestructive Testing of Pavements and Backcalculation of Moduli, Vol. 3, ASTM STP 1375, S.D. Tayabji and E.O. Lukanen, Eds., American Society for Testing and Materials, West Conshohocken, PA, 2000.

Brown, S.F., and Snaith, M.S., *The Permanent Deformation Characteristics of a Dense Bitumen Macadam Subjected to Repeated Loading*, Proc. 4th Conf. On Struct. Des of Asphalt Pavements, University of Michigan, Ann Arbor, Mich., 1978, pp. 225-248.

Buch, N., R. S. Harichandran, G. Y. Baladi, D.Y. Park, and H. B. Kim, *Calibration of Michigan's Rut and Fatigue Distress Models and Development of an Overlay Design Procedure in MICHBACK*, Michigan Department of Transportation (MDOT) Report (Report No. RC-1383), Michigan State University, East Lansing, MI, 1999.

Burmister, D.M., *The Theory of Stresses and Displacements in Layered Systems and Applications to the Design of Airport Runways*, Proceedings, Highway Research Board, 23, 1943, pp. 126-144.

Burmister, D.M., *The General Theory of Stresses and Displacements in Layered Soil Systems I, II, III*, J. Applied Physics, 16, 1945, pp. 84-94, 126-127,296-302.

Center for Research and Contract Standardization in Civil and Traffic Engineering (CROW), *Surface Cracking in Asphalt Layers*, Report of the Working Group, The Netherlands, March, 1990.

Chatti, K. and H. B. Kim, *Dissipated Energy Approach of Characterising the Fatigue Damage of Plain and Modified Asphalt Concrete Mixes Using the Indirect Tensile Test*, Final report, Project No. 0053, Composite Materials and Structure Center, Michigan State University, 1996

Chatti, K. and Yun, K.K., *SAPSI-M: Computer Program for Analyzing Asphalt Concrete Pavements Under Moving Arbitrary Loads*, Transportation Research Record No.1539, pp. 88-95, 1996

Chen, D.H., H-H. Lin, J. Bilyeu, and M. Murphy, *Temperature Correction on FWD Measurements*, 79th TRB Annual Meeting, TRB, National Research Council, Washington, D.C., 2000

Chen, H., K. Marshek, and C. Saraf, *Effects of Truck Tire Contact Pressure Distribution on the Design of Flexible Pavements: A Three-Dimensional Finite Element Approach*, Transportation Research Record 1095, TRB, National Research Council, Washington, D.C., 1986, pp. 72-86.

Cheung, Y.K. and O.C. Zienkiewicz, *Plate and Tanks on Elastic Foundations – An Application of Finite Element Method*, International Journal of Solids and Structures, Vol. 1, 1965, pp. 451-461.

Chou, Y.T. and Larew, H.G., *Stresses and Displacements in Viscoelastic Pavement Systems under a Moving Load*, Highway Research Record, 282, Highway Research Board, 1969, pp. 25-40.

Collop, A.C., D. Cebon, and M.S.A. Hardy, *Viscoelastic Approach to Rutting in Flexible Pavements*, Journal of Transportation Engineering, Vol. 121, No. 1, 1995.

Cook, R.D., Malkus, D.S., and Plesha, M.E. *Concepts and Applications of Finite Element Analysis*, 3rd edition, Wiley, New York, 1989.

*DATAPAVE,* a Software Package for Long Term Pavement Performance Information Management System (LTPP-IMS), FHWA, 1997

Dauzats, M., and A. Rampal, *Mechanism of Surface Cracking in Wearing Courses*, Proceedings, 6th International Conference Structural Design of Asphalt Pavements, The University of Michigan, Ann Arbor, MI, July 1987, pp. 232-247.

De Beer, M.m J. Groenendijk, and C. Fisher, *Three-Dimesional Contact Stresses Under the LINTRACK Wide-Base Single Tyres, Measured with the Vehicle-Road Surface Pressure Transducer Array (VRSPTA) System in South Africa*, Division of Roads and Transport Technology, Counsil for Scientific and Industrial Research, Pretoria, South Africa, Nov. 1996.

De Beer, M., C. Fisher, and F.J. Jootse, *Determination of Pneumatic Tire/Pavement Interface Contact Stresses Under Moving Loads and Some Effects on Pavements with Thin Asphalt Surfacing Layers*, Proceedings, 8th International Conference on Asphalt Pavements, University of Washington, Seattle, Washington, August 1997, pp. 179-227.

Dempsey, B.J., W.A. Herlach and A.J. Patel, *The Climatic-Materials-Structural Pavement Analysis Program*, Final Report, Federal Highway Administration Washington, D.C., FHWA/RD-84/115, Vol 3, February, 1985.

Elliott, J.F. and Moavenzadeh, F., *Analysis of Stresses and Displacements in Three-layer Viscoelastic Systems*, Highway Research Record, 345, Highway Research Board, 1971, pp. 45-57.

Gerritsen, A.H., C.A.P.M. van Gurp, J.P.J. van der Heide, A.A.A. Molenaar, and A.C. Pronk, *Prediction and Prevention of Surface Cracking in Asphaltic Pavements*, 6th International Conference Structural Design of Asphalt Pavements, The University of Michigan, Ann Arbor, MI, July 1987, pp.378-391.

Harichandran, R.S., Ramon, C.M., and Baladi, G.Y., "MICHBACK User's Manual", Department of Civil and Environmental Engineering, Michigan State University, East Lansing, Michigan, 1994.

Himeno, K., T. Ikeda, T. Kamijima, and T. Abe, *Distribution of Tire Contact Pressure of Vehicles and Its Influence on Pavement Distress*, Proceedings, 8th International Conference on Asphalt Pavements, University of Washington, Seattle, Washington, August 1997, pp. 129-139.

Huang, Y.H., *Computation of Equivalent Single-Wheel Loads Using Layered Theory*, Highway Research Record, 291, Highway Research Board, 1969, pp. 144-155.

Huang, Y.H., *Stresses and Strains in Viscoelastic Multilayer Systems Subjected to Moving Loads*, Highway Research Record, 457, Highway Research Board, 1973, pp. 60-71.

Huang, Y.H., *Pavement Analysis and Design*, Prentice-Hall Inc., Englewood Cliffs, N.J., 1993

Huhtala, M., R. Alkio, J. Pihljamaki, M. Pienmaki, and P. Halonan, *Behavior of Bituminous Materials Under Moving Wheel Loads*, Journal of the Association of Asphalt Paving Technologists, Vol. 59, 1990, pp. 422-442.

Huhtala, M. and J. Pihljamaki, *New Concepts on Load Equivalency Measurements*, Proceedings, 7th International Conference on Asphalt Pavements, Vol. 3, 1992, pp. 194-208.

Hwang, D., and M.W. Witczak, *Program DAMA (Chevron)*, User's Manual, Department of Civil Engineering, University of Maryland, 1979

I-DEAS *Master Series*, Structural Dynamics Research Corporation, 1997

Inge, E.H., and Kim, Y.R., *Prediction of Effective Asphalt Layer Temperature*, Transportation Research Record 1473, TRB, National Research Council, Washington, D.C., 1994

Johnson, A.M. and Baus, R.L. *Alternative method for temperature correction of backcalculated equivalent pavement moduli*, Transportation Research Record 1355, TRB, National Research Council, Washington, D.C., 1992

Jones, A. *Tables of Stresses in Three-layer Elastic Systems*, Bulletin 342, Highway Research Board, 1962, pp. 176-214.

Kenis, W.J., *Predictive Design Procedures, A Design Method for Flexible Pavements using the VESYS Structural Subsystem*, Proc., 4th International Conference on the Structural Design of Asphalt Pavements, 1,1977, pp.101-147.

Kenis, W.J., *Predictive Design Procedures, VESYS Users Manual-An Interim Design Method for Flexible Pavements using the VESYS Structural Subsystem*, Final Rep. No. FHWA-RD-77-154, U.S. Dept. of Transp., Washington, D.C., 1978.

Kim, H.B., N. Buch, and D.Y. Park, *Mechanistic-Empirical Rut Prediction Model for In-Service Pavements*, 79th TRB Annual Meeting, TRB, National Research Council, Washington, D.C., 2000

Kim, Y.R., S.W. Park, and L. Shao, *Statewide Calibration of Asphalt Temperature Study from 1992 and 1993*, NCDOT Report (Project 23241-95-1), North Carolina State University, Raleigh, NC, 1996.

Kuo, Chen-Ming, *Three-Dimensional Finite Element Analysis of Concrete Pavement*, Ph.D. Thesis, University of Illinois at Urbana-Champaign, 1994.

Lee, H.J. and Y.R. Kim, *Viscoelastic Constitutive Model for Asphalt Concrete under Cyclic Loading*, Journal of Engineering Mechanics, Vol. 124, No. 1, 1998.

Love, A.E.H., *Mathematical Theory of Elasticity*, 4th ed., Cambridge University Press, New York, 1927.

Lu, Y. and Wright, P.J., *Temperature Related Visco-Elastoplastic Properties of Asphalt Mixtures*, J. of Tranp. Engrg, Vol 126, No.1, 2000, pp. 58-65.

Lukanen, E.O., R. Stubstad, and R. Briggs, *Temperature Predictions and Adjustment Factors for Asphalt Pavement*, FHWA-RD-98-085, LTPP Final Report, Federal Highway Administraion, 2000

Lytton, R.L., Germann, F.P., Chou, Y.J. and Stoffels, S.M., *Determining Asphalt Concrete Pavement Structural Properties by Nondestructive Testing* (NCHRP Report 327), Transportation Research Record, Washington, D.C., 1990.

Marsheck, K., H. Chen, R. Connell, and W. Hudson, *Experimental Determination of Pressure Distribution of Truck Tire-Pavement Contact*, Transportation Research Record 1070, TRB, National Research Council, Washington, D.C., 1986, pp. 9-13.

Marsheck, K., H. Chen, R. Connell, and C. Saraf, *Effect of Truck Tire Inflation Pressure and Axle Load on Flexible and Rigid Pavement Performance*, Transportation Research Record 1070, TRB, National Research Council, Washington, D.C., 1986a, pp. 14-21.

Moavenzadeh, F., Soussou, J.E., Findakly, H.K. and Brademeyer, B., *Synthesis for Rational Design of Flexible Pavements*, Part 3, Operating Instructions and Program Documentation, Reports Prepared for FHWA under Contract FH 11-776, 1974.

Mohseni, A. and M., Symons, *Effect of improved LTPP AC pavement temperature models on SUPERPAVE performance grades*, 77th Annual TRB conference, Washington D.C., 1998

Mohseni, A. and M., Symons, *Improved AC pavement temperature models from LTPP seasonal data*, 77th Annual TRB conference, Washington D.C., 1998a

Myers, L.A., R. Roque, and B.E. Ruth, *Mechanisms of Surface-Initiated Longitudinal Wheel Path Cracks in High-Type Bituminous Pavements*, Proceedings, Vol. 67, Association of Asphalt Paving Technologist, 1998, pp.401-432

Myers, L.A., R. Roque, B.E. Ruth, and C. Drakos, *Measurement of Contact Stresses for Different Truck Tire Types to Evaluate Their Influence on Near-Surface Cracking and Rutting*, Transportation Research Record 1655, TRB, National Research Council, Washington, D.C., 1999

Neter, J., W. Wasserman, and M. Kutner, *Applied Linear Regression Models*, 2nd Edition, Irwin, Homewood, Illinois, 1989

Nilsson, R.N., I. Oost, and P.C. Hopman, *Viscoelastic Analysis of Full-Scale Pavements: Validation of VEROAD*, Transp. Res. Record, No. 1539, Transp. Res. Board, Washington, D.C., 1996, pp. 81-87.

Owusu-Antwi, E.B., Titus-Glover, L. and Khazanovich, L., *A Rutting Model for Implementation in Mechanistic Base Design Procedure*. Presented at 77th Annual Meeting, TRB, National Research Council, Washington, D.C., 1998

Park, Sun Woo and Kim, Y. Richard, *Temperature Correction of Backcalculated Moduli and Deflections using Linear Viscoelasticity and Time-Temperature Superposition, TRB 76th Annual Meeting*, Washington, D. C., 1997.

Peattie, K.R., *Stress and Strain Factors for Three-layer Elastic Systems*, Bulletin 342, Highway Research Board, 1962, pp. 215-253.

Perloff, W.H. and Moavenzadeh, F., *Deflection of Viscoelastic Medium due to Moving Load*, Proc., 2nd International Conference on the Structural Design of Asphalt Pavements, University of Michigan, 1967, pp. 269-276.

Rowe, G.M., *Performance of Asphalt Mixtures in the Trapezoidal Fatigue Test*, Journal of the Association of Asphalt Paving Technologists, Vol. 62, 1993, pp. 344-384.

Rowe, G.M., S.F. Brown, M.J. Sharrock, and M.G. Bouldin, *Viscoelastic Analysis of Hot Mix Asphalt Pavement Structures*, Transp. Res. Record, No. 1482, Transp. Res. Board, Washington, D.C., 1995, pp. 44-51.

Rowe, G.M., and S.F. Brown, *Fatigue Life Prediction Using Visco-Elastic Analysis*, Proc., International Conference on Asphalt Pavements, Seattle, Washington, 1997, pp. 1109-1122.

Shao, L., S.W. Park, and Y.R. Kim, *Simplified procedure for prediction of asphalt pavement subsurface temperatures based on heat transfer theories,* Transportation Research Record 1568, TRB, National Research Council, Washington, D.C., 1997, pp. 114-123

*Shell Pavement Design Manual*, Shell International Petroleum Company, London, England, 1978.

Southgate, H.F., *An evaluation of temperature distribution of asphalt pavements and its relationship to pavement deflection*, MSCE Thesis, University of Kentucky, Lexington, Kentucky, 1968

Sperling, L.H., *Introduction to Physical Polymer Science*, John Wiley & Sons, Inc., 2nd Edition, Singapore, 1993

Strategic Highway Research Program (SHRP) A-404, *Fatigue Response of Asphalt-Aggregate Mixes*, ITS, University of California, Berkeley, 1994

Stubstad, R.N., Baltzer, S., Lukanen, E.O., and Ertman-Larsen, H.J., *Prediction of AC Mat Temperature for Routine Load/Deflection Measurements*, 4th International Conference on Bearing Capacity of Airfields, Minnesota, 1994.

Tabatabaie-Raissi, A.M. *Structural Analysis of Concrete Pavement Joints*, Ph.D. Thesis, University of Illinois at Urbana-Champaign, 1977.

Thompson, M.R., *ILLI-PAVE based Full Depth Asphalt Concrete Pavement Design Procedure*, Proceedings, Sixth International Conference on Structural Design of Aspahlt Paqvemnts, Vol.1, pp.13-22, 1987

Thompson, M.R. *Mechanistic-Empirical Flexible Pavement Design: An Overview,* Transportation Research Record 1539, TRB, National Research Council, Washington, D.C., 1995, pp. 1-5

Uddin, W., *A Micromechanical Model for Prediction of Creep Compliance and Viscoelastic Analysis of Asphalt Pavements*, Presented at 77th Annual Meeting, TRB, National Research Council, Washington, D.C., 1998.

Uhlmeyer, J.S., K. Willoughby, L.M. Pierce, and J.P. Mahoney, *Top-Down Cracking in Washington State Asphalt Concrete Wearing Courses*, 79th TRB Annual Meeting, TRB, National Research Council, Washington, D.C., 2000

Ullidtz, P. *Pavement Analysis*, Elsevier, New York, 1987

Van de Loo, P.J., *The Creep Test, A Key Tool in Asphalt Mix Design and in the Prediction of Pavement Rutting*, Proc., Assoc. of Asphalt Paving Technologists, 47, 1978, pp. 253-281.

Van Dijk, W. and W. Visser, *The Energy Approach to Fatigue for Pavement Design*, AAPT, Vol. 46, 1997

Wahhab, H.I.A., and Balghunaim, F.A., *Asphalt Pavemnet Temperature-Related to Arid Saudi Environment*, J. Mat. in Civil Engrg., ASCE, 6(1), 1994, pp. 1-14.

Warren, H., and W.L. Dieckmann, *Numerical Computation of Stresses and Strains in a Multiple-Layer Asphalt Pavement System*, Internal Report, Chevron Research Corporation, Richmond, CA., 1963

Westergaard, H. M., *Computation of Stresses in Concrete Roads*, HRB Proc. Vol. 6, 1926.

Westergaard, H. M., *Stresses in Concrete Pavements Computed by Theoretical Analysis*, Public Roads, Vol. 7, No. 2, April, 1926.

Winkler, E., *Die Hehre von der Elastizitat und Festigkeit: The Theory of Elasticity and Stiffness*, H. Dominicus, Parague, 1867.

Yeh, Ming-Shan, *Nonlinear Finite Element Analysis and Design of Flexible Pavements*, Ph.D. Thesis, Michigan State University, 1989.

Yoder, E.J. and Witczak, M.W., *Principal of Pavement Design*, John Wiley and Sons, Inc., 2nd. Edition, New York, 1975.

Young, R.J. and P.A. Lovell, *Introduction to Polymers*, Chapman & Hall, 2nd Edition, London, UK, 1991